LaJolla INSTITUTE
DIVISION of APPLIED NONLINEAR PROBLEMS
7855 FAY AVENUE, SUITE 200
LA JOLLA, CALIFORNIA 92037 • (619) 456-5451

LJI-88-P-495

Final Report

Strange Attractors in Geophysical Flow Fields

Bruce J. West

Division of Applied Nonlinear Problems
La Jolla Institute
7855 Fay Avenue, Suite 200
La Jolla, California 92037

Prepared for:
Office of Naval Research
800 North Quincy Street
Arlington, Virginia 22217-5000

Under Contract Number N00014-88-C-0547

August 1988

LJI-88-P-495

Final Report

Strange Attractors in Geophysical Flow Fields

Bruce J. West

Division of Applied Nonlinear Problems
La Jolla Institute
7855 Fay Avenue, Suite 200
La Jolla, California 92037

Prepared for:
Office of Naval Research
800 North Quincy Street
Arlington, Virginia 22217-5000

Under Contract Number N00014-88-C-0547

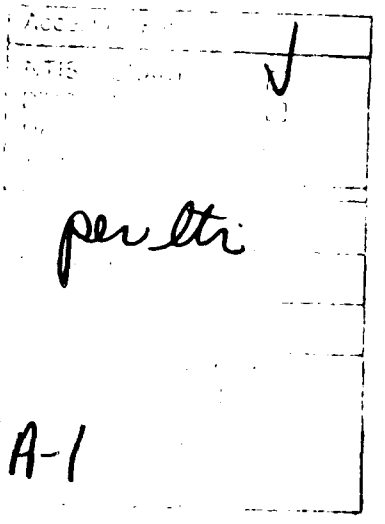

August 1988

Executive Summary

Herein we address the question of whether the techniques of nonlinear dynamics system theory can be usefully applied in a physical oceanography context. The tentative answer to this question is, yes, the dynamics of a numerically generated one-dimensional sea surface is shown to take place on a low-dimensional attractor. Further, the dimension of the attractor is fractional (noninteger) and therefore the trajectory describing the surface evolution is chaotic.

The report is segmented into four sections. In the first section we review the traditional wisdom of the mathematical modeling of waves on the sea surface. In the second section a mini-review of nonlinear dynamics is presented, in which the basic concepts of importance in understanding the influence of nonlinearities on the evolution of a system are discussed in a straightforward way. How these concepts have been applied in geophysical context, including the ocean surface, is discussed in Section 3. In particular it is shown that both climate and weather have chaotic attractors using a technique that allows one to reconstruct the attractor directly from observational data. The properties of the sea surface modeled as a fractal surface are also discussed.

In Section 4 some original research is presented in which the attractor reconstruction technique is applied to a numerically generated one-dimensional sea surface having a Phillips spectrum of waves. In these preliminary calculations we find that, like the climate and weather attractors, the water wave attractor has a low-order fractional dimension. This implies that as few as five or six degrees of freedom may be sufficient to describe the dynamics of a surface that required 512 degrees of freedom to numerically generate. The implications of this for such problems as data processing are still being considered and one discussed inpart in Section 5. We emphasize that these results are preliminary and may require substantial investigation before they can be substantiated.

Table of Contents

1. Introduction

It is well known that the geophysical data sets seem almost capricious in their variability. Indeed it is this mercurial nature of geophysical flows that makes the prediction of weather patterns, or sea states, from deterministic primitive equations so uncertain. One strategy for taking this changeability into account has been to introduce noise directly into the equations of motion, thereby replacing the deterministic equations of motion by stochastic differential equations [Landau and Lifshitz, 1959]. From these stochastic equations it is then possible to construct transport equations for the evolution of average flow properties, such as the mean velocity, the average energy, etc.. In physical oceanography, at least, this technique has *not* been very successful in describing the evolution of the energy spectral density of gravity waves [see eg., West, 1981]. In large part this failure arises because such transport equations do not properly take into account such strongly nonlinear effects as wave breaking and long wave/short wave interactions. In this report we wish to focus on certain techniques which may be able to determine the influence of strong nonlinear interactions on the evolution of water waves, as well as on weather patterns and climate. These techniques have been developed in the area of nonlinear systems theory.

In Section 2 of this report we present a mini-review of nonlinear dynamics which may be skipped over by the experts, but which the novice might find useful. In this section one will discover that dynamic systems theory emerged from a fusion of two classical areas of mathematics, topology and the theory of differential equations. Its importance to the experimental and observational sciences lies in its capacity to *quantitatively* characterize complex dynamical behavior. Herein we review how dynamical systems theory is applied in various geophysical contexts. One way in which it is applied is in the construction of simple dynamical models that give rise to solutions that resemble the observed time series data. Another way in which it is applied is through the development of data processing algorithms that capture the essential features of the dynamics of the system, such as its degree of irregularity and the structure of the attractor* on which the system's dynamics takes place [cf. Section 2]. It is obvious that the theory of differential equations is useful because it enables one to construct the dynamic equations that

* All technical terms, from nonlinear dynamics, used in the Introduction are defined in Section 2.

describe the evolution of the geophysical system of interest. Topology is of value here because it allows us to determine the unique geometrical properties of the resulting dynamic attractors. The degree of irregularity or randomness of calculated time series is closely related to the geometrical structure of the underlying attractor.

Mandelbrot (1977, 1982), the father of fractals, argues that we need a new kind of geometry to study such structures. Euclidean geometry is concerned with the understanding of straight lines and regular forms, and it is usually assumed, in geophysical and oceanography, that the world consists of continuous, smooth curves in spaces of integer dimension. When we look at billowing clouds, trees of all kinds, breaking waves and coastlines, we observe that the notions of classical geometry are inadequate to describe them. Detail does *not* become less important as regions of these various structures are magnified, but perversely more and more detail is revealed at each level of magnification. The rich texture of these structures is characteristic of fractals [Mandelbrot, 1977, 1982]. In Section 3 we show that a fractal structure is not smooth and homogeneous, and that the smaller-scale structure is similar to the large-scale form. The aspect of such structures that makes them different from what we usually experience is that there is no characteristic length scale.

But it is not only static structures that have fractal properties but dynamical processes as well. In Section 3 we also review how the fractal concept has been applied to time series in some geophysical applications and in Section 4 some preliminary applications are made to a spectrum of deep water gravity waves. Because this latter application is particularly important to us, let us now review some of the traditional wisdom regarding such wave fields.

The generation, growth, propagation and eventual dissipation of waves on the ocean surface have, over the past quarter century, been described in terms of weakly interacting, nonlinear waves [see eg., Phillips, 1966; West, 1981]. The equations of motion for the nonlinear wave field are determined by a Hamiltonian [Zakhorov, 1968; Miles, 1977] for an incompressible, inviscid, irrotational fluid. To describe the process of wave generation, evolution, and the subsequent development of wave instabilities, it is often convenient to express the observables at the ocean surface as series expansions in the eigenfunction of the linearized system. For water waves these eigenfunctions are simple sines and cosines and the eigenfunction expansion is merely a Fourier decomposition of the

surface. The expansion coefficients are interpreted as the constant amplitudes of independent waves in a linear wave field, and as the time varying amplitudes in a nonlinear wave field. The Hamiltonian for this system can be expressed as a series in which the nonlinear terms appear as products of the mode amplitudes, see eg. West (1981). These nonlinear interactions, interpreted as the scattering or coupling of the once linear waves, induce variations in both the amplitudes and phases of the linear modes in the equations of motion.

The sea surface gravity wave field is described as a conservative Hamiltonian system and Hamilton's equations of motion provides a deterministic description of its evolution [Hasselmann, 1968; Broer, 1974; Watson and West, 1975; Miles, 1977; West, 1981]. If we assume that this field is well represented by N degrees of freedom, where N may be large but finite (a field has an infinite number of degrees of freedom), then the system can be represented by $2N$ coupled, deterministic, nonlinear rate equations for the mode amplitudes. Moser (1973) separates the interactions into resonant and nonresonant groups. The nonresonant interactions provide for a stable evolution of the wave field, whereas the resonant interactions produce instabilities. The existence of resonances in water wave dynamics was explicitly pointed out by Phillips (1960). He demonstrated that just as for resonances in linear systems, the nonlinear resonances in wave/wave interactions produce an initial secular growth of new waves. Benny (1962) extended these arguments to show how the nonlinear interactions also saturate, thereby quenching the apparent instability. Chirikov (1979) pointed out that the instabilities generated by such nonlinear resonances are always bounded, unlike linear resonances which grow without limit. This bounding of the instability is produced by the nonlinear dispersion relation, i.e., the amplitude dependence of the frequencies in the equations of motion. Weak nonlinearities, therefore, act to stabilize the water wave system and inhibit explosive instabilities.

The concept of dominant resonant interactions have formed the basis for many analytic-numeric calculations of the properties of surface water waves [Hasselmann, 1962, 1963a, b; Zakhorov, 1968; Yuen and Lake, 1982; Peregrine, 1983; Bryant, 1984]. The evolution of capillary and gravity-capillary waves has been described by mode rate equations with cubic nonlinearities, i.e., four-wave interactions. The nonresonant interactions had been thought to be unimportant in describing the evolution of the wave field; however, Watson and West (1975), using perturbation theory, and West (1981),

using canonical transformations of variables, demonstrated that the nonresonant terms contribute substantially to the strength of the resonant interactions among the surface waves and are therefore not negligible. Thus, in the numerical results discussed in Section 4, we include *both* resonant and nonresonant effects.

The motion of the free surface of an incompressible, irrotational, inviscid fluid $\zeta(\mathbf{x}, t)$ is determined by Bernoulli's equation

$$\frac{\partial}{\partial t}\phi + \tfrac{1}{2}\mathbf{v}\cdot\mathbf{v} + g\zeta = 0 \quad , z = \zeta \quad , \tag{1.1}$$

with the fluid velocity $\mathbf{v}(\mathbf{x}, z, t)$ given by the gradient of the velocity potential $\phi(\mathbf{x}, z, t)$,

$$\mathbf{v} = \nabla\phi \tag{1.2}$$

and the vertical motion of the free surface by

$$\frac{\partial}{\partial t}\zeta(\mathbf{x}, t) + \mathbf{v}\cdot\nabla\zeta(\mathbf{x}, t) = \frac{\partial\phi}{\partial z} \equiv W \quad , z = \zeta \quad . \tag{1.3}$$

In the interior of the incompressible fluid,

$$\nabla\cdot\mathbf{v} = 0 \tag{1.4}$$

so that the velocity potential satisfies Laplace's equation

$$\nabla^2\phi = 0 \quad . \tag{1.5}$$

These equations can be converted to equations at the free surface, where

$$\phi_s(\mathbf{x}, t) \equiv \phi[\mathbf{x}, z = \zeta(\mathbf{x}, t), t] \tag{1.6}$$

with the result [Watson and West, 1975],

$$\frac{\partial}{\partial t}\phi_s + \tfrac{1}{2}(\nabla_s\phi_s)^2 + g\zeta = \tfrac{1}{2}[1 + (\nabla_s\zeta)^2]W^2 \quad , \tag{1.7}$$

$$\frac{\partial\zeta}{\partial t} + \nabla_s\phi_s\cdot\nabla_s\zeta = [1 + (\nabla_s\zeta)^2]W \quad , \tag{1.8}$$

where ∇_s is the horizontal gradient operator. The numerical integration of (1.7) and (1.8) is based on the method of Watson and West (1975) and is done by taking the indicated products of the field quantities in configuration space; fast Fourier transforming (FFT) the configuration equations and time incrementing the transformed equations to obtain the components of the appropriate field variables, then transforming (FFT) back to configuration space to again evaluate the nonlinear products and start the process again.

This numerical procedure, developed by West, Brueckner, Janda, Milder and Milton (1987), does not distinguish between resonant and nonresonant interactions, so that it includes terms explicitly neglected or approximated by most calculations involving the use of nonlinear mode rate equations.

The question of interest here is whether the sea surface described by these equations, and therefore explicitly determined by the evolution of $2N$ degrees of freedom can also be described by a low-dimensional dynamic attractor. This question is addressed in Section 4, where the techniques discussed in Section 2 and 3 are applied to the time series generated by the numerical code. The tentative answer to the question is, yes, the dynamics of the one-dimensional sea surface does take place on a low-dimensional attractor. Further, the attractor seems to have a fractional (fractal) dimension and therefore the trajectory describing the evolution is chaotic. We emphasize that these results are preliminary and may require substantial investigation before they can be substantiated.

2. Mini-Review of Nonlinear Dynamics

In this section we sketch the concepts from nonlinear dynamics that will be the most useful in attempting to determine if the surface, or interior, of the ocean can be usefully modeled as a low-dimensional attractor. One of the most fruitful and brilliant ideas of the second half of the 1600's was the idea that the concept of a function and the geometric representation of a curve are related. Geometrically the notion of a linear relation between two quantities implies that if a graph is constructed with the ordinate denoting the values of one variable and the abscissa denoting the values of the other variable, then the relation in question appears as a straight line. In general, the graph or curve lies in the "space" defined by the independent coordinate axes. In a dynamic system the coordinate axis are defined by the possible values of the independent dynamic variables.

The state of a given system is defined by a point in the above space, often called either the state space or phase space of the system. As time moves on the point traces out a curve, called an orbit or trajectory, which describes the history of the system's evolution. This geometrical representation of dynamics is one of the most useful tools in dynamic systems theory for analyzing the time-dependent properties of nonlinear systems. By nonlinear we mean the output of a system is not proportional to the input. One implication of this is the following: If the system is linear, than two trajectories initiated at nearby points in phase space evolve in close proximity, so that at any point in future time the two trajectories (and therefore the states of the system they represent) are also near to one another. If the system is nonlinear then two such trajectories could diverge from one another and at subsequent times the two trajectories could be arbitrarily far apart, i.e., the distance between the orbits does not evolve in a proportionate way. Of course this need not *necessarily* happen in a nonlinear system, it is a question of stability.

This brings us back to our recurrent example of the weather and to the question of its predictability. Its elusive nature has only recently come into sharper focus and made clear two distinct views of the character of the evolution of deterministic dynamic systems. These views were articulated by their respective proponents, Laplace and Poincaré, writing nearly 100 years apart.

Laplace (1825) believed in strict determinism and to his mind this implied complete predictability. Uncertainty for him is a consequence of imprecise knowledge, so that probability theory is necessitated by incomplete and imperfect observations. This view is clearly expressed in the quotation:

"The present state of the system of nature is evidently a consequence of what it was in the preceding moment, and if we conceive of an intelligence which at a given instant comprehends all the relations of the entities of this universe, it could state the respective positions, motions, and general affects of all these entities at any time in the past or future."

"Physical astronomy, the branch of knowledge which does the greatest honor to the human mind, gives us an idea, albeit imperfect, of what such an intelligence would be. The simplicity of the law by which the celestial bodies move, and the relations of their masses and distances, permit analysis to follow their motions up to a certain point; and in order to determine the state of the system of these great bodies in past or future centuries, it suffices for the mathematician that their position and their velocity be given by observation for any moment in time. Man owes that advantage to the power of the instrument he employs, and to the small number of relations that it embraces in its calculations. But ignorance of the different causes involved in the productions of events, as well as their complexity, taken together with the imperfection of analysis, prevents our reaching the same certainty about the vast majority of phenomena. Thus there are things that are uncertain for us, things more or less probable, and we seek to compensate for the impossibility of knowing them by determining their different degrees of likelihood. So it is that we owe to the weakness of the human mind one of the most delicate and ingenious of mathematical theories, the science of chance or probability."

Poincaré 1906 on the other hand sees an intrinsic inability to make predictions due to a sensitive dependence of the evolution of the system on the initial state of the system. He expressed this in the following way:

"A very small cause which escapes our notice determines a considerable effect that we cannot fail to see, and then we say that the effect is due to chance. If we knew exactly the laws of nature and the situation of the universe at the initial moment, we could predict exactly the situation of that same universe at a succeeding moment. But even if it were the case that the natural laws had no longer any secret for us, we could still only know the initial situation *approximately*. If that enabled us to predict the succeeding situation with *the same approximation*, that is all we require, and we should say that the phenomenon had been predicted, that it is governed by laws. But it is not always so; it may happen that small differences in the initial conditions produce very great ones in the final phenomena. A small error in the former will produce an enormous error in the latter. Prediction becomes impossible, and we have the fortuitous phenomenon."

Thus we can clearly distinguish between the "traditional" view of Laplace and the "modern" view of Poincaré. The latter is considered modern because we have now discovered that deterministic systems with only a few degrees of freedom can generate aperiodic behavior that for many purposes is indistinguishable from random fluctuations. We emphasize that the random aspect is fundamental to the system dynamics and gathering more information will not reduce the degree of uncertainty. Randomness generated in this way is now called *chaos* [see eg. Crutchfield et al., 1987]. To understand chaos we need to discuss the dynamics of nonlinear systems.

We introduced the notion of a phase space and a trajectory to describe the dynamics of a system. Each choice of an initial state for the system produces a different trajectory. If, however, there is a limiting set in phase space to which all trajectories are drawn after a sufficiently long time, we say that the system dynamics are asymptotically described by an attractor. The attractor is the geometric limiting set on which all the trajectories eventually find themselves, i.e., the set of points in phase space to which the trajectories are attracted. Attractors come in many shapes and sizes, but they all have the property of occupying a finite volume of phase space. As a system evolves it sweeps through the attractor, going through some regions rather rapidly and others quite slowly, but always staying on the attractor. Whether or not the system is chaotic is determined by how two initially adjacent trajectories cover the attractor over time. As Poincaré stated, if a small change in the initial separation of trajectories (error) produces an enormous change in their final separation (error), then the evolution is unpredictable. One question is how this growing separation, indicative of chaos, is accomplished on an attractor of finite size. The answer has to do with the layered structure of the attractor necessary for it to be chaotic.

Rössler (1976) described chaos as resulting from the geometric operations of stretching and folding. Two initially nearby orbits cannot rapidly separate forever on an attractor of finite size, therefore the attractor must eventually fold over onto itself. Once folded the attractor is again stretched and folded again. This process is repeated over and over yielding an attractor structure with an infinite number of layers to be traversed by the various trajectories. The infinite richness of the attractor structure affords ample opportunity for trajectories to diverge and follow increasingly different paths. The finite size of the attractor insures that these diverging trajectories will eventually pass close to one another again, albeit on different layers of the attractor. Crutchfield et al. (1987)

visualize thes orbits on a chaotic attractor as being shuffled by this stretching and folding process, much as a deck of cards is shuffled by a dealer. Thus the randomness of the chaotic orbits is a consequence of this shuffling process. This operation of stretching and folding creates folds within folds ad infinitum, resulting in the attractor often having a fractal structure in phase space.

The degree of irregularity (chaos) of the dynamic observable is closely related to the geometrical structure of the underlying attractor. There are a number of measures of the degree of chaos of these attractors. One is its *dimension*; integer values of the dimension indicate a simple attractor, non-integer dimension indicates a chaotic attractor in phase space.

A second measure of the degree of irregularity generated by a chaotic attractor is the ''entropy'' of the motion. The entropy is interpreted by Crutchfield et al. (1987) as the average rate of stretching and folding of the attractor, or alternatively, as the average rate at which information is generated. The application of the information concept in the dynamic systems context has been championed by Shaw (1981,1984) and Nicolis (1985,1986). One can view the preparation of the initial state of the system as initializing a certain amount of information. The more precisely the initial state can be specified, the more information one has. This corresponds to localizing the initial state of the system in phase space, the amount of information is inversely proportional to the volume of state space localized by measurement. In a regular attractor, trajectories initiated in a given local volume stay near to one another as the system evolves, so the initial information is preserved in time and no new information is generated. Thus the initial information can be used to predict the final state of the system. In a chaotic attractor the stretching and folding operations smear out the initial volume, thereby destroying the initial information as the system evolves and the dynamics create new information. Thus the initial uncertainty in the specification of the system is eventually smeared out over the entire attractor and all predictive power is lost, ie., all causal connection between the present and the future is lost.

Let us denote the region of phase space as initially occupied by V_i (initial volume) and the final region by V_f. The change in the observable information I is then [Shaw, 1981; Nicolis and Tsuda, 1985]

$$\delta I = \log_2 \frac{V_f}{V_i} \quad . \tag{2.0.1}$$

The rate of information creation or dissipation is given by

$$\frac{dI}{dt} = \frac{1}{V}\frac{dV}{dt} \quad . \tag{2.0.2}$$

In non-chaotic systems, the sensitivity of the flow to the initial conditions grows with time at most as a polynomial, eg., let $\omega(t)$ be the number of distinguishable states so that

$$\omega(t) \sim t^n \tag{2.0.3}$$

since $V_f/V_i = \omega_f/\omega_i$ we have [Shaw 1981]

$$\frac{dI}{dt} \sim \frac{n}{t} \quad . \tag{2.0.4}$$

Thus the rate of information generation converges to zero as $t \to \infty$ and the final state is predictable from the initial information. On the other hand, in chaotic systems the sensitivity of the flow to the initial conditions grow exponentially with time,

$$\omega(t) \sim e^{nt} \tag{2.0.5}$$

so that

$$\frac{dI}{dt} \sim n \quad . \tag{2.0.6}$$

This latter system is therefore a continuous source of information, the attractor itself generates the information independently of the initial conditions.

The final measure of the degree of chaos associated with an attractor with which we will be concerned is the set of Lyapunov exponents. These exponents quantify the average exponential convergence or divergence of nearby trajectories in the phase space of the dynamical systems. Wolf, Swift, Swinney and Vastano (1985), among others, believe the spectrum of Lyapunov exponents provides the most complete qualitative and quantitative characterization of chaotic behavior. A system with one or more positive Lyapunov exponents is defined to be chaotic. The local stability properties of a system are determined by its response to perturbations; along certain directions the response can be stable whereas along others it can be unstable. If we consider a d-dimensional sphere of initial conditions and follow the evolution of this sphere in time, then in some directions the sphere will contract, whereas in others it will expand, thereby forming a d-dimensional ellipsoid. Thus, a d-dimensional system can be characterized by d exponents where the j^{th} Lyapunov exponent quantifies the expansion or contraction of

the flow* along the j^{th} ellipsoidal principal axis. The sum of the Lyapunov exponents is the average divergence of the flow, which for a dissipative system (possessing an attractor) must always be negative.

Consider a three dimensional phase space in which the limiting set (the attractor) can be characterized by the triple of Lyapunov exponents $(\lambda_1,\lambda_2,\lambda_3)$. The qualitative behavior of the attractor can be specified by determining the signs of the Lyapunov exponents only, ie., $(sign\,\lambda_1, sign\,\lambda_2, sign\,\lambda_3)$. As shown in Figure (2.0.1a) the triple (-,-,-) corresponds to an attracting fixed point. In each of the three directions there is an exponential contraction of trajectories, so that no matter what the initial state of the system it will eventually wind up at the fixed point. This fixed point need not be the origin, as it would be for a dissipative linear system, but can be anywhere in phase space. The arrows shown in the figure do not necessarily represent trajectories since the fixed point can be approached at any angle by the evolving nonlinear system.

An attracting limit cycle is denoted by (0,-,-) in which there are two contracting directions and one that is neutrally stable. In Figure (2.0.1b) we see that this attractor resembles the orbit of a harmonic oscillator with a particular energy, but that is not the case. The orbit of a harmonic oscillator does not attract points from off the orbit onto itself. On the other hand in a nonlinear dynamical system an orbit has a basin of attraction so that all systems whose initial state lies in the basin eventually wind up on the limit cycle.

The triple (0,0,-) has two neutral directions and one that is contracting so that the attractor is the 2-torus depicted in Figure (2.0.1c). An example of such a system would be two coupled harmonic oscillators, where the two positions and two velocities would describe the dynamics. The constant energy (no dissipation) reduces the number of variables in this coupled system to three so that the system is described by the two constant radii and the two angles locating the trajectory on the surface of the torus.

Finally (+,0,-) corresponds to a chaotic attractor in which the trajectories expand in one direction, are neutrally stable in another and contracting in a third. In order for the trajectories to continuously expand in one direction and yet remain on a finite attractor,

* By "flow" we mean the behavior on phase space of a bundle of trajectories having a distribution of initial conditions.

the attractor must undergo the stretching and folding operations in this direction as discussed by Rössler (1978). Figure (2.0.1d) is the two-dimensional projection of the Rössler attractor.

The resolution of the apparent conflict between the traditional and the modern view of dynamic systems theory as presented in classical mechanics is that chaos is not inconsistent with the traditional notion of solving deterministic equations of evolution. As Ford (1987) states:

"...Determinism means that Newtonian orbits exist and are unique, but since existence-uniqueness theorems are generally nonconstructive, they assert nothing about the character of the Newtonian orbits they define. Specifically, they do not preclude a Newtonian orbit from passing every computable test for randomness of being humanly indistinguishable from a realization of a truly random process. Thus, popular opinion to the contrary notwithstanding, there is absolutely no contradiction in the term "deterministically random." Indeed, it is quite reasonable to suggest that the most general definition of chaos should read: chaos means deterministically random..."

2.1 Nonlinear Oscillator

In the physical sciences the dynamics of a system are determined by the equations describing how the physical observables change in time. These equations are obtained by means of some general principle, such as the conservation of energy and/or momentum, applied to the system of interest. The appropriate conservation law follows from a symmetry of the system which determines a rule by which the system evolves. If a set of circumstances is specified by an N-component vector $\mathbf{X}=(X_1, X_2, .., X_N)$ then in order to predict the future state of the system from its present configuration, we must specify a rule for the systems' evolution. In the physical sciences the traditional strategy is to construct a set of differential equations. These equations are obtained by considering each component of the system to be a function of time, then as time changes so too do the circumstances. If in a short time interval Δt we can associate an attendant set of changes $\Delta\mathbf{X}=(\Delta X_1, ..., \Delta X_N)$ as determined by $\Delta\mathbf{X}=F(\mathbf{X}, t)\Delta t$ then in the limit $\Delta t \rightarrow 0$ one would write the "equations of motion"

$$\frac{d}{dt}\mathbf{X}(t)=\mathbf{F}(\mathbf{X}, t) \tag{2.1.1}$$

which is a statement about the evolution of the system in time. If at time $t=0$ we

specify the components $\mathbf{X}(0)$, i.e., the set of circumstances characterizing the system, and if $\mathbf{F}(\mathbf{X}, t)$ is an analytic function of its arguments, then the evolution of the system is determined by direct integration of the equations of motion away from the initial state.

The mathematicians have categorized the solutions to such equations for the simplest kinds of systems. One way to describe such systems is by means of geometric constructions in which the solution to an equation of the above form is depicted by a curve in an appropriate space. The coordinate axes necessary for such a construction are the continuum of values that the vector $\mathbf{X}(t)$ can assume, each axis is associated with one component of the vector $\mathbf{X}$; this is called a phase space. Consider a two-dimensional phase space having axes labeled by the components of the dynamical system $\mathbf{X}=(X_1, X_2)$. A point in the phase space $\mathbf{x} = (x_1, x_2)$ gives a complete characterization of the dynamical system at a point in time. As time proceeds this point traces out a curve as shown in Figure (2.1.1), starting from the initial state $[X_1(0), X_2(0)]$ and proceeding to the final state $[X_1(t), X_2(t)]$ at time t. A trajectory or orbit in phase space traces out the evolution of the dynamical system. Time is a parameter which indexes each point along such a solution curve. The field of trajectories initiated from a set of initial conditions is often referred to as the flow field. If for example the flow field asymptotically ($t \rightarrow \infty$) converges to a single point in phase space, this is called a fixed point (or focus) [cf. Figure (2.1.2)]. If the flow field converges to a single closed curve this is called a limit cycle [cf. Figure (2.1.3)]. Such limit cycles appear as periodic behavior in the variables of interest.

A nonlinear oscillator which is "weakly" nonlinear is capable of oscillating at essentially a single frequency and can produce a signal that is very low in harmonic content. Although the output from such an oscillator system is sinusoidal at a single frequency, there are fundamental and crucial differences between such an oscillator and the classical harmonic oscillator, the latter being a conservative system which is loss-free. The basic difference is that the nonlinear oscillator can oscillate at one and only one frequency and one and only one amplitude, the amplitude and frequency being dependent on one another for a given configuration of parameters. In contrast, the amplitude and frequency are independent in the classical linear oscillator, which can oscillate at any arbitrary level for a given set of parameter values. These differences are illustrated in the description of the limit cycle. The phase plane of a Hamiltonian (loss-free) oscillator is

depicted in Figure (2.1.4) together with the limit cycle for an oscillator with nonlinear dissipation [cf. Figure (2.1.3)]. Although there are superficial resemblances between these diagrams, there are, in fact, fundamental differences between these two physical systems. While the linear conservative oscillator can be described by an infinite family of closed ellipses, as shown in Figure (2.1.4), the nonlinear oscillator approaches a *single limit cycle* as seen in Figure (2.1.3). This limit cycle is reached asymptotically whether the initial conditions correspond to an infinitesimal perturbation near the origin or to a finite perturbation far beyond the limit cycle. In either case the phase point spirals to the limit cycle, which is a stable final state. On the other hand, the conservative linear oscillator does not display this "structural stability." Any perturbation causes it to leave one ellipse and move to another, i.e. the orbits are neutrally stable.

In linear systems the term equilibrium is usually applied in connection with conservative forces, with the point of equilibrium corresponding to the vanishing of all forces with the system being at rest. The stability of such an equilibrium state is then defined by the behavior of the system when it is subject to a small perturbation i.e., a small displacement away from the equilibrium state in phase space. Roughly speaking, the terms stability and instability indicate that after the perturbation is applied the system returns to the equilibrium state (stable) or that it continues to move away from it (unstable) or that it does not move (neutral stability).

(a) Strange attractors (deterministic chaos)

The appellation "strange attractor" was given to those attractors on which, unlike the system just discussed, the system dynamics are aperiodic. This means that a deterministic equation of motion gives rise to a trajectory whose corresponding time series nowhere repeats itself over time; it is chaotic. The term "chaotic" refers to the dynamics of the attractor, whereas "strangeness" refers to the topology of the attractor. From the point of view of classical statistical mechanics the idea of randomness has traditionally been associated with the weak interaction of an observable with the rest of the universe. The traditional view requires there to be many (an infinite number) degrees of freedom that are not directly observed, but whose presence is manifest through fluctuations in the physical observations [see eg., West and Lindenberg, 1987]. More recently it has been learned that in a nonlinear system with even a few degrees of freedom chaotic motion can be observed [Lorenz, 1963].

What we present in this subsection are some of the recent results obtained in nonlinear dynamics that lead to chaos. First we briefly review the classical work of Lorenz (1963) on a deterministic continuous dissipative system with three variables. The phase space orbit for the solution to the Lorenz system is on an attractor, but of a kind on which the solution is aperiodic and therefore *strange*. We discuss this family of aperiodic solutions and discover that chaos lurks in a phase space of dimension three. Rössler (1978) points out that if oscillation is *the* typical behavior of low-dimensionai dynamical systems, then chaos, in the same way, characterizes three-dimensional continuous systems.

The modern view of randomness discussed in the Introduction can be traced back to Poincaré, but the recent avalanche of interest dates from the attempts of Lorenz to understand the short term variability of weather patterns and thereby enhance their predictability [see eg., Halloway and West, 1984]. His approach was to represent a forced dissipative geophysical hydrodynamic flow by a set of deterministic nonlinear differential equations with a finite number of degrees of freedom. By forcing we mean that the environment provides a source of energy for the flow field, which in this case is a source of heat at the bottom of the atmosphere. The dissipation in this flow extracts energy from the temperature gradient but the forcing term puts energy back in. For the particular physical problem Lorenz was investigating, the number of degrees of freedom he was eventually able to use was three, let's call them X, Y, and Z. In the now standard form these equations are

$$\frac{dX}{d\tau} = -\sigma X + \sigma Y \tag{2.1.2}$$

$$\frac{dY}{d\tau} = -XY + r X - Y \tag{2.1.3}$$

$$\frac{dZ}{d\tau} = XY - bZ \tag{2.1.4}$$

where σ, r and b are parameters. The solutions to the Lorenz model can be identified with trajectories in phase space. What is of interest here are the properties of the nonperiodic bounded solutions in this three dimensional phase space. A bounded solution is one that remains within a restricted domain of phase space as time goes to infinity.

The phase space for the set of equations (2.1.2) - (2.1.4), is three-dimensional and the solution to them traces out a curve $\Gamma_t(x,y,z)$ given by the locus of values of $\mathbf{X}(t) = [X(t), Y(t), Z(t)]$ [cf. Figure (2.1.5)]. We can associte a small volume $V_0(t) = X_0(t) Y_0(t) Z_0(t)$ with a perturbation of the trajectory and investigate how this

volume of phase space changes with time. If the original flow is confined to a region R then the rate of change of the small volume with time $\partial V_0/\partial t$ must be balanced by the flux of volume $\mathbf{J}(t) = V_0(t)\,\dot{\mathbf{X}}(t)$ across the boundaries of R. The quantity $\dot{\mathbf{X}}(t)$ in the flux $\mathbf{J}$ represents the time rate of change of the dynamical variables in the absence of the perturbations, i.e., the unperturbed flow field that can sweep the perturbation out of the region R. The balancing condition is expressed by an equation of continuity and in the physics literature is written

$$\frac{\partial}{\partial t}\, V_0(t) + \nabla \cdot \mathbf{J}(t) = 0 \tag{2.1.15}$$

or in detail

$$\frac{1}{V_0(t)}\,\frac{d}{dt} V_0(t) = \partial_X \dot{X} + \partial_Y \dot{Y} + \partial_Z \dot{Z} \tag{2.1.16}$$

where d/dt ($\equiv \partial_t + \dot{\mathbf{x}} \cdot \nabla_x$) is the so-called *convective* or *total* derivative of the volume. Using the equations of motion (2.1.2) - (2.1.4) in (2.1.6) we obtain

$$\frac{1}{V_0(t)}\,\frac{d}{dt} V_0(t) = -(\sigma + b + 1) \quad . \tag{2.1.7}$$

Equation (2.1.7) is interpreted to mean that as an observer moves along with an element of phase space volume $V_0(t)$ associated with the flow field, the volume will contact at a rate $b + \sigma + 1$, i.e., the solution to (2.1.7) is $V_0(t) = V_0(t=0) \exp[-(b+\sigma+1)t]$. Hence the volume goes to zero as $t \to \infty$ at a rate which is independent of the solutions $X(t), Y(t)$ and $Z(t)$. As pointed out by Lorenz , this does not mean that each small volume shrinks to a point in phase space; it may simply become flattened into a surface, one with a fractional dimension, ie. a non-integer dimension between two and three. Consequently the total volume of the region initially enclosed by the surface R shrinks to zero at the same rate, resulting in all trajectories become asymptotically confined to a specific subspace having zero volume and a fractal dimension [Ott, 1985].

To understand the relation of this system to the kind of dynamical situation we were discussing in the preceding section we must study the behavior of the system on the limiting manifold to which all trajectories will be ultimately confined. This cannot be done analytically because of the nonlinear nature of the equations of motion for the Lorenz model. Therefore, these equations are integrated numerically on a computer and the resulting solution is depicted as a curve in phase space for particular values of the

parameters σ, b and r. The technical details associated with the mathematical understanding of these solutions is available in the literature, see e.g., Ott (1985) or Eckmann and Ruelle (1985) and of course the original discussion of Lorenz (1963).

In Figure (2.1.6) we display the behavior of $Y(t)$ for 3000 time units. After reaching an early peak at $t = 35$, $Y(t)$ relaxes so a relatively stable value at $t = 85$ which persists, subject to systematically amplified oscillations, until near $t \approx 1650$. Beyond this time $Y(t)$ becomes pulse-like and appears to change signs at apparently random intervals. This irregularity is not just in the spacing between maxima but also in the sign of the adjacent maxima, i.e., the irregular occurrence of a number of peaks of one sign before a peak of the opposite sign occurs.

In Figure (2.1.7a) the solution manifold in the three dimensional phase space is shown and (2.1.7b) projects the solution manifold onto the (z,y)-plane and the (x,y)-plane. The trajectory indicated is not complete, but is that segment traversed in the time interval $t = 1400$ to 1900. The points C and C' are the fixed points of the equations, i.e., the values of $x, y,$ and z for which $\dot{X} = \dot{Y} = \dot{Z} = 0$ in (2.1.2)-(2.1.4), which for $r > 1$ yield $X = Y = \pm[b(r-1)]^{1/2}, Z = r-1$. These two views of the trajectory indicate that the erratic behavior apparent in the $Y(t)$ plot [cf. Figure (2.1.6)] arises from the orbit spiraling around one of the fixed points C or C' for some arbitrary period and then jumping to the vicinity of the other fixed point, spiraling around that for a while and then jumping back to the other and on and on. If the number of times the orbit circled C and C' were recorded and ordered, the resulting sequence would be random. Virtually all trajectories finally end up on this highly unstable manifold.

The strange attractor depicted in Figure (2.1.5) is not the only solution to the Lorenz system of equations. This solution was obtained for the parameter values $\sigma = 10, b = 8/3, r = 28$. If the values $\sigma = 10$ and $b = 8/3$ are held fixed and r is increased from zero, a wide range of attractors and subsequent dynamic behaviors are obtained. The possible flow patterns make the transition from stable equilibria independent of initial conditions, to chaotic attractors that are sensitively dependent on initial conditions, to "chaotic transients" [Yorke and Yorke 1979] in which, for certain initial conditions, an apparently chaotic trajectory emerges and asymptotically decays into a stable equilibria. The decay time is a sensitive function of the initial state.

Lorenz, in examining the solution to his equations, deduced that the trajectory is apparently confined to a surface. Ott (1985) comments that the apparent "surface" must have a small thickness, and it is inside this thickness that the complicated structure of the strange attractor is embedded. This is where the folding discussed in the Introduction actually occurs. If one were to pass a transverse line through this surface, the intersection of the line with the surface is a set of dimension D with $0 \leq D \leq 1$. The structure of the attractor is therefore fractal, and the stretching and folding of the trajectory discussed earlier is a geometric property of the attractor.

The erratic behavior in the time series depicted in Figure (2.1.6) is also apparent in the associated spectrum. The spectrum is the mean square value of the Fourier transform of a time series, i.e., the Fourier transform of the correlation function. Consider the solution $X(t)$; it will have a Fourier transform over a time interval T defined by

$$\hat{X_T}(\omega) = \int_{-T/2}^{T/2} X(t)\, e^{-i\omega t}\, \frac{dt}{2\pi} \tag{2.1.8}$$

and a power spectral density (PSD)

$$S_{xx}(\omega) \equiv \lim_{T \to \infty} \frac{|\hat{X_T}(\omega)|^2}{T} \quad . \tag{2.1.9}$$

In Figure (2.1.8) we display the power spectral densities (PSD) $S_{xx}(\omega)$ and $S_{zz}(\omega)$ as calculated by Farmer, Crutchfield, Froehling, Packard and Shaw (1980) using the trajectory shown. It is apparent from the power spectra density using the $X(t)$ time series that there is no dominant periodic x–component to the dynamics of the attractor, although lower frequencies are favored over higher ones. The power spectral density for the $Z(t)$ time series has a much flatter spectrum overall, but there are a few isolated frequencies at which energy is concentrated. This energy concentration would appear as a strong periodic component in the time trace of $Z(t)$. From this one would conclude that $X(t)$ is non-periodic, but that $Z(t)$ possesses both periodic and non-periodic components. In fact from the linearity of the Fourier transform (2.1.8) we would say that $Z(t)$ is a superposition of these two parts:

$$Z(t) = Z_p(t) + Z_{np}(t) \quad . \tag{2.1.10}$$

The implication of (2.1.10) is that the auto-correlation function

$$C_{zz}(\tau) = \lim_{t \to \infty} < Z(t)Z(t+\tau) > \qquad (2.1.11)$$

may be written as the sum of a nonperiodic components $< Z_{np}(t)Z_{np}(t+\tau) >$ that decays to zero at $\tau \to \infty$ and a periodic component $< Z_P(t)Z_p(t+\tau) >$ that does not decay.

To summarize: we have here a new kind of attractor that is referred to as "strange" whose dynamics are "chaotic" and with a power spectra density resulting from the time series of the trajectory that has broadband components. Dynamical systems that are periodic or quasi-periodic have a PSD composed of delta functions, i.e., very narrow spectral peaks; non-periodic systems have broad spectra with no dramatic emphasis of any particular frequency. It is this broad band character of the PSD that is currently used to identify non-periodic behavior in experimental data.

So what does this all mean? In part what it means is that the dynamics of a complex system might be random even if its description can be "isolated" to a few (three or more) degrees of freedom that interact in a deterministic but nonlinear way. If the system is dissipative, i.e., information is extracted from the system on the average, but the system is open to the environment, i.e., information is supplied to the system by means of boundary conditions, then a "strange attractor" is not only a possible manifold for the solutions to the dynamic equations; it, or something like it, may even be probable.

We show subsequently that the aperiodic or chaotic behavior of an attractor is a consequence of a sensitivity to initial conditions: trajectories that are initially nearby exponentially separate as they evolve forward in time on a chaotic attractor. Thus as Lorenz observed: microscopic perturbations (unobservable changes in the initial state of a system) are amplified to affect macroscopic behavior. This property is quite different from the qualitative features of nonchaotic attractors. In the latter, orbits that start out near one another remain close together forever. Thus small errors or perturbations remain bounded and the behavior of individual trajectories remain predictable.

Of course these considerations are not of much practical value unless they can be implemented in the determination of the properties of a real data set. This will be done subsequently. The rationale for their application was also developed by Lorenz in his seminal work, but the full extent of its importance has only recently begun to emerge, see e.g. Lanford (1976). He (Lorenz) observed that the trajectory leaves the spiral centered at C say, [see Figure (2.1.5)], only after exceeding some critical distance from the center.

Further, the degree to which this critical distance is exceeded determines the point at which the next spiral, i.e., that centered at C', is entered as well as the number of circuits executed prior to making the transition back to the C center again. Thus he concludes that "some single feature of a given circuit should predict the same feature of the following circuit." As an example he selected the maximum value of the $Z(t)$ variable along the trajectory which occurs whenever the circuit is nearly completed.

In Figure (2.1.9) the abscissa is labeled by the value of the n^{th} maxima Z_n of $Z(t)$ and the ordinate is labeled by the value of the following maximum Z_{n+1}. It is clear that the points generated lie along a curve if the spaces between points are filled in. This is shown for example by Shaw (1981) using the increased computing capacity that has developed in the intervening years. The computer generated function clearly prescribe a two- to-one relation between Z_n and Z_{n+1}. From this relation one could formulate an empirical prediction scheme using the geometry of the attractor as a data set without a knowledge of the underlying dynamic equations. In the next section, after we learn about mappings, we will see how this is done.

A second example of a dynamic system whose solutions lie on a chaotic attractor was given by Rössler (1976) for a chemical process. He has in fact provided over half a dozen examples of such attractors [cf. Rössler (1978)], but we will not discuss all of them here. It is useful to consider his motivation for constructing such a variety of chaotic attractors. In large part it was to understand the detailed effects of the stretching and folding operations in nonlinear dynamical systems. These operations mix the orbits in phase space in the same way a baker mixes bread by kneading it, i.e., rolling it out and folding it over. Visualize a drop of red food coloring placed on top of a ball of dough. This red spot represents the initially nearby trajectories of a dynamic system. Now as the dough is rolled out for the first time the red spot is stretched into an ellipse, which eventually is folded over. After a sufficiently long time the red blob is stretched and folded many times, resulting in a slab of dough with alternating layers of red and white. Crutchfield et al. (1987) point out that after 20 such operations the initial blob has been stretched to more than a million times its original length, and its thickness has shrunk to the molecular level. The red dye is then thoroughly mixed with the dough, just as chaos thoroughly mixes the trajectories in phase space on the attractor.

The dynamic equations for Rössler's (1976) three degree of freedom system is

$$\dot{X} = -(Y+Z) \tag{2.1.12}$$

$$\dot{Y} = X + aY \tag{2.1.13}$$

$$\dot{Z} = b + XZ - cZ \tag{2.1.14}$$

where a, b and c are constants. For one set of parameter values, Farmer et al. (1980) referred to the attractor as "the funnel," the obvious reason for this name is seen in Figure (2.1.10). Another set of parameter values yields the "simple Rössler attractor," [cf. Figure (2.1.11d)]. Both of these chaotic attractors have one positive Lyapunov exponent. As we mentioned earlier, a Lyapunov exponent is a measure of the rate at which trajectories separate one from the other [cf. Section (2.0)]. A negative exponent implies the orbits approach a common fixed point. A zero exponent means the orbits maintain their relative positions; they are on a stable attractor. Finally, a positive exponent implies the orbits exponentially separate; they are on a chaotic attractor.

Equations (2.1.19) - (2.1.21) is one of the simplest sets of differential equation models possessing a chaotic attractor. Figure (2.1.11) depicts a projection of the attractor onto the (x,y)-plane for four different values of the parameter c. Notice that as c is increased the trajectory changes from a simple limit cycle with a single maximum [Figure (2.1.11a)], to one with two maxima [Figure (2.1.11b)] and so on until finally the orbit becomes aperiodic [Figure (2.1.11d)]. Here again, as with the Lorenz attractor, we can relate the n^{th} maximum of say $X(t)$ to the $(n+1)^{st}$ maximum. This can be done by noting the intersection of the trajectory in Figure (2.1.11) to a line placed transverse to the attractor. In this way we obtain the plot of the maximum shown in Figure (2.1.12), the curve yielding the functional equation $x_{n+1} = f(x_n)$ which is a difference equation. This figure suggests how we can replace a continuous model by one which is discrete. We shall return to this procedure in the following section.

2.2 Nonlinear Mappings

Now that we have seen the brand of chaos that a continuos strange attractor gives we examine a one-dimensional noninvertible nonlinear map. This mapping is the discrete analog of the logistic equation and leads to a subharmonic bifurcation of the solution eventually resulting in a kind of chaos that is distinct from that generated by the Lorenz attractor. The results are quite general for maps with a single maxima. A third

kind of chaos is related to that found on the Lorenz attractor in that a two-dimensional invertible map is shown to have an attractor which is *strange*, i.e., it is the discrete analog of the Lorenz attractor.

One of the fascinating aspect of these maps is that they appear to be the natural way in which to describe the time development of systems in which successive generations are quite distinct. The result of the mathematical analysis is that for certain parameter regimes there are a large number of classes of discrete dynamical models (maps) with chaotic solutions. The *chaos* associated with these solutions is such that the orbits are periodic or erratic in time, but the chaos of one class has not been shown to be the same as that of another class. However, they all indicate that one must abandon the notion that the deterministic nonlinear evolution of a process implies a predictable result. One may be able to solve the discrete equations of motion only to find a chaotic solution that requires a distribution function for making predictions.

Just as in Section 2.1 we wish to describe the dynamics of a system characterized by an N-component vector $\mathbf{X}=(X_1,X_2,...,X_N)$ and again in order to determine the future evolution of the system from its present state we must specify a dynamic rule for each of the components. For many systems the variables need not be considered continuous functions of time, but rather to be functions of a discrete time index specifying successive generations. The minimum unit of time change for the dynamic equations would in this case be given by unity, i.e., the change of a single generation. Thus the equations of motion instead of being given by (2.1.1) would be of the form

$$\mathbf{X}(n+1)=\mathbf{F}[\mathbf{X}(n)] \tag{2.2.1}$$

where the changes in the vector $\mathbf{X}(n)$ between generation n and $n+1$ is determined by the function $\mathbf{F}[\mathbf{X}(n)]$. If at generation $n=0$ we specify the components of $\mathbf{X}(0)$, i.e., the set of circumstances characterizing the system, then the evolution of the system is determined by iteration (mapping) of the recursion relation (2.2.1.) away from the initial state. Even in systems that are perhaps more properly described by continuous time equations of motion it is thought by many, see e.g. Collete and Eckmann (1980), that a discrete time representation may be used to isolate simplifying features a certain dynamical systems.

(a) One-dimensional maps

The evolution equation in a discrete representation is called a *map* and the evolution is given by iterating the map, ie., by repeated application of the mapping operation to the newly generated points. Thus iterations of the form $X_n \rightarrow X_{n+1} = f(X_n)$, where f maps the one-dimensional interval [0,1] onto itself, is interpreted as a discrete time version of a continuous dynamical system. The choice of interval [0,1] is arbitrary since the change of variables $Y = (X-1)/(b-a)$ will replace a mapping of the interval $[a,b]$ into itself by one that maps [0,1] into itself. For example, consider the continuous trajectory in the two-dimensional phase space depicted in Figure (2.2.1). The intersection points of the orbit with the X-axis are denoted by $X_1, X_2, \cdots$. The point X_{n+1} can certainly be related to X_n by means of the function f determined by the trajectory. Thus, instead of solving the continuous differential equations that describe the trajectory, in this approach one produces models of the mapping function f and studies the properties of $X_{n+1} = f(X_n)$. Here, as we have said, n plays the role of the time variables. This strategy has been applied to models for biological, social, economic, chemical and physical systems. May (1976) has pointed out a number of possible applications of the fundamental equation for a single variable

$$X_{n+1} = f(X_n) \quad . \tag{2.2.2}$$

In genetics, for example, X_n could describe the change in the gene frequency between successive generations; in epidemiology, the variable X_n could denote the fraction of the population infected at time n; in psychology, certain learning theories can be cast in the form where X_n is interpreted as the number of bits of information that can be remembered up to generation n; is sociology, X_n might be interpreted as the number of people having heard a rumor at time n and (2.2.2) would then describe the propagation of rumors in societies of various structures see, e.g., Kemeny and Snell (1972). The potential applications of such modeling equations are therefore restricted only by our imaginations.

Consider the simplest mapping, also called a recursion relation, in which a population X_n of organisms per unit area, on a petri dish for example, in the n^{th} generation is strictly proportional to the population in the preceding generation with a proportionality constant μ:

$$X_n = \mu X_{n-1} \ , \quad n = 1, 2, \cdots \tag{2.2.3}$$

The proportionality constant is given by the difference between the birth rate and death rate and is therefore the *net* birth rate of the population. Equation (2.2.3) is quite easy to solve. Suppose that the population has a level $X_0 = N_0$ at the initial generation, then the recursion relation yields the sequence of relation

$$X_1 = \mu N_0 \ , \quad X_2 = \mu X_1 = \mu^2 N_0 , \cdots \tag{2.2.4}$$

so that in general

$$X_n = \mu^n N_0 \tag{2.2.5}$$

This rather simple solution already exhibits a number of interesting properties. Firstly, if the net birth rate μ is less than unity, then we can write $\mu^n = e^{-n\beta}$ where $\beta > 0$, so that the population decreases exponentially between successive generation (note $\beta = -\ln \mu$). This is a reflection of the fact that with $\mu < 1$, the population of organisms fails to reproduce itself from generation to generation and therefore it exponentially approaches extinction:

$$\lim_{n \to \infty} X_n = 0 \ \text{ if } \ \mu < 1 \ . \tag{2.2.6}$$

On the other hand if $\mu > 1$, then we can write $\mu^n = e^{n\beta}$ where $\beta \ (= \ln \mu) > 0$, so the population increases exponentially from generation to generation. This is a reflection of the fact that with $\mu > 1$ the population has an excess at each generation resulting in a population explosion. This is the Malthus' exponential population growth:

$$\lim_{n \to \infty} X_n = \infty \ \text{ if } \ \mu > 1 \ . \tag{2.2.7}$$

The only value of μ for which the population does not have these extreme tendencies is $\mu = 1$, when, since the population reproduces itself exactly in each generation, we obtain the unstable situation:

$$\lim_{n \to \infty} X_n = N_0 \tag{2.2.8}$$

Of course this simple model is no more valid than the continuous growth law of Malthus (1798), which he used to describe the exponential growth of human populations. A more scientifically oriented investigator, Verhulst (1844) , put forth a theory that somewhat mediated the pessimistic view of Malthus. Verhulst noted that the growth of real populations is not unbounded. He argued that such factors as the availability of food, shelter, sanitary conditions, etc. all restrict (or at least influence) the growth of populations. He included these effects by making the growth rate μ a function of the population level. His arguments allows us to generalize the discrete model to include the effects of limited resources. In particular, the birthrate is assumed to decrease with increasing population in a linear way:

$$\mu \rightarrow \mu(X_n) = \mu [\, 1 - X_n/\Theta \,] \tag{2.2.9}$$

Where Θ is the saturation level of the population. Thus the linear recursion relation (2.2.3) is replaced with the nonlinear discrete *logistic equation* ,

$$X_{n+1} = \mu X_n [\, 1 - X_n/\Theta \,] \quad . \tag{2.2.10}$$

It is clear that when $X_n << \Theta$ the population grows exponentially since the nonlinear term is negligible. However at some point the ratio X_n/Θ is going to be of the order unity and the rate of population growth will be retarded. When $X_n = \Theta$ there are no more births in the population. Biologically the regime $X_n > \Theta$ corresponds to a negative birthrate, but this does not make biological sense and so we restrict the region of *interpretation* of this model to $[1 - X_n/\Theta] > 0$. Finally, we reduce the number of parameters from two, μ and Θ, to one by introducing $Y_n = X_n/\Theta$ the fraction of the saturation level achieved by the population. In terms of this *ratio* variable the recursion relation (2.2.10) becomes

$$Y_{n+1} = \mu Y_n [\, 1 - Y_n \,] \quad . \tag{2.2.11}$$

Segal (1984) challenges the readers of his book (at this point in the analysis of this mapping) to attempt and predict the type of behavior manifest by the solution to (2.2.11), e.g. Are there periodic components to the solution? Does extinction ever occur?, etc. His intent was to alert the reader to the inherent complexity contained in the deceptively simple looking equation (2.2.11). We will examine some of these general properties shortly, but first let us explore our example a bit more fully. Our intent is to introduce the reader

to a number of fundamental dynamical concepts that will be useful in the subsequent study of water wave data. Note that saturation inducing models such as (2.2.11) have been used to describe the transport of energy in physical oceanography.

We noticed that extinction was the solution to the simple system (2.2.3) when $\mu<1$. Is extinction a possible solution to (2.2.11)? If it is, then once that state is attained, it must remain unchanged throughout the remaining generations. Put differently, extinction must be a steady-state solution of the recursion relation. A steady-state solution is one for which $Y_n = Y_{n+1}$ for all n. Let us assume the existence of a steady-state level Y_{ss} of the population such that (2.2.11) becomes

$$Y_{ss} = \mu Y_{ss}(1 - Y_{ss}) \tag{2.2.12}$$

for all n, since in the steady-state $Y_{n+1} = Y_n = Y_{ss}$. Equation (2.2.12) defines the quadratic equation

$$Y_{ss}^2 + (1/\mu - 1) Y_{ss} = 0 \tag{2.2.13}$$

which has the two roots $Y_{ss} = 0$, and $Y_{ss} = (1 - 1/\mu)$. The $Y_{ss} = 0$ root corresponds to extinction, but we now have a second steady solution to the mapping, that being $Y_{ss} = 1 - 1/\mu$. One of the questions that is of interest in the more general treatment of this problem is to determine to which of these steady states the population evolves as time go by, ie., extinction or some finite constant level.

Before we examine the more general properties of (2.2.11) and equations like it, let us use a more traditional tool of analysis and examine the stability of the two steady states found above. Traditionally the stability of a system in the vicinity of a given value is determined by perturbation theory. We use that technique now and write

$$Y_n = Y_{ss} + \xi_n \tag{2.2.14}$$

where $\xi_n << 1$ so that (2.2.14) denotes a small change in the relative population from its steady-state value. If we now substitute (2.2.14) into (2.2.11) we obtain

$$Y_{ss} + \xi_{n+1} = \mu(Y_{ss} + \xi_n) [1 - Y_{ss} - \xi_n] \quad . \tag{2.2.15}$$

Then using (2.2.12) to eliminate certain terms and neglecting terms quadratic in ξ_n we obtain

$$\xi_{n+1} = (\mu - 2Y_{ss}) \xi_n \tag{2.2.16}$$

as the recursion relation for the perturbation. In the neighborhood of extinction, the $Y_{ss}=0$ steady state, (2.2.16) reduces to (2.2.3) in the variable ξ_n rather than X_n. Therefore if $0<\mu<1$ then the fixed point $Y_{ss}=0$ is stable and if $\mu>1$ the fixed point is unstable. By stable we mean that $\xi_n \to 0$ as $n \to \infty$ if $0<\mu<1$ so that the system returns to the fixed point, i.e., ξ_n decreases exponentially in n. By unstable we mean that $\xi_n \to \infty$ as $n \to \infty$ if $\mu>1$ so that the perturbation grows without bound and never returns to the fixed point, i.e., ξ_n increases exponentially with n. Of course $\mu=1$ means the fixed point is neutrally stable, i.e., it neither return to nor diverges from $Y_{ss}=0$.

In the neighborhood of the steady state $Y_{ss}=1-1/\mu$ the recursion relation becomes

$$\xi_{n+1}=(2-\mu)\xi_n \quad . \tag{2.2.17}$$

The preceding analysis can again be repeated with the result that if $1>2-\mu>-1$ the fixed point $Y_{ss}=1-1/\mu$ is stable and implies that the birthrate is in the interval $1<\mu<3$. The stability is monotonic for $1<\mu<2$, but because of the changes in sign it is oscillatory for $2<\mu<3$. Similarly the fixed point is unstable for $0<\mu<1$ (monotonic) and $\mu>3$ (oscillatory).

Following Olsen and Degn (1985) we examine the nature of the solutions to (2.2.11) as a function of the parameter μ a bit more closely. This can be done using a simple computer code to evaluate the iterates Y_n. For $0<\mu\leq 4$ insert an initial value $0\leq Y_0\leq 1$ into (2.2.11) and generate a Y_1, which is also in the interval [0,1]. This second value of the iterate is then inserted back into (2.2.11) and a third value Y_2 is generated; here again $0\leq Y_2\leq 1$. This process of generation and reinsertion constitutes the dynamic process, which is a mapping of the unit interval into itself in a two- to-one manner, i.e., two values of the iterate at step n can be used to generate a particular value of the iterate at step $n+1$. In Figure (2.2.2a) we show Y_n as a function of n for $\mu=2.8$ and observe that as n becomes large ($n>10$) the value of Y_n becomes constant. This value is a fixed point of the mapping equal to $1-1/\mu=0.643$, and is approached by all initial conditions $0<Y_0<1$ i.e., it is an attractor. Quite a different behavior is observed for the same initial point when $\mu=3.2$. In Figure (2.2.2b) we see that after an initial transient the process becomes periodic, that is to say that the iterate alternates between two values. This periodic orbit is called a 2-cycle. Thus, the fixed point becomes unstable at the parameter value $\mu=3$ and bifurcates into a 2-cycle. Here the 2-cycle becomes the attractor for

the mapping. For a slightly larger value of μ, $\mu = 3.53$, the mapping settles down into a pattern in which the value of the iterate alternates between two large values and two small values [cf. Figure (2.2.2c)]. Here again the existing orbit, a 2-cycle, has become unstable at $\mu = 3.444$ and bifurcated into a 4-cycle. Thus, we see that as μ is increased a fixed point changes into a 2-cycle, a 2-cycle changes into a 4-cycle, which in turn will change into an 8-cycle and so on. This process of period doubling is called subharmonic bifurcation since a cycle of a given frequency ω_0 bifurcates into periodic orbits which are subharmonics of the original orbit, i.e., for k bifurcations the frequency of the orbit is $\omega_0/2^k$. The attractor for the dynamic process can therefore be characterized by the appropriate values of μ.

As one might have anticipated, the end point of this period doubling process is an orbit with an infinite period (zero frequency). An infinite period implies that the system is aperiodic, that is to say, the pattern of the values of the iterate does not repeat itself in any finite number of iterations, i.e., finite time interval, [cf. Figures (2.2.2d)]. We will see presently about any process that does not repeat itself as time goes to infinity is completely unique and hence is random. It was this similarity of the mapping to discrete random sequences that motivated the coining of the term chaotic to describe such attractors. The deterministic mapping (2.2.11) can therefore generate chaos for certain values of the parameter μ.

Returning now to the more general context it may appear that limiting the present analysis to one-dimensional systems is unduly restrictive; however, we recall that the system is pictured to be a projection of a more complicated dynamical system onto a one-dimensional subspace [cf. e.g., Figure (2.2.1)]. A substantial literature based on (2.2.11) has developed in the past decade, much of which is focused on the purely mathematical properties of such mappings. The physicists and mathematicians have been quite actively exploring the consequences of these results for physical and chemical systems.

For the moment we shall make the assumption that the maps (dynamic systems) of interest contain a single maximum and that $f(X)$ is monotonically increasing for value of X below this maximum and monotonically decreasing for values of X above this maximum. Maps such as these, i.e., maps with a single maximum, are called noninvertible, since, given X_{n+1} there are two possible values of X_n and therefore the functional

relation cannot be inverted. If the index n is interpreted as the discrete time variable, as we did above, the recursion relation generates new values of X_n forward in time but not backward in time, see e.g. Ott (1985). This assumption corresponds to the reasonable requirement that the dynamic law stimulates X to grow when it is near zero, but inhibits its growth when it reaches some saturation value. An example of this is provided by the discrete version of the Verhulst equation for population growth that we have just examined. Equation (2.2.10) is often called the discrete logistic equation and has been intensively studied in the physical sciences, usually in the scaled form (2.2.11). Thus the mapping function is $f(Y_n)=\mu Y_n(1-Y_n)$ and when graphed versus Y_n yields the quadratic curve depicted in Figure (2.2.3).

The mapping operation is one that is accomplished by applying the function f to a given initial values Y_0 to generate the next point, and applied sequentially to generate the successive images of this point. The point Y_n is generated by applying the mapping f, n times to the initial point Y_0:

$$Y_n = f^n(Y_0) \tag{2.2.18}$$

using the relation $f^n(Y_0)=f[f^{n-1}(Y_0)]$. This is done graphically in Figure (2.2.3a) for $n=3$ using the rule: starting from the initial point Y_0 a line is drawn to the function yielding the value $Y_1=f(Y_0)$ along the ordinate, then from symmetry the same value is obtained along the abscissa by drawing a line to the diagonal (45°) line. An application of f to Y_1 is then equivalent to dropping a line from the diagonal to the f-curve to yield $Y_2=f(Y_1)=f[f(Y_0)]=f^2(Y_0)$. The value Y_3 is obtained in exactly the same way from $Y_3=f^3(Y_0)$. The intersection of the diagonal with the function f defines a point Y^* having the property

$$Y^* = f(Y^*) \tag{2.2.19}$$

which is called a *fixed point* of the dynamic equation, i.e., Y^* is the Y_{ss} from (2.2.12). The fixed point corresponds to the steady-state solution of the discrete equation and for (2.2.11) $Y^* = 1 - 1/\mu$ (nontrivial) and $Y^* = 0$ (trivial). We can see in Figure (2.2.3b) that the iterated points are approaching Y^* and as $n \to \infty$ they will reach this fixed point. To determine if a mapping will approach a fixed point asymptotically, i.e., if the fixed point is stable, we examine the slope of the function at the fixed point, see e.g., May (1976) ; Li and Yorke (1975) ; Collet and Eckmann (1980). The function acts like a curved

mirror either focusing the ray towards the fixed point under multiple reflections or diverging the ray away. The asymptotic direction (either towards or away from the fixed point) is determined by the slope of the function at Y^*, which is depicted in Figure (2.2.4) by the dashed line and denoted by $f'(Y^*)$ i.e., the (tangent) derivative of $f(Y)$ at $Y=Y^*$. As long as $|f'(Y^*)|<1$ the iterations of the map are attracted to $Y=Y^*$, just as the perturbation ξ approaches zero in (2.2.14) near the stable fixed point. Again using a logistic map as an example, we have $f'(Y^*)=2-\mu$, so that the equilibrium point is stable and attracts all trajectories originating in the interval $0<Y<1$ if and only if $1<\mu<3$. This is of course the same result we obtained using linear stability theory [cf. Eq. (2.2.17)] for the logistic map.

When the slope of f is such that the fixed point becomes unstable, i.e., when $|f'(Y^*)|>1$, then the solution "spirals" out. If the parameter μ is continuously increased until this instability is reached then the orbit will spiral out until it encounters a situation where $Y_2^*=f(Y_1^*)$ and $Y_1^*=f(Y_2^*)$, i.e., the orbit becomes periodic. Said differently, the mapping f has a *periodic orbit* of period 2 since $Y_2^*=f(Y_1^*)=f^2(Y_2^*)$ and $Y_1^*=f(Y_2^*)=f^2(Y_1^*)$ since Y_1^* and Y_2^* are fixed points of the mapping f^2 and not of the mapping f. In Figure (2.2.4a) we illustrate the mapping f^2 and observe it to have two maxima rather than the single one of f. As the parameter μ is increased further the dimple between the two maxima increases as do the height of the peaks along with the slopes of the intersection of f^2 with the diagonal [cf. Figure (2.2.4b)].

For $1<\mu<3$ the fixed point is stable and Y^* is a degenerate fixed point of f^2, i.e., $Y^*=f^2(Y^*)$. At $\mu=3.414$ the fixed point becomes unstable and two new solutions to the quadratic mapping emerge. These are the two intersections of the quadratic map with the diagonal having slopes with magnitude less than unity, Y_1^* and Y_2^*. The chain rule of differentiation of the derivative of f^2 at Y_1^* and Y_2^* is the product of the derivatives along the periodic orbit

$$f^{2\prime}(Y_1^*)=f'[f(Y_1^*)]\,f'(Y_1^*)=f'(Y_1^*)f'(Y_2^*)=f^{2\prime}(Y_2^*) \qquad (2.2.20)$$

so that the slope is the same as both points of the period 2 orbit, see e.g., Li and Yorke (1975), and in fact the slope is the same at all k of the values of a period k orbit. This is in fact a continuous process starting from the stable fixed point Y^* when $|f'|<1$; as μ is increased this point becomes unstable at $|f'|=1$ and generates two new stable points with $|f^{2\prime}|<1$ for a period 2 orbit; as μ is increased further these points become unstable

at $|f'| = 1$ and generates two new stable points with $|f^{2\prime}| < 1$ for a period 2 orbit; as μ is increased further these points become unstable at $|f^{2\prime}| = 1$ and generates four new stable points with $|f^{4\prime}| < 1$ for a period 4 orbit. This bifurcation sequence is tied to the value of the parameter μ. As this parameter is increased the discrete equation undergoes a sequence of bifurcations from the fixed point to stable cycles with periods 2, 4, 8, 16, 32 ... 2^k. In each case the bifurcation process is the same as that for the transition from the stable fixed point to the stable period 2 orbit. A graph indicating the location of the stable values of Y for a given μ is given in Figure (2.2.5). Here we see that the μ interval between successive bifurcations is diminishing so that the "window" of values of μ wherein any one cycle is stable progressively diminishes. If we denote by μ_k the value of μ where the orbit bifurcates from length 2^{k-1} to 2^k, then

$$\lim_{k \to \infty} \frac{\mu_k - \mu_{k-1}}{\mu_{k+1} - \mu_k} = \text{universal constant} \qquad (2.2.21)$$

a result first obtained numerically by Feigenbaum (1979). This result indicates that a constant μ_∞ is being approached by this sequence. This critical parameter value is a point of accumulation of a period 2^k cycles. For (2.2.11) the critical value of this parameter is $\mu_\infty = 3.5700$. The numerical value of μ_∞ is dependent on the particular map considered, although the existence of an accumulation point does not, and more importantly the universal constant in (2.2.21) has a value 4.69210 ... and is also independent of the specific choice of the map.

In Figure (2.2.5) we use the logarithm of μ as the abscissa in order to clearly distinguish the bifurcation points. In Figure (2.2.6) we replot this sequence linearly in μ. In the latter figure we distinguish from left to right, a stable fixed point, orbit of period 1; a stable orbit of period 2, then 4, 8 and then a haze of orbits starting along the in μ_∞, then another orbit of period 6 then 5, and 3. Collet and Eckmann (1980) comment: "The astonishing fact about this arrangement of stable periodic orbits is its *independence* of the particular one-parameter family of maps." The haze of points beyond μ_∞ consists of an infinite number of fixed points with different periodicities, along with an infinite number of different periodic orbits. In addition there are an uncountable number of aperiodic trajectories (bounded) each of which is associated with a different initial point Y_0. Two such adjacent initial points generate orbits that become arbitrarily distant with iteration

number; no mater how long the time series generated by $f(Y)$ is iterated, the two patterns never repeat. As mentioned, Li and Yorke (1975) have applied the term *chaotic* to this hazy region where an infinite number of different trajectories can occur.

Thus we have arrived at the remarkable fact that a simple discrete deterministic equation can generate trajectories that are aperiodic. In particular in order to form a one-dimensional map to exhibit chaotic behavior, it must noninvertible.

(b) Two-dimensional maps

In the above discussion we defined a mapping in terms of a projection of a higher order dynamic system onto a one-dimensional line. This same definition can be applied for the intersection of the trajectories of a higher order dynamic process with a two-dimensional plane. In Figure (2.2.7) a sketch of a trajectory in three dimensions is shown, the intersection of the orbit with a plane defines a set of points that can be obtained by means of the two-dimensional map:

$$X_{n+1} = f_1(X_n, Y_n) \ , \ Y_{n+1} = f_2(X_n, Y_n) \ . \qquad (2.2.22)$$

Here we follow Ott (1985) and consider only invertible maps where (2.2.22) can be solved uniquely for X_n and Y_n as functions of X_{n+1} and Y_{n+1}; $X_n = g_1(X_{n+1}, Y_{n+1})$ and $Y_n = g_2(X_{n+1}, Y_{n+1})$. If n is the time index then invertibility is equivalent to time reversibility, so that these maps are reversible in time whereas those in the preceding discussion were not. The maps in this section are analogous to the Hamiltonian dynamic equations discussed in physics and chemistry and not the dissipative equations leading to the strange attractors such as the Lorenz model.

The reason for examining higher order maps, such as the two-dimensional example given by (2.2.22) is that under certain conditions these maps have many of the properties of the so called strange attractors discussed earlier even though they are conservative. In particular we will establish the connection between these invertible maps and the strange attractor of Lorenz as well as the fractal dimension discussed earlier.

The one-dimensional noninvertible maps were obtained by projecting a higher order trajectory onto a one-dimensional line. Let us now reverse the process and expand the space of the noninvertible map from one to two-dimensions by introducing the coordinate Y_n in the following way:

$$X_{n+1} = f(X_n) + Y_n \qquad (2.2.23)$$

$$Y_{n+1} = \beta X_n \quad . \tag{2.2.24}$$

Of course, if f is noninvertible and $\beta = 0$ (2.2.23) collapses back onto the one-dimensional map (2.2.11). For any non-zero β, however, the map (2.2.23) is invertible, i.e., $X_n = Y_{n+1}/\beta$ and $Y_n = X_{n+1} - f(Y_{n+1}/\beta)$. Thus we have transformed a noninvertible map to an invertible one by extending the space. As Ott (1985) points out, however, if β is sufficiently small the distinction between the invertible two-dimensional map and the noninvertible one-dimensional map may not be measurable.

Let us examine the behavior of a small phase space volume as the two-dimensional map is iterated from $X_n Y_n = V_n$ to $X_{n+1} Y_{n+1} = V_{n+1}$ in analogy to what was done with the Lorenz model. The relation between the two volumes is

$$V_{n+1} = JV_n \tag{2.2.25}$$

where J is the Jacobian of the map:

$$J \equiv \begin{vmatrix} \dfrac{\partial X_{n+1}}{\partial X_n} & \dfrac{\partial X_{n+1}}{\partial Y_n} \\ \dfrac{\partial Y_{n+1}}{\partial X_n} & \dfrac{\partial Y_{n+1}}{\partial Y_n} \end{vmatrix} \tag{2.2.26}$$

Inserting (2.2.23) and (2.2.24) into (2.2.26) we find $J = -\beta$ so that the volume at consecutive times (2.2.25) is given by

$$V_{n+1} = -\beta V_n \tag{2.2.27}$$

which for an initial volume V_0 has the solution

$$V_{n+1} = (-1)^{n+1} \beta^{n+1} V_0 \quad , \tag{2.2.28}$$

so that if $|\beta| < 1$ the volume will contract by a factor $|\beta|$ at each application of the mapping. This contraction does *not* imply that the solution goes over to a point in phase space, but only that it is attracted to some bounded region of dimension lower than that of the initial phase space. If the dimension of the attractor is non-integer, then the attractor is fractal; see e.g. in Mandelbrot (1980) where the observation that the fractal dimension of a set may or may not be consistent with the term *strange*. Following Eckmann (1981), we employ the property that, if all the points in the initial volume V_0 converge to a single attractor, but that points which are arbitrarily close initially separate exponentially in time, then that attractor is called strange. This property of nearby trajectories to

exponentially separating in time is called *sensitive dependence on initial conditions* and gives rise to the aperiodic behavior of strange attractors. There exists however a large variety of attractors which are neither periodic orbits nor fixed points and which are not strange attractors. All of these, states Eckmann (1981), seem to present more or less pronounced chaotic features. Thus there are attractors that are erratic but not strange. We will not pursue this general class here.

As an example of the two-dimensional invertible mapping we first transform the logistic equation (2.2.1) into the family of maps $X_{n+1} = 1 - cX_n^2$ with the parametric identification $c = (\mu/2 - 1)\mu/2$ and $0 < c \leq 2$, since $2 < \mu \leq 4$ and X_n maps the interval $[-1, 1]$ onto itself. Then using (2.2.23) and (2.2.24) we obtain the mapping first studied by Henon (1976):

$$X_{n+1} = 1 - cX_n^2 + Y_n \tag{2.2.29}$$

$$Y_{n+1} = \beta X_n \tag{2.2.30}$$

In Figure (2.2.8) we have copied the loci of points for the Henon system in which 10^4 successive points from the mapping with the parameter values $c = 1.4$ and $\beta = 0.2$ initiated from a variety of choice of (x_0, y_0). Ott (1985) points out that, as the map is iterated, points come closer and closer to the attractor eventually becoming indistinguishable from it. This, however, is an illusion of scale. If the boxed region of the figure is magnified one obtains Figure (2.2.9a) from which a great deal of structure of the attractor can be discerned. If the boxed region in this latter figure is magnified, then what had appeared as three unequally space lines appear in Figure (2.2.9b) as three distinct parallel intervals containing structure. Notice that the region in the box of Figure (2.2.9a) appears the same as that in Figure (2.2.9b). Magnifying the boxed region in this latter region we obtain Figure (2.2.9c), which aside from resolution is a self-similar representation of the structure seen on the two preceding scales. Thus we observe scale invariant, Cantor-set-like structure transverse to the linear structure of the attractor. Ott (1985) concludes that because of this self-similar structure the attractor is probably strange. In fact it has been verified by direct calculation that initially nearby points separate exponentially in time; [see eg. Feit, 1978; Curry, 1979], thereby coinciding with at least one definition of the strange attractor.

(c) The Lyapunov exponent

We have adopted the definition that chaotic systems are those that have a sensitive dependence on initial conditions. This sensitivity requires that orbits initially near to one another exponentially separate as they evolve forward in time. A computable quantitative measure of the rate at which orbits separate is the Lyapunov exponent. For a one-dimensional map the Lyapunov exponent is defined by the slope of the map:

$$\sigma = \lim_{n\to\infty} \frac{1}{N} \sum_{n=1}^{N} ln \mid \frac{df(Y_n)}{dY} \mid \tag{2.2.31}$$

where $Y_{n+1} = f(Y_n)$. Shaw (1981) has shown that σ is also the *average* information change over the entire interval of iteration. He argues that a map may be interpreted as a machine that takes a single input Y_0 and generates a string of numbers during the iteration process. If the string has a pattern such as would arise for an attractor that is a fixed point or periodic orbit, then after a very short time the machines gives *no new information.* On the other hand if the orbit is chaotic so that the string of numbers is random, then each iterate is new to the observer, and gives a new piece of information. Shaw convincingly demonstrates that a chaotic process is a generator of information. He argues that a negative σ implies a periodic orbit and the magnitude of σ measures the degree of stability of that orbit against perturbations. If an orbit is initiated at a point off the periodic orbit, but within its basin of attraction, the initial data will be lost as the orbit damps to its stable values. The parameter σ determines the rate at which this information is lost to the macroscopic world. If σ is positive, then it determines the rate of divergence of nearby trajectories which is the same as the rate of information production, see Oseledec (1968).

As an example let us take $\mu = 4$ in (2.2.11). Then if we define a new variable

$$Z_n = \frac{2}{\pi} \sin^{-1} (\sqrt{Y_n}) \tag{2.2.32}$$

the logistic map transforms to the "tent map"

$$Z_{n+1} = \begin{cases} 2Z_n & 0 \le Y_n \le 0.5 \\ 2(1 - Z_n) & 0.5 \le Y_n \le 1 \end{cases} . \tag{2.2.33}$$

From this we obtain for the slope of the map to be used in (2.2.31)

$$\left| \frac{df(Z_n)}{dZ} \right| = 2 \tag{2.2.34}$$

for all Z, so that

$$\sigma = \ln 2 \approx 0.693 > 0 \quad . \tag{2.2.35}$$

Since this quantity is *invariant* under coordinate transformations this proves that the logistic map with $\mu = 4$ meets our definition of a chaotic dynamical system, i.e., 0.693 bits of information are generated in each iteration. In fact this mapping is chaotic for all $\sigma > \sigma_\infty = 3.57\cdots$ since $\sigma > 0$ for all these values.

Let us consider an N-dimensional map, i.e., $\mathbf{X} = (X^1, X^2, \ldots, X^N)$,

$$\mathbf{X}_{n+1} = \mathbf{f}(\mathbf{X}_n) \tag{2.2.36}$$

for which we have a trajectory $\mathbf{X'}_n$ in this phase space with initial condition $\mathbf{X}_0$ and a nearly trajectory $\mathbf{X}_n$ with initial condition $\mathbf{X}_0 + \Delta\mathbf{X}_0$ and $\| \Delta\mathbf{X}_0 \| << \| \mathbf{X}_0 \|$. Here the double bars denote the norm of the vector. The difference between the two trajectories $\Delta\mathbf{X}_0$ defines the tangent vector $\mathbf{u}_n \equiv \Delta\mathbf{X}_n$ such that (2.2.36) can be used to write

$$\mathbf{u}_{n+1} = \mathbf{f}(\mathbf{X'}_n) - \mathbf{f}(\mathbf{X}_n) \cong \frac{\partial \mathbf{f}}{\partial \mathbf{X}} \cdot \mathbf{u}_n + \cdots \tag{2.2.37}$$

which defines the linearized mapping

$$\mathbf{u}_{n+1} = \mathbf{A}(\mathbf{X}_n) \cdot \mathbf{u}_n \quad . \tag{2.2.38}$$

where $\mathbf{A}$ is the $N \times N$ matrix defined by

$$\mathbf{A}(\mathbf{X}_n) = \frac{\partial}{\partial \mathbf{X}} \mathbf{f}(\mathbf{X}_n) \tag{2.2.39}$$

so that the map (2.2.38) is linearized along the trajectory $\mathbf{X}_n$. Following Nicolis (1986) the solution to (2.2.38) for a given initial condition $\hat{\mathbf{e}}_0$ at the n^{th} iteration can be written as

$$\mathbf{u}_n = U_{n,n-1}\, U_{n-1,n-2} \cdots U_{21}\, U_{10}\, \hat{\mathbf{e}}_0 \quad , \tag{2.2.40}$$

where $\mathbf{U}$ is the fundamental solution matrix. The indexing on $\mathbf{U}$ indicates the iteration for which it is the solution to the mapping. Let us interpret (2.2.40) starting with the right-most factor: $U_{10}\hat{\mathbf{e}}_0 = \mathbf{u}_1$, is the solution (2.2.38) for the initial condition $\mathbf{X}_0$. The solution $\mathbf{u}_1$ is a vector of length d_1 and director $\hat{\mathbf{e}}_1$:

$$U_{10}\,\hat{\mathbf{e}}_0 = d_1\,\hat{\mathbf{e}}_1 \tag{2.2.41}$$

and $\hat{\mathbf{e}}_1$ has a unit norm. Now we apply U_{21} to $\hat{\mathbf{e}}_1$ and obtain a vector of length d_2 and

direction $\hat{\mathbf{e}}_2$. Finally we can rewrite (2.2.40) as the product of n numbers

$$\mathbf{u}_n = d_n\, d_{n-1} \cdots d_1\, \hat{\mathbf{e}}_n \quad , \; |\hat{\mathbf{e}}_n| = 1 \tag{2.2.42}$$

instead of a product of n matrices. The maximal Lyapunov exponent is then defined as

$$\begin{aligned} \sigma &= \lim_{n\to\infty} \frac{1}{n}\, ln\, |\, d_1\, \hat{\mathbf{e}}_n| \\ &= \lim_{n\to\infty} \frac{1}{n} \sum_{j=1}^{n} ln\; d_n \quad . \end{aligned} \tag{2.2.43}$$

We see from the definition of $d_k = |\, U_{k,k-1}\; \hat{\mathbf{e}}_{n-1}|$ that $ln\, d_k$ is the exponential change of the length of $\hat{\mathbf{e}}_0$ during the time interval when the system (2.2.36) moves between the iterates $\mathbf{X}_{k-1}$ and $\mathbf{X}_k$.

Rather than finding just the maximal Lyapunov exponent we can define a Lyapunov exponent for each of the N variables that describe the dynamic system. To do this we note [cf. Benettin, Golgani and Strelcyn, 1976] that one can introduce eigenvalues $\lambda_j(n)$ of the matrix

$$\mathbf{A}_n = \left[\mathbf{A}(\mathbf{X}_n)\; \mathbf{A}(\mathbf{X}_{n-1}) \cdots \mathbf{A}(\mathbf{X}_1)\right]^{1/n} \quad , \tag{2.2.44}$$

where $\mathbf{A}_n$ is defined by (2.2.39) and is the Jacobian matrix of $\mathbf{f}$. The Lyapunov exponents are then given by

$$\sigma_j = = \lim_{n\to\infty} ln\, |\; \lambda_j(n)| \tag{2.2.45}$$

These eigenvalues λ_j are often called the Lyapunov numbers.

Let us consider the example given by Ott (1985) [cf. Figure (2.2.10)]. For a two-dimensional map, the Lyapunov numbers are given by λ_1 and λ_2 and are interpreted as the average principle stretching factors for a very small initial circular area of radius $\varepsilon(0)$. More formally we can write

$$\begin{aligned} \lambda_j = \lim_{n\to\infty} \Big\{ & \text{ magnitude of the } j^{th} \text{ eigenvaues of} \\ & \left[\mathbf{A}(X_n, Y_n)\; \mathbf{A}(X_{n-1},\, Y_{n-1}) \cdots \mathbf{A}(X_1, Y_1)\right]^{1/n} \Big\} \end{aligned} \tag{2.2.46}$$

where $\mathbf{A}(X, Y)$ is the Jacobian matrix of the map:

$$\mathbf{A}(X,Y)=\begin{bmatrix} \dfrac{\partial f_1(X,Y)}{\partial X} & \dfrac{\partial f_1(X,Y)}{\partial Y} \\ \dfrac{\partial f_2(X,Y)}{\partial X} & \dfrac{\partial f_2(X,Y)}{\partial Y} \end{bmatrix} . \tag{2.2.47}$$

The functions f_1 and f_2 are the components of the mapping vector **f** in (2.2.36); and, of course, $(X_1 Y_1), \cdots, (X_n, Y_n)$ is a sequence generated by the map. Then the Lyapunov numbers specify the average stretching rate of nearby points. If the map is to be chaotic, for $\lambda_1 > \lambda_2$ say, then λ_1 must be greater than unity, so that the distance between almost nearby points increases in successive iterations. If the map is area contracting then $\lambda_1 \lambda_2 < 1$, the distance between almost nearby points decreases in successive iterations; if it is area preserving then $\lambda_1 \lambda_2 = 1$ and the distance remains unchanged.

2.3 Measures of Strange Attractors

In broad outline we have attempted to give some indications of how simple nonlinear dynamic equations can give rise to a rich variety of dynamic behaviors. In particular we have, in large part, focused on the phenomenon of chaos described from the point of view of mathematics and modeling, but little or no effort was made to relate these results to actual data sets. Thus the techniques may not appear to be as useful as they could be to the experimentalist who observes large variations in his/her data and wonders if the observed fluctuations are chaos or noise. For a number of geophysical phenomena there may be no reliable dynamical model describing the behavior of the system, so the investigator must use the data directly to distinguish between the two. As we mentioned earlier, a traditional method for determining the dynamic content of a time series is to construct the power spectrum for the process by taking the Fourier transform of the autocorrelation function, or equivalently by taking the Fourier transform of the time series itself and forming its absolute square [cf. (2.1.9)]. The autocorrelation function provides a way to use the data at one time to determine the influence of the process on itself at a latter time. It is a measure of the relation of the value of a random process at one instant of time, $X(t)$ say, to the value at another instant τ seconds later, $X(t+\tau)$. If we have a data record extending continuously over the time interval $(-T/2, T/2)$, then the autocorrelation function is defined as

$$C_{xx}(\tau) \equiv \lim_{T\to\infty} \frac{1}{T} \int_{-T/2}^{T/2} X(t)X(t+\tau)\,dt \quad . \tag{2.3.1}$$

Note that for a finite sample length, i.e. for T finite, the integral defines an *estimate* for the autocorrelation function $C_{xx}(\tau, T)$ so that $C_{xx}(\tau) = \lim_{T \to \infty} C_{xx}(\tau, T)$. In Figure (2.3.1) a sample history of $X(t)$ is given along with its displaced time trace $X(t + \tau)$. The point by point product of these two series is given in (2.3.1) and then the average over the time interval $(-T/2, T/2)$ is taken. A sine wave, or any other harmonic deterministic data set, would have an autocorrelation function which persists over all time displacements. Thus the autocorrelation function can provide a measure of deterministic data embedded in a random background.

Similar comments apply when the data set is discrete rather than continuous, as it would be for the mappings in Section 2.2. In the discrete case we denote the interval between samples as $\Delta (= T/N)$ for N equally spaced intervals and r as the lag or delay number so that the estimated autocorrelation function is

$$C_{xx}(r\Delta, N) = \frac{1}{N - r} \sum_{j=1}^{N-r} X_j X_{j+r} \ , \ r = 0, 1, \cdots, m \qquad (2.3.2)$$

and m is the maximum lag number. Note that $C_{xx}(r\Delta, N)$ is analogous to the estimate of the continuum autocorrelation function and becomes the true autocorrelation function in the limit $N \to \infty$. These considerations have been discussed at great length by Wiener (1949) in his classic book on time series analysis, and is still recommended today as a text from which to capture a master's style of investigation.

The frequency content is extracted from the autocorrelation function by applying a filter in the form of a Fourier transform. This yield the power spectral density

$$S_{xx}(\omega) = \frac{1}{\pi} \int_{-\infty}^{\infty} e^{-i\omega t} C_{xx}(t)\, dt \qquad (2.3.3)$$

of the time series $X(t)$. Equation (2.3.3) relates the autocorrelation function to the power spectral density and is known as the *Weiner-Khinchine* relation which is in agreement with (2.1.8). One example of its use is provided in Figure (2.3.2a) where the exponential form of the autocorrelation function $C_{xx}(t) = e^{-t/\tau_c}$ used in Figure (2.3.2b) yields a frequency spectrum of the Cauchy form

$$S_{xx}(\omega) = \frac{1}{\pi} \ \frac{\tau_c}{1 + \omega^2 \tau_c^2} \ . \qquad (2.3.4)$$

At high frequencies the spectrum (2.3.4) is seen to fall-off as ω^{-2}.

As we mentioned, a periodic signal in the data will show sharp peaks in the spectrum corresponding to the fundamental frequency and its higher harmonics [cf. Section 2.1(b)]. On the other hand the spectrum corresponding to aperiodic variations in the time series will be broadband in frequency with no discernible structure. In themselves spectral techniques have no way of discriminating between chaos and noise and are therefore of little value in determining the *source* of the fluctuations in a data set. They were in fact very useful, as shown in Section 2.1(b), in establishing the *similarities* between stochastic processes and chaos defined as the sensitive dependence on initial conditions in a dynamic process.

One way in which some investigators have proceeded in discriminating chaos from noise is to visually examine time series for period doublings. This is a somewhat risky business, however, and may lead to misinterpretations of data sets. Also, period doubling is only one of the possible routes to chaos in dynamic systems.

It has been suggested that fractal processes associated with scaled, broadband spectra are "information-rich." Periodic states, in contrast, reflect narrow-band spectra and are defined by monotonous, repetitive sequences, depleted of information content. In Figure (2.3.3) we depict the spectrum of the time series $X(t)$ obtained from the funnel attractor solution of the equation set (2.1.2)-(2.1.14). The attractor itself is shown in Figure (2.1.10). We see that the spectrum is broad band as was that of the Lorenz attractor [cf. Figure (2.1.8)], with a number of relatively sharp spikes. These spikes are manifestations of a strong periodic components in the dynamics of the funnel attractor. Thus the dynamics could easily be interpreted in terms of a number of harmonic components in a noisy background, but this would be an error. One way to distinguish between these two interpretations is by means of the information dimension of the time series. The dimension decreases as a system undergoes a transition from chaotic to periodic dynamics.

Thus we conclude that more systematic methods for distinguishing between chaos and noise are desirable and necessary. We turn to those methods now.

(a) Correlational dimension

In the preceding discussion we presented the standard example of a correlation function having an exponential form. Such a correlation function could describe a random time series having a memory or correlation time τ_c. It could not describe a dynamical system having an asymptotic stationary or periodic state. Similarly it could not

describe a nonlinear dissipative dynamical system that has a chaotic attractor. Grassberger and Procaccia (1983a, b, c) developed a correlational technique by which one can exclude various choices for the kind of attractor on which the dynamics for a given data set exists. They wanted to be able to say that the attractor for the data set is not multiply periodic, or that the irregularities are not due to external noise, etc. As we have just seen Fourier analysis would tell us if the attractor were multiply periodic, but not the source of the fluctuations. They proposed a measure obtained by considering correlations between points of a time series taken from a trajectory on the attractor after the initial transients have died away.

Consider the set $\{X_j, j = 1, 2, \cdots, N\}$ of points on the attractor taken from a time series $X(t)$, i.e., we take $X_j \equiv X(j\Delta)$ where Δ is a fixed time interval between successive measurements. We see that this set of points could also be determined from a mapping where j denotes the iterate of the map. If the attractor is chaotic then since nearby trajectories exponentially separate in time, we expect that most pairs of points X_j, X_k $j \neq k$ will be dynamically uncorrelated. Even though these points may appear to be essentially random, they do all lie on the same attractor and therefore are correlated in phase space. As we discuss in the next section, the single time series can be used to construct an m-dimensional representation of the data by shifting the data as follows: $X_j^{(1)} = X(j\Delta); X_j^{(2)} = X(j\Delta - \tau), \ldots, X_j^{(m)} = X[j\Delta - (m-1)\tau]$, where τ has a value that is after determined by trial and error. The single time series X_j is thus replaced by the vector time series $\mathbf{X}_j \equiv \{X_j^{(1)}, X_j^{(2)}, \ldots, X_j^{(m)}\}$ where m is called the embedding dimension.

Grassberger and Procaccia (1983) introduced the correlation integral $C(r)$ defined by

$$C_m(r) \equiv \lim_{N\to\infty} \frac{1}{N^2} \sum_{i,j=1}^{N} \Theta(r - |\mathbf{X}_i - \mathbf{X}_j|)$$

$$\equiv \int_0^r d^m r' \, c(\mathbf{r}') \qquad (2.3.5)$$

where $\Theta(x)$ is the Heaviside function, $= 0$ if $x \leq 0$ and $= 1$ if $x > 0$, and $c(\mathbf{r}')$ is the traditional correlation function in Euclidian volume of m-dimensions

$$c(\mathbf{r}) = \lim_{N\to\infty} \frac{1}{N^2} \sum_{i,j=1, i\neq j}^{N} \delta^m(\mathbf{X}_i - \mathbf{X}_j - \mathbf{r}) \quad . \qquad (2.3.6)$$

and $|\mathbf{X}_i - \mathbf{X}_j|$ is the Euclidean norm of the m-dimensional vector. The virtue of the integral function is that for a chaotic or strange attractor the correlational integral has the power-law form

$$\lim_{m \to \infty} C_m(r) \sim r^{\nu} \tag{2.3.7}$$

and moreover, the "correlation exponent" ν is closely related to the fractal dimension D and the information dimension σ of the attractor. They argue that the correlation exponent is a useful measure of the local properties of the attractor whereas the fractal dimension is a purely geometric measure and is rather insensitive to the local dynamic behavior of the trajectories on the attractor. The information dimension is somewhat sensitive to the local behavior of the trajectories and is a lower bound on the Hausdorff dimension. In fact they observe that in general one has

$$\nu \leq \sigma \leq D \quad . \tag{2.3.8}$$

Thus if the correlation integral obtained from an experimental data set has the power-law form (2.3.7) with $\nu < m$, one knows that the data set arises from deterministic chaos rather than random noise, because noise will result in $C_m(r) \sim r^m$ for a constant correlation function over the distance r. Note that for periodic sequences $\nu = 1$; for random sequences it should equal the embedding dimension, while for chaotic sequences it is finite and non-integer.

Grassberger and Procaccia (1983) point out that one of the main advantages of the correlation dimension ν is the ease with which it can be measured. In particular it can be measured more easily than either σ or D for cases when the fractal dimension is large (≥ 3). Just as they anticipated, the measure ν has proven to be most useful in experimental situations, where typically high dimensional systems exist.

To test their ideas they studied the behavior of a number of simple models for which the fractal dimension is known. In Figure (2.3.4) we display three of the many calculations they did. In each case the logarithm of the correlation integral is plotted as a function of the logarithm of a dimensionless length which according to the power-law relation (2.3.7) should yield a straight line of positive slope. The slope of the line is the correlational dimension ν. We see from these examples that the technique successfully predicts the correlational behavior for both mappings and differential equations having chaotic attractors.

(b) Attractor reconstruction from data

More often than not the geophysical observer does not have the luxury of a mathematical model to guide the measurement process. What is usually available are a few partial theories, securely based on assumptions often made more for convenience than for reality, and a great deal of phenomenology. Therefore in a system known to depend on a number of independent variables it is not clear how many kinds of measurements one should make. In fact it is often unrealistically difficult to take more than the measurement of a single degree of freedom. What then can one say about a complex system given this single time series? It turns out that quite a lot may be learned using methods developed in nonlinear dynamics. In particular a method has been devised that enables one to reconstruct a multidimensional attractor from the time series of a single observable. The application of this technique to a number of geophysical data sets will be reviewed in the next chapter, but for the moment we concentrate on the exposition of the underlying theory.

Packard, Crutchfield, Farmer and Shaw (1980) who constituted the nucleus of the *Dynamic Systems Collective* at the University of California, Santa Cruz in the late 70's and early 80's, were the first investigators to demonstrate how one reconstructs a chaotic attractor from an actual data set. They used the time series generated by one coordinate of the three-dimensional chaotic dynamical system studied by Rössler (1978) i.e., (2.1.12)-(2.1.14) with the parameter values a = 0.2, b = 0.4 and c = 5.7. The reconstruction method is based on the hueristic idea that for such a three-dimensional system, any three ''independent'' time varying quantities are sufficient to specify the state of the system. The three dynamic coordinates $X(t)$, $Y(t)$ and $Z(t)$ are only one of the many possible choices. They conjectured that; ''any such sets of three independent quantities which uniquely and smoothly label the states of the attractor are diffeomorphically equivalent.'' In English this means that an actual dynamic system does not know of the particular representation chosen by us, and that any other representation containing the same dynamic information is just as good. Thus, an experimentalist sampling the values of a single coordinate need not find the ''one'' representation favored by nature, since this ''one'' does not in all probability exist.

Packard et al. (1980) playing the role of experimentalists sampled the $X(t)$ coordinate of the Rössler attractor. They then noted a number of possible alternatives to the phase space coordinates (x, y, z) that could give a faithful representation of the dynamics using the time series they had obtained. One possible set was the time series itself plus two replicas of it displaced in time by τ and 2τ, i.e. $X(t)$, $X(t-\tau)$ and $X(t-2\tau)$. Note that implicit in this choice is the idea that $X(t)$ is so strongly coupled to the other degrees of freedom that it contains dynamic information about these coordinates as well as itself. A second representation set could be obtained by making the time interval τ an infinitesimal, so that by taking differences between the variables we would obtain $X(t)$, $\dot{X}(t)$ and $\ddot{X}(t)$.

Figure (2.3.5a) shows a projection of the Rössler chaotic attractor on the (x, y) plane. Figure (2.3.5b) depicts the reconstruction of that attractor from the sampled $X(t)$ time series in the $(x, \dot{x})$ plane. It is clear that the two attractors are not identical, but it is just as clear that the reconstructed one retains the topological characteristics and geometrical form of the experimental attractor. One quantitative measure of the equivalence of the experimental and reconstructed attractors is the Lyapunov exponent associated with each one. This exponent can be determined by constructing a *return map* for each of the attractors and then applying the relation (2.2.31).

A return map is obtained by constructing a Poincaré surface of section. In this example of an attractor projected onto a two-dimensional plane, the Poincaré surface of section is the intersection of the attractor with a line transverse to the attractor. We indicate this by the dashed line in Figure (2.3.5b) and the measured data are the sequence of values $\{X_n\}$ denoting the crossing of the line by the attractor in the positive direction. These data are used to construct a next amplitude plot in which each amplitude X_{n+1} is plotted as a function of the preceding amplitude X_n. It is possible for such a plot to yield anything from a random spray of points to a well defined curve. If in fact we find a curve with a definite structure then it may be possible to construct a return map for the attractor. For example, the oscillating chemical reaction of Belousov and Zhabotinskii was shown by Simoyi, Wolf, and Swinney (1982) to be describable by such a one-dimensional map. In Figure (2.3.6) we indicate the return map constructed from the experimental data of Simoyi et al. (1980), also Figure (2.1.9) for the Lorenz attractor.

Simoyi et al. (1982) point out that there are 25 distinct chemicals in the Belousov-Zhabotinskii reaction, many more than can be reliably monitored. Therefore there is no practical way to construct the twenty-five dimensional phase space $\{X_j^{(m)}\}$, $m = 1, \cdots, 25$ from the experimental data. Instead they use the embedding theorems of Whitney (1936) and Takens (1981) to justify the monitoring of a single chemical species, in this case the concentration of the bromide ion, for use in constructing an m-dimensional phase portrait of the attractor $\{X(t), X(t-\tau), \cdots X[t-(m-1)\tau]\}$ for sufficiently large m and for almost any time delay τ. They find that for their experimental data m=3 is adequate and the resulting one-dimensional map [cf. Figure (2.3.6)] provided the first example of a physical system with many degrees of freedom that can be so modeled in detail.

Let us now recap the technique. We assume that the system of interest, a geophysical time series say, can be described by m variables, where m is large but *unknown*, so that at any instant of time there is a point $\mathbf{X}(t) = (X^{(1)}(t), X^{(2)}(t), \cdots, X^{(m)}(t))$ in an m-dimensional phase space that completely characterizes the system. This point moves around as the system evolves, in some cases approaching a fixed point or limit cycle asymptotically in time. In other cases the motion appears to be purely random and one must distinguish between a system confined to a chaotic attractor and one driven by noise. In experiments, one often only records the output of a single detector, which selects one of the m components of the system for monitoring. In general the experimentalist does not know the size of the phase space since the important dynamic variables are usually not known and therefore he/she must extract as much information as possible from the single time series available, $X^{(1)}(t)$ say. For sufficiently long delay times τ one uses the embedding theorem to construct the sequence of displaced time series $\{X^{(1)}(t), X^{(1)}(t+\tau), \cdots, X^{(1)}[t-(m-1)\tau]\}$. This set of variables has been shown to have the same amount of information as the m-dimensional phase point. Thus, as time goes to infinity, we can build from the experimental data a one-dimensional phase space $X^{(1)}(t)$, a two-dimensional phase space with axes $\{X^{(1)}(t), X^{(1)}(t-\tau)\}$, and so on. One then determines if the system dynamics are confined to a low-dimensional attractor.

3. Review of Some Geophysical Applications of the Reconstruction technique and other Nonlinear Concepts

In the previous Sections we have made every effort to develop some rather difficult mathematical concepts and techniques in a context that would make their importance self-evident in a geophysical setting. In the present section we review how a number of these ideas have been applied to geophysical problems and argue for their continued refinement and application. This list of examples is representative rather than exhaustive. In particular we focus on the attractor reconstruction technique because it provides a way to extract the greatest amount of modeling information from observational data. The attractor that is reconstructed from the data is shown to clearly distinguish between noise and chaos, and since the way to influence systems contaminated by noise are quite different from those manifesting fluctuations due to low order nonlinear interactions, being able to distinguish between the two is often crucial. When such an attractor can be reconstructed from a time series it explicitly gives the number of variables required to faithfully model the phenomenon of interest.

In this section, our discussion spans the realm of activity from that of climate to weather to fully developed wave fields on the ocean surface.

3.1 Weather and Climate Attractors

A dominant characteristic of meteorological data is its extreme variability. As discussed by Monin (1972), it is this broadband response that makes the predictability of weather patterns from deterministic primitive equations so uncertain. The fluctuations in atmospheric flow field that give rise to indeterminacy have been associated with small-scale turbulence. The scales of these fluctuations are unresolved in global circulation models even though their effects are manifest on these large scales. One technique for treating these fluctuations analytically is to replace the deterministic equations by stochastic equations [eg. Thompson, 1957; Landau and Lifshitz, 1959; Lorenz, 1969; Hasselman, 1976; Egger, 1982]. Such replacements have in the past been purely phenomenological, but more recent studies [West, 1982; Lindenberg and West, 1984] suggest how one may proceed more systematically from the deterministic to the stochastic representation. A third alternative has been to replace these complex field models with low-order dynamical models having chaotic solutions, such as first done by Lorenz (1963). It is this last approach that we adopt in this section.

We discussed the Lorenz model at some length in Section (2.1b) and showed that the basic structure of the observed flow depends on only a small number of degrees of freedom in phase space. The general hypothesis (hope) is that this may be true for observed flow fields. Nicolis and Nicolis (1984) were the first to apply the attractor reconstruction technique to a geophysical data set in hopes of finding a climatic attractor. They applied the technique to the isotope record of a deep sea core to estimate the number of variables governing the long-time climate evolution during the past million years. They used the method of Grassberger and Procaccia (1983) to measure the dimensionality of the data set, and thereby deduce the number of degrees of freedom necessary to control the underlying dynamics of the climate. They used 500 single variable values of the isotope record which were actually interpolated from 184 actual measurements. The value of the correlation dimension they obtained, $\nu = 3.1$, was criticized by Grassberger (1986) as resulting from the smoothing process implicit in extending the data set and not from the dynamics of the climate attractor. Subsequent analyses have not suffered from such criticism [Essex, Lookman and Nerenberg, 1987; Tsonis and Elsner, 1988; Fraedrich, 1986].

In Section (2.3a) we discussed the correlation dimension as a measure of the kind of attractor on which the dynamics for a given data set exists. Here we follow the more intuitive approach used by Fraedrich (1986) toward a general definition of dimension. A number of small boxes $N(L)$, each of side L, are used to fill a d-dimensional volume V:

$$\mathrm{V} = \sum_{N(L)} L^d = N(L) L^d \quad . \tag{3.1.1}$$

Thus, for a constant volume V, the number of boxes filling the volume increases inversely with L^{-d}. The dimension is obtained from (3.1.1) to be

$$d = -\frac{\ln N(L)}{\ln L} + \frac{\ln \mathrm{V}}{\ln L} \quad . \tag{3.1.2}$$

Taking the limit of decreasing box size leads to the more general definition of dimension

$$d = \lim_{L \to 0} \frac{\ln N(L)}{\ln (1/L)} \tag{3.1.3}$$

first developed by Hausdorff and more recently called the fractal dimension by Mandelbrot (1977). If the volume V denotes the attractor in phase space, then $N(L)$ is the number of boxes required to cover the attractor, and the attractor has a fractal dimension d.

The exponent d determines how fast $N(L)$ increases with decreasing L and may be determined by plotting $\ln N(L)$ versus $\ln(1/L)$. However, algorithms to count these boxes have been shown to be impractical in determining the dimension of chaotic attractors because of their slow convergence. This motivated Grassberger and Procaccia (1983) to develop another method which would estimate a lower bound on the fractal dimension, i.e., the correlation dimension in Section (2.3a). Recall that $\mathbf{X}(t_j)$ denotes the trajectory at time t_j in an m-dimensional phase space $\mathbf{X} = (X^{(1)}, X^{(2)}, \cdots, X^{(m)})$. The number $N(\,)$ of pairs of points whose separation distance is smaller than r, $r > |\mathbf{X}(t_j) - \mathbf{X}(t_k)|$, is formally determined by

$$N(r) = \sum_{j,k=1}^{N} \Theta[r - |\mathbf{X}(t_j) - \mathbf{X}(t_k)|] \tag{3.1.4}$$

and N is the total number of points. The cumulative distribution function $C(r)$ is normalized by the total of $N^2[\approx N(N-1)]$ pairs and describes how the number of pairs grows with increasing distance threshold r. For $N \to \infty$, the growth rate changing with the dimension d is determined by

$$C(r) = \lim_{N \to \infty} \frac{N(r)}{N^2} \sim r^d \quad . \tag{3.1.5}$$

For example, consider data points homogeneously distributed on a line, then the number of all points that are up to a distance r apart grow linearly with r, i.e., are proportional to r. For data homogeneously distributed over a plane (in a volume), the number of points grows quadratically (cubically) with r, i.e., are proportional to $r^2 (r^3)$. Thus, the dimension of the attractor in phase space can be obtained from

$$d = \frac{\ln C(r)}{\ln r} \tag{3.1.6}$$

where $C(r)$ is the frequency distribution of distance of the pairs of points situated on the time trajectory of the dynamical system in an m-dimensional phase space.

Because we do not know the dimension of the attractor in advance, one successively determines the correlation dimension d and correlation integral $C(r)$, for various values of the embedding dimension m, i.e., $d(m)$ and $C_m(r)$:

$$d(m) = \frac{\ln C_m(r)}{\ln r} \quad . \tag{3.1.7}$$

and $d(m) \rightarrow \nu$ as m increases. This corresponds to the m-dimensional phase space $\mathbf{X}(t) = \{X(t), X(t+\tau), \cdots, X(t-[m-1]\tau)\}$ where τ is the time lag [Ruelle, 1981]. In experimental data, noise always destroys part of the attractor. If the noise has a characteristic scale r_{noise}, then in an m-dimensional phase space the noisy trajectory is space filling on a length scale r smaller than r_{noise}:

$$C_m(r) \sim r^m \quad \text{for } r < r_{noise} \quad . \tag{3.1.8}$$

Whereas for length scales greater than that of the noise level:

$$C_m(r) \sim r^d \quad \text{for } r > r_{noise} \quad . \tag{3.1.9}$$

Thus, on a plot of $\ln C(r)$ versus $\ln r$, there should be a break in the curve denoting the change in slope between (3.1.8) and (3.1.9). The position of the break $r = r_{noise}$ supplies information on the noise level of the system.

(a) Surface Pressure and Relative Sunshine

To test the above ideas on real data sets Fraedrich (1986) selected daily values of surface pressure and relative sunshine duration as time series. In Figure (3.1.1) is depicted a three dimensional embedding of the single pressure time series $p(t)$ for three different time delay. Note how the trajectory changes from one tightly constrained to nearly a plane when $\tau = 3$ hours, to one that seems to fill the three dimensional volume for $\tau = 3$ days.

In Figure (3.1.2) the $\ln C_m(r)$ versus $\ln r$ is given for different embedding dimensions ($1 \leq m \leq 20$) for $\tau = 3$ days corresponding to the decorrelation time of the synoptic disturbances. The cumulative distribution of pressure distances grows with increasing threshold distance r. When r reaches its upper limit, the distribution function converges to unity. Distribution functions are shown for 15 year records and the related random series having the same mean, variance and number of data points. A random data set of finite length (number of observations), and produced by a random number generator, is not expected to follow the proportionality $d = m$, but merely the inequality $d \leq m$. In Figure (3.1.2) we see that the observational data and the random time series for the daily surface pressure appear quite similar. In Figure (3.1.3) Fraedrich shows the $d(m)$ versus m for a number of time lags and we see that there is some tendency for $d(m)$ to saturate at a value d_∞, but what that value is, is not clear from the figure. It is clear, however, that the dimension is below that of the random time series. Fraedrich points out that the data

in Figure (3.1.3) may not be sufficiently embedded because the time series include weather phenomena from winter and summer, the long-range process from season to season and the interannual variability.

Separating the records into winter seasons (commencing on November 1) and summer seasons (commencing on May 1), Fraedrich processes the data for 14 winters and 15 summers in Figures (3.1.3b) and (3.1.3c). In these figures the dimension values clearly saturate; $d_\infty \approx 3.2$ for the winter seasons and $d_\infty \approx 3.9$ for the summer seasons. Thus we conclude that although summers and winters separately have a weather attractor, that the combined data does not. Such a situation could arise if there are distinct flow regimes in phase space for each of the seasons rather than just one region for which the value of a parameter is changing between seasons.

Similar results were obtained by Fraedrich for the sunshine duration data, $d_\infty \approx 3.1$ for winter and $d_\infty \approx 4.3$ for summer, and the zonal wave amplitudes of the 500 *mb* geopotential waves along 50 ° N ($d_\infty \approx 3.0$ for winter and $d_\infty \approx 3.6$ for summer).

Essex, Lookman and Nerenberg (1987), as well as Fraedrich, also used these ideas from dynamical systems theory for the study of global climate. These authors used two variants of the embedding method on nine sets of 12,084 measurements yielding 108,756 values in all of daily local geopotential values at 500 *mb* taken at 12 *UT* extending over a span of 40 years. These data are very like one of the sets used by Fraedrich, however, the earlier study had less than 7.1×10^3 data points. The first method of Essex et al., treated the data from each location as independent measurements from a single site by concatenating the different time series from each site to create one large time series. The results of this method are shown in Figure (3.1.4) and summarized by the crosses in Figure (3.1.5). The straight line fits in Figure (3.1.4) of $\ln C_m(r)$ to $\ln r$ are fairly good over a reasonable range of r.

The second method used the data from each site as a separate coordinate of a point. The embedding was done by introducing the data from progressively more sites as additional coordinates. The results are indicated in Figure (3.1.5) as triangles. Figure (3.1.6) shows the value of $d(m)$ at each r for $m = 9$ using this method. In spite of the variation in the data points the plateau region is quite clear. In Figure (3.1.5) both methods are seen to yield a convergence to $d_\infty \approx 6$. This suggest that on the time scale of decades, climates might be represented as a system with as few as seven degrees of freedom. Thus

Essex et al., agree with the earlier conclusion of Nicolis and Nicolis that the atmosphere and oceans exhibit properties of a low dimensional attractor, although the two analysis involve data that differ by orders of magnitude.

This shortening of the time scales was brought to its logical conclusion by Tsonis and Elsner (1988) who used data on the order of hours, again orders of magnitude shorter time scales than those considered by Essex et al.. Nicolis and Nicolis using single-variable values of the oxygen isotope records of deep-sea cores spanning the past million years calculated a climatic attractors dimension of 3.1. Fraedrich and Essex et al., analysed weather data over time scales of 15 to 40 years and obtained a dimension of the weather attractor of between 6 and 7. Tsonis and Elsner using wind velocity measurements over time scales of minutes calculated a weather attractor of 7.3.

The time series consisting of 10 second averages of the vertical wind velocity recorded 10 m above the ground over an 11 hour period is shown in Figure 3.1.7a. The total number of data points is 3,960. The autocorrelation function and spectral density are also in Figure (3.1.7). From the autocorrelation function a conservative estimate of the time lag was made; 20 seconds. In Figure (3.1.8) the logarithm of the number of pairs versus $\ln r$ for $\tau = 10sec$ for embedding dimensions $m = 4, 6, 8, 10, 12$ are depicted. The scaling regions are indicated by the straight line segments indicated. These $d(m)$ are denoted by crosses in Figure (3.1.9) where as m increases we see that $d(m) \rightarrow d_{\infty} = 7.3$. Therefore, we can conclude that the system reresented by the vertical wind velocity series possesses an attractor. The non-integer dimension of the attractor suggests that it is chaotic, i.e., that the submanifold is a fractal set.

3.2 Fractal Dimension and the Ocean Surface

Recently the importance of nondifferentiable curves and surfaces have become apparent in different areas of the physical science. This growing awareness is due in no small part to the efforts of Mandelbrot (1977, 1982) in drawing attention to the fractal paradigm in modeling a wide variety of natural phenomena. We have pointed out that a fractal object is one that possesses no smallest scale. Of course in real systems there is always a largest and smallest scale, it is a question of the size of the interval overwhich no characteristic scale is apparent. For some applications a single decade of data is sufficient, for others one would want two or three decades of scale-free data before the process was pronounced a fractal. In a geophysical context Ausloos and Berman (1985)

have recently used a fractal function to model undersea topography and Stiassne (1988) used one to model the surface of the ocean. We review these two applications in this section.

The German mathematician Karl Weierstrass cast the argument for fractals into a particular mathematical form. His intent was to construct a series representation of a continuous, non-differentiable function. His function was a superposition of harmonic terms:

$$W(t) = \sum_{n=0}^{\infty} \frac{1}{a^n} \cos(b^n \omega_0 t) \tag{3.2.1}$$

a fundamental with frequency ω_0 and unit amplitude, a second periodic term of frequency $b\,\omega_0$ with amplitude $1/a$, a third periodic term of frequency $b^2\omega_0$ with amplitude $1/a^2$, and so on. The resulting function is an infinite series of periodic terms, each term of which has a frequency that is a factor b larger ($b>1$) than the preceding term and an amplitude that is a factor $1/a$ smaller ($a>1$).

Note that for this concept of a fractal function, or fractal set, there is no smallest or characteristic scale. For $b>1$ in the limit of n terms, $n\rightarrow\infty$, the frequency $b^n\omega_0\rightarrow\infty$, and there is no highest frequency contribution to the Weierstrass function. Of course, if one thinks in terms of periods rather than frequencies, then the shortest period contributing to the series is zero. Consider what is implied by this lack of a smallest scale in period, or equivalently by the lack of a largest scale in frequency. Imagine a continuous line on a two-dimensional Euclidean plane and suppose that the line has a fractal dimension greater than unity but less than two. How would such a curve appear? In this case we are superimposing smaller and smaller wiggles; the curve would be like the irregular line on a map representing a very rugged sea coast.

At first glance this curve would seem to be a ragged line with many abrupt changes in direction, as in Figure (3.2.1a). If we now magnify a small region of the line, as in Figure (3.2.1b), we see that the enlarged region appears qualitatively the same as the original curve. If we now magnify a small region of this new line, as in Figure (3.2.1c), we again obtain a curve that is qualitatively indistinguishable from the first two. The procedure can be repeated indefinitely [as long as $n\rightarrow\infty$ in (3.2.1)], and the behavior of the mathematical function is analogous to the discontinuous, inhomogeneous clumping of matter in space. The equivalence of the function from one scale to the next is called

self-similarity and the measure of the degree of self-similarity in the Weierstrass function (in terms of frequency and amplitude), is precisely the fractal, or Hausdorff-Bessiovich dimension: $d = \ln a / \ln b$.

Because of the infinite layers of detail, one cannot draw a tangent to a fractal curve, which means that the function, although continuous, is not differentiable. It also means that the more terms one allows to contribute to the function (the more accurately one maps the coastline), the longer the curve becomes, and there is no upper limit to its length.

Lévy introduced a generalization of the Weierstrass function which was later discussed by Mandelbrot (1977) and subsequently analysed in extensive detail by Berry and Lewis (1980). This function was called the Weierstrass-Mandelbrot function by the last authors, but here we refer to it as the extended Weierstrass function since there will be a number of such generalizations. Here again we have a superposition of sinusoidal terms with geometrically spaced frequencies and amplitudes that follow an inverse power law:

$$W(t) = \sum_{n=-\infty}^{\infty} b^{-n(2-D)} [\, 1 - e^{ib^n \omega_0 t}] e^{i\phi_n} \quad , \tag{3.2.2}$$

where the phase ϕ_n is arbitrary, $1 < D < 2$, and we have set $2 - D = \ln a / \ln b$. In the following discussion we scale time in such a way that $\omega_0 = 1$. For a complete discussion of the properties of (3.2.2) we refer the reader to Berry and Lewis (1980); here we merely record some of them that are important for our discussion.

The set of phases $\{\phi_n\}$ may be chosen either deterministically or randomly. If ϕ_n is a random variable uniformly distributed on the interval $(0, 2\pi)$, then each choice of $\{\phi_n\}$ constitutes a member of an ensemble for the stochastic function $W(t)$. If the phases are also independent and $b \to 1+$, then $W(t)$ is a Gaussian random function. The condition $1 < D < 2$ is required to ensure the convergence of the sum.

To generalize the extended Weierstrass function Ausloos and Berman preserved two properties: homogeneity and scaling (statistical properties). Consider the increments of W:

$$\begin{aligned} \Delta W(t, \tau) &= W(t + \tau) - W(t) \\ &= \sum_{n=-\infty}^{\infty} b^{-n(2-D)} [\, e^{ib^n t} - e^{ib^n (t+\tau)}] e^{i\phi_n} \quad , \end{aligned} \tag{3.2.3}$$

and assume that the ϕ_n are independent, random variables uniformly distributed on the

interval $(0, 2\pi)$. The mean square increment is then

$$V(\tau) \equiv <|\Delta W(t,\tau)|^2>$$

$$= \sum_{n=-\infty}^{\infty} b^{-n(4-2D)} 2[1-\cos(b^n\tau)] \qquad (3.2.4)$$

where the brackets denote an average over an ensemble of realizations of the ϕ_n-fluctuations. The right hand side of (3.2.4) is independent of t, i.e., it depends only on the time difference τ, so that $W(t)$ is homogeneous (also called stationary when t refers to the time).

Equation (3.2.4) also leads to the scaling property of the extended Weierstrass function:

$$V(b\tau) = b^{2(2-D)} V(\tau) \quad . \qquad (3.2.5)$$

If the sum giving the extended Weierstrass function (3.2.2) covered the interval from $n = 0$ to $n = \infty$, then the scaling property expressed in (3.2.5) would hold only approximately. A two-variable scalar extended Weierstrass function $W(\mathbf{r})$ is proposed by Ausloos and Berman to be one such that

$$V(\rho) = <|\Delta W(\mathbf{r},\rho)|^2> \qquad (3.2.6)$$

so that for all $\mathbf{r}$

$$V(b\rho) = b^{2(3-D)} V(\rho) \qquad (3.2.7)$$

where in this case $2 < D < 3$.

After discussing some candidate functions that for one physical reason or another were considered unsatisfactory, Ausloos and Berman decided on one that is a random superposition of weighted "ridge-like" surfaces:

$$W(\mathbf{r}) = \left[\frac{\ln b}{M}\right]^{1/2} \sum_{m=1}^{M} A_m \sum_{n=-\infty}^{\infty} (k_0 b^n)^{D-3} [1 - e^{ib^n k_0 r\cos(\theta-\alpha_m)}] e^{i\phi_{mn}} \quad . \qquad (3.2.8)$$

Here k_0 is a wave number that can be used to scale horizontal variations; the normalization factor is chosen to make the series converge as $b \to 1+$ and $M \to \infty$; the angle α_m gives the orientation of the corrugation of the surface having an amplitude A_m; and the phases ϕ_{mn} are again defined as random variables. It is a simple matter to verify that (3.2.8) has the scaling property of (3.2.7) and that $V(\rho)$ is homogeneous.

Ausloos and Berman present a number of computer plots of the surfaces generated by the extended Weierstrass function (3.2.8). Their interest was in measuring the effect of the small length scales on long-range acoustic propagation in the ocean. Here we are more interested in the possible use of this function to model the ocean surface. Therefore let us examine some of their computer plots interpreted as snap-shots of the sea surface.

In Figure (3.2.2) we see a figure that could be interpreted as a one-dimensional sea surface consisting of long ridges of random height and wavelength. This is not unlike the surface profiles shown on pages 330 and 331 of Neumann and Pierson (1966). In Figure (3.2.3) two of these surfaces at right angles are superposed to give rise to a two-dimensional random surface which resembles that of a high sea. To the unaided eye the most convincing example of a sea surface is given in Figure (3.2.4). Here we seem to see the ever present small scale structure riding on top of a large scale wave.

A different extended Weierstrass function, but one that has both properties of (3.2.1) and its extension to two spatial dimensions (3.2.2) is considered by Falconer (1985) to be

$$W(\mathbf{r}) = \left[\frac{\ln b}{M}\right]^{1/2} \sum_{m=1}^{M} A_m \sum_{n=0}^{\infty} b^{-n(3-D)} \cos\left[k_0 b^n (x\cos\theta_m + y\sin\theta_m) + \Phi_{mn}\right] \quad . \quad (3.2.9)$$

If we interpret the phase as the time-dependent quantity

$$\Phi_{mn} = \phi_{mn} - \omega_n t \quad (3.2.10)$$

where ω_n is the frequency of a deep water gravity wave having wavenumber $k_n = k_0 b^n$,

$$\omega_n = \sqrt{g k_n} = \sqrt{g k_0} b^{n/2} \quad (3.2.11)$$

and g is the acceleration of gravity. Thus we have

$$W(\mathbf{r}) = \left[\frac{\ln b}{M}\right]^{1/2} \sum_{m=1}^{M} A_m \sum_{n=0}^{\infty} b^{-n(3-D)} \cos\left[k_0 b^n (x\cos\phi_m + y\sin\theta_m)\right.$$

$$\left. + \phi_{mn} - \omega_0 b^{n/2} t\right] \quad , \quad (3.2.12)$$

in which a superposition of propagating waves has been made to form $W(\mathbf{r})$. Following Stiassnie, the amplitudes A_m can be chosen in such a way that the mean square value of $W(\mathbf{r})$ is the same as that of the sea surface. To do this we recall that the surface wave spectrum is given by

$$\Psi(\mathbf{k}) = \left[\frac{B u_*}{g^{1/2}}\right] G(\theta)/k^{\beta} \quad (3.2.13)$$

where the function $G(\theta)$ accounts for the directionality of the waves, u_* is the wind function velocity and $B \approx 0.012$. Noting that we have selected a geometric series in wavenumber we replace the differential $kdkd\theta$, by the discrete versions $\theta_m = m\Delta\theta$ and $dk_n = k_n \ln b$ so that

$$\Psi(\mathbf{k})kdkd\theta \rightarrow \frac{2\pi}{M} k_n dk_n A_m^2 = \frac{2\pi B u_*}{M g^{1/2}} \ln b G(\theta_m) k_0^{2-\beta} b^{n(2-\beta)} \quad . \qquad (3.2.14)$$

Using (3.2.14) to replace A_m in (3.2.12) therefore yields

$$W(\mathbf{r}) = \left[\frac{2\pi}{M} \frac{B u_* \ln b}{g^{1/2} k_0^{2(3-D)}} \right]^{1/2} \sum_{m=1}^{M} [G(\theta_m)]^{1/2} \sum_{n=0}^{\infty} b^{-n(3-D)}$$

$$\cos [k_0 b^n (x \cos\theta_m + y \sin\theta_m) + \phi_{mn} - \omega_0 b^{n/2} t] \qquad (3.2.15)$$

if the exponents of k_0 are equal, i.e.,

$$D = 4 - \beta/2 \qquad (3.2.16)$$

Thus the surface represented by (3.2.15) has a fractal dimension D dependent on the index of the observed surface wave spectrum. If we take $\beta = 7/2$ as suggested by Kitaigorodskii (1983) then the fractal dimension of the sea surface is $D = 2.25$.

As Stiassne points out, surface tension introduces a cut-off at say $k = k_s$ so that the actual sea surface is only approximately fractal. It has a fractal-like structure, over length scales from $2\pi/k_s$ to $2\pi/k_0$, which corresponds to approximately 0.1 m to 100 m in the open ocean.

4. Water Wave Attractor

We now turn to the question of whether these dynamic techniques are useful in interpreting data sets from either the open ocean or from wave tanks. Traditionally we think of surface wave interaction phenomena as consisting of both broad band and narrow band processes. The mode/mode energy transfer resulting from the nonlinear hydrodynamic interactions is broad band, as is the general wave train instability. On the other hand, the Benjamin Feir instability mechanism and recurrence, as well as surface envelope solitons are narrow band phenomena. These processess have been understood on the basis of the weak interaction theory of interacting nonlinear gravity waves [see eg. West (1981)].

Many of these weak interaction effects are discussed by West (1981) and as summarized by Phillips (1979) these phenomena share the following characteristics:

(1) The weak interaction phenomena may be manifest *only by the longer (dominant) waves in the wave field*; the behavior of short waves (wavelengths less than the dominant one) is determined by strong interactions with long waves rather than by weak interaction processes. This is due in part to the fact that only the dominant waves maintain their integrity sufficiently long for the mechanism to work.

(2) They are evolutionary phenomena with *a common time scale of order* ε^{-2} *times the wave period*, where ε is the slope of the dominant wave. Under most oceanic conditions, this time scale is of order 100 wave periods (minimally) of the dominant wave. Equivalently, the distance that waves travel before these effects become significant is of order ε^{-2} times the dominant wavelength. The shorter waves disappear and are refreshed by the wind on a much shorter space-time scale. These interactions lead to Gaussian statistics of the surface wave field [Benny and Newell (1967), Hasselmann (1968)].

(3) The state of a wave field at a given point is, in part, the result of these processes acting over the preceding time, but the modification they can produce in the wave field in a limited distance or time (a few wavelengths or periods) is small, of order ε^{-2}, characteristically one percent or less. Consequently, they are intrinsically unable account for any observed local response in the wave field to a local disturbance such as the modulation of a short wave near the peak of a long wave in a wind generated field.

The strong interactions are those which occur on a time scale of the same order as the wave period of interest. They include the instability leading to wave breaking, wave breaking itself, wave-current interactions, the distortion of a short wave energy packet by a long wave, the process of parasitic capillary formation and micro-scale breaking induced by surface wind drift. These phenomena provide the possibility of a rapid response to oceanic perturbations and are much less studied than the above weak interactions. Again summarizing the discussion of Phillips (1979) and West (1981):

(1) The surface wave train modulation produced by internal waves or other currents is a strong interaction effect in that it can be produced by a single internal wave pulse (though it is frequently described as a "resonance," a weak interaction phenomena).

(2) A wave train or packet of short waves, interacting with a longer wave, varies in amplitude and scale with respect to its position on the long wave. The modulation pattern of the packet has a spectral signature that is distributed over a range of frequencies proportional to the *long* wave speed and is approximately proportional to the long wave slope. As the long wave slope increases, the spectral signature is dominated more and more by the properties of the short waves *near the long wave crest*, and less by those at other points of the long wave cycle. This implies that the surface fluctuations cannot be homogeneous in space.

(3) Micro-scale surface properties such as the formation of parasitic capillary waves and microscale breaking, i.e., the formation of sheets of bubbles, have densities (number of occurrences per unit area) that, in an active wind-generated sea, respond rapidly to energy exchanges with short gravity waves and more sensitively than changes in the short wave amplitudes themselves. In this way, they can serve as indicators to perturbations on the scale of internal waves and other internal flow-fields. This appears as large scale and long time correlations in the surface statistics.

Here we wish to determine if the surface wave field can be described by a low-dimensional attractor, which in the present context would be viewed as a strong interaction. To do this we need to analyze a "time" series characteristic of the sea surface. For this we use a numerically generated surface wave field using the new numerical method for surface hydrodynamics developed by West, Brueckner, Janda, Milder and Milton (1987).

4.1 Numerically Generated Data

We use the computer code of West et al., (1987) to numerically generate a one-dimensional surface displacement $\zeta(x,t)$. For this purpose we use 512 wavenumber modes in units such that $k_0 = 2\pi/L = 1$ and the acceleration of gravity is unity:

$$\zeta(x,t) = -Im\left[\sum_{n=1}^{512} a_n(t)e^{i(nx-\sqrt{n}t)}\right] \quad . \tag{4.1.1}$$

The initial mode amplitudes $\{a_n(0)\}$ are selected so as to have a Phillips spectrum k^{-3} and independent random phases uniformly distributed on the interval $(0,2\pi)$. The equations of motion given in West et al. are then integrated forward in time to their values $\{a_n(t)\}$ on a Cray computer. The surface displacement is then used in two ways. First, at a fixed time t, the frozen surface on the spatial interval $(0,2\pi)$ is segmented into M points which constitute the "time" series. Secondly, at a fixed spatial point, x, the variation in the surface elevation in time is treated as the time series. The latter use of the data is what one would record with a wave staff located at x measuring the passage of a wave field.

We compare the above data with a completely random data set generated by the function

$$R(t) = \sum_{n=1}^{N} \cos(\sqrt{n}t + \phi_n) \tag{4.1.2}$$

where ϕ_n is a random variable uniform on the interval $(0,2\pi)$ and N is the number of modes in the sum. The variable $R(t)$ becomes a zero-centered Gaussian random variable for large N which we also segment into M points for our random time series.

The "experimental" data in method 1 are given by the set $\{\zeta_j \equiv \zeta(x_j,t)\}$ where we divide the continuous spatial curve into 1024 equally spaced points. We use these data to construct the set of variables $\{\zeta_j, \zeta_{j-\tau}, \cdots, \zeta_{j-(m-1)\tau}\}$ in an m-dimensional embedding space and apply the Grassberger-Procaccia correlation algorithm to determine the dimensionality of the data. In Figure (4.1.1) we depict $\ln C_m(r)$ versus $\ln r$ for a number of embedding dimensions. In Figure (4.1.2) we show the correlation dimension for the data set using two lag times τ as a function of embedding dimension. The random data, partitioned in the same way, yields the result $d(m) = m$ as expected. The surface data, however, clearly show a tendency to saturate for both $\tau = 8$ and $\tau = 15$. This implies that

although the surface was generated using 512 degrees of freedom (in the spectral sense) as few as five or six degrees of freedom may be adequate to describe its spatial behavior. Note that in method 1 our data describe points in space, not points in time. Therefore the interpretation of these results is not as straightforward as the earlier applications.

We note the kink in the $\ln C_m(r)$ versus $\ln r$ curve in Figure (4.1.1) for large m. At first it was not clear how one might interpret this result, but analyses due to Theiler in his Ph.D. thesis (1987) suggests that the kink may be due to correlation in the data set. In his analysis, Theiler considers a stochastic data set that is Gaussian with a prescribed correlation time α. The correlation time is observed to produce a kink [cf. Figure 4.1.3] just of the form seen in Figure (4.1.1) and to result in the correlational dimension not increasing linearly with the embedding dimension. This observation suggests that the longest wavelength waves on the sea surface modulate the short wavelength waves, and this modulation is picked up as a correlation of the small scale structure at the higher embedding dimensions. Theiler developed a technique to suppress this correlation which we propose to test in the present context. The method involved deleting the $n-$ nearest neighbors in the calculation of the correlation function, but we will not pursue that technique further here.

We now turn to the second method of collecting data in which we record the height of the sea surface as a function of time at a fixed spatial location. We segment the spatial interval $(0, 2\pi)$ into 16 equi-distant points. At each point we record the surface elevation for an interval of time four units long. This corresponds to two periods of the longest wave present on the sea surface. Each of the 16 time series is discretized into 1024 points, yielding a total of 16,384 data points if we were to concatenate all the data as done, for example, by Essex et al., (1987) in their global climate study.

We concatenate the data from eight adjacent locations to define a single time series consisting of 8,192 data points. In method 1 we picked the value of τ by inspection. In the present method we were guided in our choice by calculating the time at which the auto correlation function first goes through zero. The preferred technique would have been to calculate the first minimum in the mutual information, but calculating the autocorrelation function was faster. The τ value determined by the autocorrelation function is 50, so we selected a value substantially above that, i.e., $\tau = 80$. In Figure (4.1.4) we see that there are two distinct scaling regimes for the data above $m = 8$. The largest regime

has $\nu \approx 2$ and is fairly independent of the embedding dimension. The second regime is plotted in Figure (4.1.5) as a function of embedding dimension and is seen to saturate around $\nu = d_{\infty} \approx 6$.

5. Conclusions and Speculations

The physicist-mathematician Mars Kac was fond of pointing out the difference between a demonstration and a proof. He maintained that a demonstration would convince a reasonable man of the truth of a mathematical statement, whereas it required a proof to convince a mathematician. Herein we have *demonstrated* the utility of certain generic concepts from nonlinear dynamical systems theory in geophysics and physical oceanography. We have reviewed how the phase space reconstruction technique can be used to determine the minimum number of variables necessary to describe certain geophysical phenomena. Since we are accustomed to describing geophysical flows by fields which are spatially continuous and therefore have an infinite number of degrees of freedom, this notion of representing such flows by low-dimensional attractors is admittedly a surprising one, but not so surprising as being able to determine the dimensions of the attractor, and thereby the number of variables needed to describe the system directly from a single time series of sufficient length.

Let us recap the attractor (phase space) reconstruction technique. We assume the system of interest; the isotope concentration from a deep ocean core, the duration of sunshine as a function of time at a measuring station, the speed of the wind at a given location and the height of the sea surface measured by a wave staff, can each be described by m-variables, where m is large but unknown. At any instant of time there is a pont $\mathbf{X}(t) = \{X^{(1)}(t), X^{(2)}(t), \ldots, X^{(m)}(t)\}$ in an m-dimensional phase space that completely characterizes the system. The point moves around as the system evolves. In the geophysical cases discussed herein the motion had previously appeared to be purely random so that one must distinguish between a system confined to a chaotic attractor from one driven by noise. For many reasons geophysical observations are often restricted to the output of a single detector which selects one of the m components of the system for monitoring. In general the scientist does not know the dimension of the phase space since the important dynamic variables are usually unknown and therefore as much information as possible must be extracted from the single time series, $X^{(1)}(t)$ say. For sufficiently long delay times τ one use the embedding theorem to construct the sequence of displaced time series $\{X^{(1)}(t), X^{(1)}(t-\tau), \ldots, X^{(1)}[t-(m-1)\tau]\}$. In this m-dimensional phase space one then determines if the system dynamics is confined to a low-dimensional attractor.

This procedure was followed in the examples listed in Section 3 and the Grassberger-Proccacia method of determining the correlation dimension was used to determine if chaotic attractors exist in geophysical data sets. Nicolis and Nicolis (1984) were the first to find a climate attractor albeit with an insufficient data base they found $\nu \cong 3.1$. Essex et al. (1987) and independently Fraedrich (1986) found climate attractors but with a dimension more than twice that found by Nicolis and Nicolis. Using daily values of surface pressure and sunshine duration Fraedrich found separate weather attractors for summer and winter with dimensions in the intervals $3.2 \leq \nu \leq 4.3$. Essex et al. used the local geopotential value to find a weather attractor with $\nu \approx 6$. Tsonis and Elsner used vertical wind velocity measurements to calculate a weather attractor with $\nu \approx 7.3$. The time series used to determine these various attractors spanned millions of years for the single values of the oxygen isotope records of deep-sea cores down to wind velocity measurements over time scales of a few hours.

Our own calculation of water wave attractors in Section 4 suggests that the one-dimensional sea surface may be describable by as few as two degrees of freedom in one domain and as many as six in another. The first domain is not unlike the result obtained using the generalized Weierstrass function to model the sea surface. The possible relation between these two approaches has not as yet been explored in the present geophysical context. It is of interest, however, to consider how these techniques may be used for the remote sensing of the sea surface.

The fundamental problem of remotely sensing patterns on the sea surface is the detection of a signal in a large dynamic range background. This can be seen from even a superficial examination of the variety of physical processes underlying the signal processing problems of interest. Consider the surface of the ocean; the nonlinear, wind-generated, surface disturbances constitute the noisy background, [see e.g. West, 1981] and the modulation of them by surface current disturbances constitute the signal. Probing the ocean's surface via radar relies on an understanding of the ocean surface modulation mechanism since the scattering is from very short Bragg waves (wavelengths of a few centimeters) and the currents of interest have scales of tens of hundreds of meters. Going now into the ocean interior, the acoustic signal generated by rainfall or the breaking of surface is also of interest. In the far field region the pressure and/or velocities generated by these sources have been contaminated by the dynamics of the intervening medium, e.g., by internal waves, patches of turbulence and acoustic noise from the sea

surface. These undersea phenomena also influence surface currents and act to degrade the signal. The motion of conducting sea water also perturbs the earth's magnetic field, e.g. internal waves give rise to a clear magnetic field signature.

The remote detection and identification of undersea phenomena is therefore a problem of indirect measurement in that one must be able to correctly interpret the disturbances of the ambient surface waves using radar (or light) backscattered from the sea surface and the perturbation in the earth's magnetic field produced by the currents' passage.

Techniques for processing the perturbed radiation whether electromagnetic, acoustic or thermal run the gamut from the application of statistical pattern recognition methods, to procedures for coherent data acquisition, to artificial neural systems. These and other techniques have their proponents, but they by-and-large miss an essential feature of the geophysical problem; the sea surface and interior are described by nonlinear dynamic (hydrodynamics) processes, [Phillips, 1977].

Historically the aperiodic component of experimental time series, such as the back scattered radiation, has been interpreted as random noise. Thus the processing procedures have relied on techniques that separate the 'signal' from the 'noise' in a linear additive way. This view is consistent with, and is probably a consequence of, the traditional interpretation of stochastic processes in the physical sciences. It results from a dynamic system being coupled to a complicated environment, i.e., the environment induces a random component into the system dynamics. A Fourier decomposition of such a time series, one consisting of a deterministic signal linearly superimposed on a noise, would yield a spectrum consisting of sharp spectral peaks at the natural frequencies of the signal and a broad band background depicting the power of the noise. This interpretation has become so ingrained that its inverse is often applied, that is to say that a spectrum such as shown in Figure 2.3.3, consisting of a broad band spectral level on which a number of peaks are superimposed, often suggests the linear additive model of signal and noise. That interpretation cannot in fact be applied to the spectrum in Figure 2.3.3 because the underlying time series was generated by a nonlinear equation of motion having a *chaotic* solution. The traditional techniques that were based on the classical signal/ noise paradigm must be modified to process data generated by processes in which the signal and noise cannot be so separated.

Herein we have shown that low-dimensional deterministic dynamical systems can generate time series that appear to have many of the characteristics of random noise. We can, however, distinguish between a chaotic and a completely random time series by

means of the attractor reconstruction technique. The time series data used in the reconstruction of attractors can be the vertical displacement of the sea surface, a component of the horizontal fluid velocity at a fixed point on the sea surface or in its interior, measurements at multiple points, and so on. These data may then be used to reconstruct the dynamic attractors determining the local behavior of the sea. The underlying assumption is that the nonlinear hydrodynamic interactions are sufficiently strong that a single variable is influenced by each of the other variables to such a degree that the time lagged variables contain the same information as the original set of variables characterizing the hydrodynamics. It is worth mentioning that the more variables that are measured, velocities at multiple space points, or the vertical velocity of the surface as well as its displacement, all give additional confidence in the attractor reconstructed from the time series.

Of course, the existence of such attractors, are of interest to physical oceanographers, but what is perhaps of more interest is how the ambient attractor could be modified by the disturbances generated by a surface current. Said differently, what we want to accomplish is to use the time series $X(t)$ to *predict* the future evolution of the wave field beyond the available data and to examine how various currents disrupt this evolution. Barnsley (1986) has been able to use chaos to predict chaos. He developed an algorithm[†] to replicate a chaotic curve generated by a laboratory experiment at a finite number of points. The resulting numerically generated curve "fits" the experimental curve surprisingly well both inside and *outside* the fitted interval.

Previous processing techniques assume the wave/wave and other hydrodynamic interactions to be weak and predict a weak modulation of the surface wave spectrum in the Bragg wave region. Such analyses have been based on perturbation theory, keeping only the lowest order interactions between the surface waves and surface currents. The signal is then given by the modulation in the clutter cross section of the sea surface and is directly proportional to the surface current [Thompson and West, 1975]. Improvements on this approach involve integrating along the direction of the current to provide a coherent gain in the signal; using multiple frequency radars to sample the modulation in different spectral domains as well as others. We do not have room here to critique the relative merits of each of these techniques. We can point out, however, that none of

[†] He regards the experimentally generated curve as the chaotic attractor of some descriptive map. Then he constructs this dissipative map by forming the union of a sequence of dissipative maps randomly selected from a predetermined, finite set.

them take the basic nonlinear hydrodynamic aspects of the sea surface and interior into account in their processing. The attractor reconstruction approach is the only one that intrinsically depends on the nonlinear nature of the time series for its implementation.

In the same way the contamination of the acoustic signal by undersea phenomena is treated perturbatively, relying on the classic signal/noise paradigm to describe the influence of internal waves and/or turbulence on the propagating pressure field. Again there are established techniques similar to those described above intended to enhance the signal-to-noise ratio that do not capitalize on the intrinsic nonlinearity of the dynamics of the intervening medium and its interaction with the acoustic wave. It is not yet clear how these traditional techniques apply when the dynamics are chaotic. We note that there already exists a simple model of internal waves based on the strange attractor concept [Abarbanel, 1983].

The relation between the hydrodynamic patterns observed in nature and the nonlinear dynamics of fluid particles has, over the past decade, become increasingly well understood. Although fluid mixing remains a mystery, some of the concepts underlying the formation of coherent structures and their eventual breakup due to chaos are becoming clearer [Wiggins, 1988; Ottino, Lsong, Rising and Swanson, 1988].

Acknowledgement

The author would like to thank the Office of Naval Research (Contract N00014-88-C-0547) for the support of this work, and K. Brueckner and R. Janda for the numerical calculations.

References

H.D.I. Abarbanel, J. Fluid Mech. **135**, 407 (1983).

M. Ausloos, and D.H. Berman, "A multivariate Weierstrass-Mandelbrot function," Proc. Roy. Soc. Lond. **400A**, 331-350 (1985)

M. F. Barnsley in *Chaotic Dynamics and Fractals*, ed. M. F. Barnsley and S. G. Demko, Academic Press, New York (1986),

G. Benettin, L. Golgani and J. M. Strelcyn, "Kolmogorov entropy and numerical experiments," Phys. Rev. **14A**, 2338 (1976).

P. J. Benney, "Nonlinear gravity wave interactions," J. Fluid Mech., **14**, 577-589, (1962).

P. J. Benney and A. C. Newell, J. Math. and Phys. **46**, 363 (1967).

M. V. Berry and Z. V. Lewis, Proc. Roy. Soc. Lond. **370A**, 459 (1980).

L.J. Broer, "On the Hamiltonian theory of surface waves," Appl. Sci. Res., **30**, 430-466, (1974).

P.J. Bryant, "Oblique wave groups in deep water," J. Fluid Mech., **146**, 1-20, (1984).

B. Chirkov, "A universal instability of many-dimensional oscillator systems," Phys. Rep., **52**, 263-379, (1979).

P. Collet and J. P. Eckmann, *Iterated Maps on the Interval as Dynamical Systems*, Birkhäuser, Bassel (1980).

M. Conrad, "What is the use of chaos?" in *Chaos*, (Ed.) A.V. Holden, Manchester University Press, Manchester UK (1986).

J. P. Crutchfield, D. Donnelly, D. Farmer, G. Jones, N. Packard and R. Shaw, Phys. Lett. **76**, 1 (1980).

J. P. Crutchfield, J. D. Farmer, N. H. Packard and R. S. Shaw, "Chaos," Scientific American, 46-57 (1987).

J. H. Curry, "On the Henòn transformation," Commun. Math. Phys. **68**, 129 (1979).

J. P. Eckmann and D. Ruelle, "Ergodic theory of chaos and strange attractors," Rev. Mod. Phys. **57**, 617-656 (1985).

J. P. Eckmann, "Roads to turbulence in dissipative dynamic systems," Rev. Mod. Phys. **53**, 643 (1981).

J. Egger, "Stochastically driven large-scale circulations with multiple equilibria," J. Atmos. Sci. **38**, 2606-2618 (1982).

C. Essex, T. Lookman and M.A.H. Nerenberg, "The climate attractor over short time scales," Nature **326**, 64-66 (1987).

D. Farmer, J. Crutchfield, H. Froehling, N. Packard and R. Shaw, "Power spectra and mixing properties of strange attractors," Ann. N. Y. Acad. Sci. **357**, 453-472 (1980).

M. J. Feigenbaum, J. Stat. Phys. **19**, 25 (1978); J. Stat. Phys. **21**, 669 (1979).

S. D. Feit, "Characteristic exponents and strange attractors," Commun. Math. Phys. **61**, 249 (1978).

K. Fraedrich, "Estimating the dimension of weather and climate attractors," J. Atmos. Sci. **43**, 419-432 (1986).

P. Grassberger, Nature **323**, 609-612 (1986).

P. Grassberger and I. Procaccia, "Measuring the strangeness of strange attractors," Physica **9D**, 189-208 (1983a).

P. Grassberger and I. Procaccia, "Characterization of strange attractors" Phys. Rev. Lett. **50**, 346 (1983b).

P. Grassberger and I. Procaccia, Phys. Rev.**28A**, 2591 (1983c).

K. Hasselmann, "On the nonlinear energy transfer in a gravity-wave spectrum, I, General theory," J. Fluid Mech., **12**, 481-500, (1962), "II, Conservation theorems, wave-particle correspondence, irreversibility," **15**, 237-281, (1963a), "III, Evaluation of the energy flux and swell-sea interaction for a Neumann spectrum," **15**, 385, (1963b).

K. Hasselmann, "Weak-interaction theory of ocean waves," in *Basic Development in Fluid Mechanics, Vol. 2*, edited by M. Hoyt, pp. 117-182, Academic, Orlando, Fla., (1968).

K. Hasselmann, "Stochastic climate models: part I. theory," Tellus **28**, 473-484 (1976).

M. Henon, "A two-dimensional mapping with a strange attractor," Comm. Math. Phys. **50**, 69 (1976).

G. Holloway and B. J. West, eds. "Predictability of Fluid Motions," Am. Inst. Phy. Conf. Proceed., vol. **106, 45-53 (1983).**

J. Kemeny and J. L. Snell, *Mathematical Models in the Social Sciences*, MIT Press, Cambridge, Mass. (1972).

S. A. Kitaigorodskii, "On the theory of the equilibrium range in the spectrum of wind-generated gravity waves," J. Phys. Ocean. **13**, 816-827 (1983).

S. H. Koslow, A. J. Mandell and M. F. Shlesinger, (Eds.) *Perspectives in Biological Dynamics and Theoretical Medicine*, Ann. N. Y. Acad. Sci. **504** (1987).

L. D. Landau and E. M. Lifshitz, "Fluid Mechanics," Pergamon, New York (1959).

O. E. Lanford, in *Statistical Mechanics and Dynamical Systems*, Math. Dept. Duke Univ., Durham, N. C., Chap. 4 (1976).

T. Y. Li and J. A. Yorke, Am. Math. Mon. **82**, 985 (1975).

K. Lindenberg and B. J. West, "Fluctuations and dissipation in a barotropic flow field," J. Atmos. Sci. **41**, 3021 (1984).

W. P. London and J. A. Yorke, Am. J. Epidem **98**, 453 (1973).

E. N. Lorenz, J. Atmos. Sci. **20**, 130 (1963).

E. N. Lorenz, "The predictability of a flow which possesses any scales of motion," Tellus **21**, 289-307 (1969).

B. B. Mandelbrot, *Fractals, Form and Chance*, W. H. Freeman (1977).

B. B. Mandelbrot, *The Fractal Geometry of Nature*, W. H. Freeman (1982).

R. T. Malthus, *Population: The First Essay* (1798), Univ. Mich. Press, Ann Arbor (1959).

R. M. May, "Simple mathematical models with very complicated dynamics," Nature **261**, 459-467 (1976).

J.W. Miles, "On Hamilton's principle for surface waves, J. Fluid Mech., **83**, 153-164, (1977).

A. S. Monin, *Weather Forecasting as a Problem in Physics*, MIT Press (1972).

E. W. Montroll and B. J. West, "On an enriched collection of stochastic processes," in *Fluctuation Phenomena*, 2nd ed, E. W. Montroll and J. L. Lebowitz, North-Holland Personal Library, Amsterdam (1987).

E. W. Montroll and M. F. Shlesinger, "On $1/f$ noise and distributions with long tails," PNAS **79**, 3380-3383 (1982).

J. Moser, *Stable and Random Motions in Dynamical Systems*, Princeton University Press, Princeton, N.J., (1973).

G. Neumann and W. J. Pierson, Jr., *Principles of Physical Oceanography*, Prentice-Hall, New Jersey (1966).

C. Nicolis and G. Nicolis, Nature **311**, 529-533 (1984).

C. Nicolis and G. Nicolis, Proc. Natl. Acad. Sci. USA **83**, 536 (1986).

J. S. Nicolis and I. Tsuda, "Chaotic dynamics of information processing: The magic number seven plus minus two revisited," Bull. Math. Biol. **47**, 343-365 (1985).

J. S. Nicolis, "Chaotic dynamics applied to information processing," Rep. Prog. Phys. **49**, 1109-1196 (1986).

L. F. Olsen and H. Degn, "Chaos in biological systems," Q. Rev. Biophys. **18**, 165-225 (1985).

J. M. Ottino, C. W. Leong, H. Rising and P. D. Swanson, "Morphological structures produced by mixing in chaotic flows," Nature **333**, 419-425 (1988)

V. I. Oseledec, "A multiplicative ergodic theorem, Lyapunov characteristic numbers for dynamical systems," Trudy Mosk. Mat. Obsc. **19**, 179 [Moscow Math. Soc. **19**, 197 (1968)].

E. Ott, "Strange Attractors and chaotic motions of dynamical systems," Rev. Mod. Phys. **57**, 655-671 (1985).

N. H. Packard, J. P. Crutchfield, J. D. Farmer and R. S. Shaw, Phys. Rev. Lett. **45**, 712-716 (1980).

P. J. E. Peebles, *The Large-scale Structure of the Universe*, Princeton Univ. Press (1980).

D.H. Peregrine, "Water waves, nonlinear Schrödinger equations and their solutions," J. Aust. Math Soc., **B24**, 16-43, (1983).

O.M. Phillips, "On the dynamics of unsteady gravity of finite amplitude," J. Fluid Mech., **9**, 193-217, (1960).

O.M. Phillips, *The Dynamics of the Upper Ocean* Cambridge University Press, New York, (1966).

O. M. Phillips, unpublished report (1979).

O. E. Rössler, Ann. N.Y. Acad. Sci **316**, 376-392 (1979).

O. E. Rössler, Phys. Lett. **57A**, 397 (1976).

O. Rössler, "Continuous chaos-four prototype equations," in *Bifurcation Theory and Applications to Scientific Disciplines*, Ann. N.Y. Acad. Sci. **316**, 376-392 (1978).

J. C. Roux, R. M. Simoyi and H. L. Swinney, Physica **D8**, 257 (1983).

L. A. Segal, *Modeling Dynamic Phenomena in Molecular and Cellular Biology*, Cambridge Univ. Press, London (1984).

R. Shaw, "Strange attractors, chaotic behavior, and information flow," Z. Naturforsch **36A**, 80-112 (1981).

R. Shaw, *The Dripping Faucet as a Model Chaotic System*, Ariel Press, Santa Cruz, CA (1984).

R. H. Simoyi, A. Wolf and H. L. Swinney, "One-dimensional dynamics in a multicomponent chemical reaction," Phys. Rev. Lett. **49**, 245-248 (1982).

J. M. Smith and R. J. Cohen, Proc. Natl. Acad. Sci. **81**, 233 (1984).

M. Stiassnie, "The fractal dimension of the ocean surface," preprint (1986).

F. Takens, in *Lecture Notes in Mathematics, 898*, ed. D. A. Rand and L. S. Young, Springer-Verlag, Berlin (1981).

J. Theiler, "Quantify chaos: practical estimation of the correlation dimension," Ph.D. Thesis, California Institute of Technology (1987).

P. D. Thompson, "Uncertainty of initial state as a factor in the predictability of large scale atmospheric flow patterns," Tellus **9**, 275-295 (1957).

J.A.L. Thomson and B. J. West, J. Phys. Ocean. **5** (1975).

A. A. Tisonis and J. B. Elsner, "The weather attractor over very short timescales," Nature **333**, 545-547 (1988).

P. F. Verhulst, Mem. Acad. Roy. Bruxelles **28**, 1 (1844).

K.M. Watson, and B.J. West, "A transport-equation description of nonlinear ocean surface wave interactions," J. Fluid Mech., **70**, 815-826, (1975).

B. J. West, *Deep Water Gravity Waves*, Springer, New York, (1981).

B. J. West, "Resonant-test-field model of fluctuating nonlinear waves," Phys. Rev. **25A**, 1683-1691 (1982).

B. J. West and K. Lindenberg, "Comments on statistical measures of predictability," in *Predictability in Fluid Motions*, eds. G. Holloway and B. J. West, Am. Inst. Phys. Conf. Proceed. vol. **106**, 45-53 (1983).

B. J. West, *An Essay on the Importance of Being Nonlinear*, Lect. Notes in Biomathematics **62**, Springer-Verlag, Berlin (1985).

B. J. West, K. A. Brueckner, R. Janda, D. M. Milder and R. L. Milton, "A new numerical method for surface hydrodynamics," J. Geophys. Res. **92**, 11863 (1987).

H. Whitney, Ann. Math. **37**, 645 (1936).

N. Wiener, *Time Series*, MIT press, Cambridge, Mass. (1949).

S. Wiggins, "Stirred but not mixed," Nature **333**, 395-396 (1988).

A. Wolf, J. B. Swift, H. L. Swinney and J. A. Vastano, "Determining Lyapunov exponents from a time series," Physica **16D**, 285-317 (1985).

H. C. Yuen and M. M. Lake, "Nonlinear dynamics of deep-water gravity waves," in *Advances in Applied Mechanics*, vol. 22, 67-229, Academic Press, Orlando, Fla. (1982).

J. A. Yorke and E. D. Yorke, J. Stat. Phys. **21**, 263 (1979).

V.E. Zakharov, "Stability of periodic waves of finite amplitude on the surface of a deep fluid," J. Appl. Mech. Tech. Phys., Engl. Transl., **2**, 190-194, (1968).

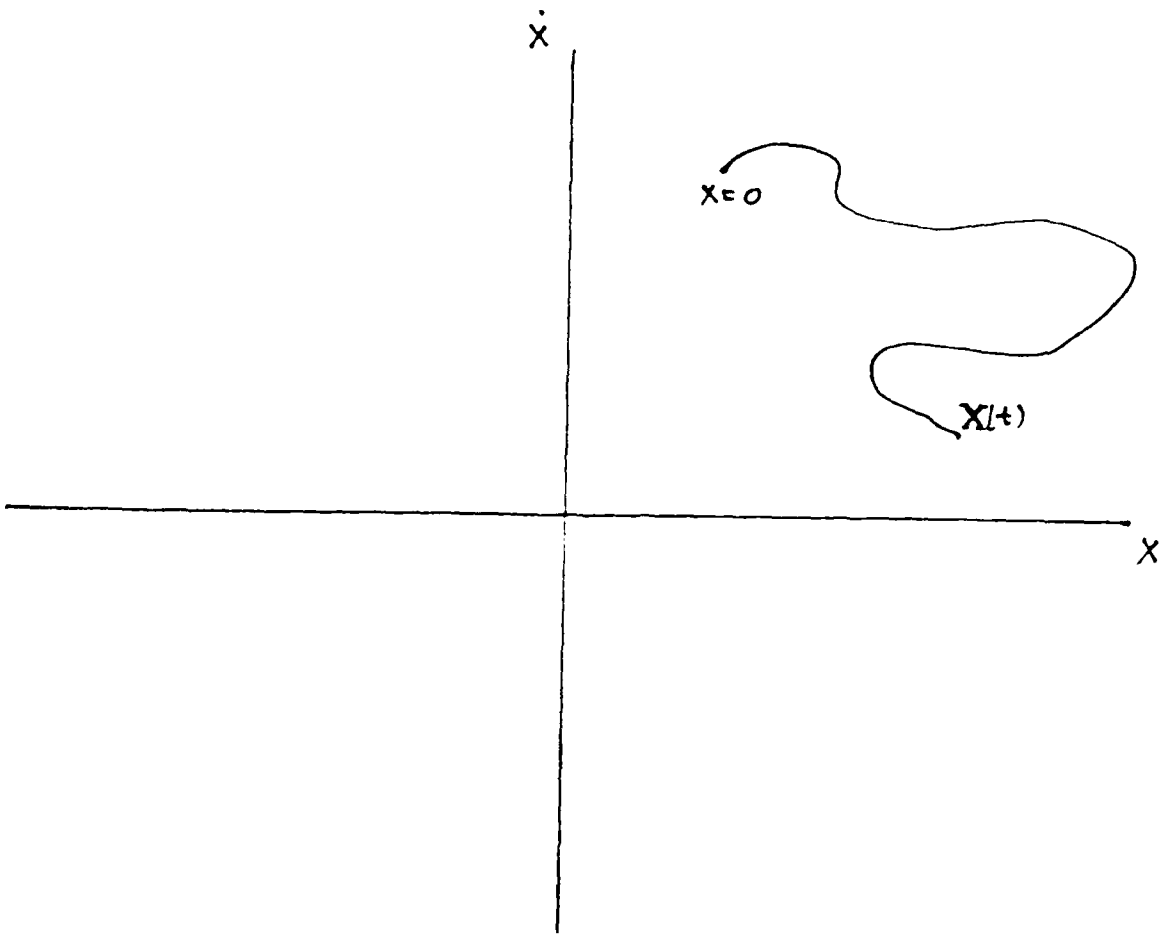

Figure (2.1.1) The (x_1, x_2) plane constitutes a two-dimensional phase space for a dynamical system. The curve is a schematic representation of the instantaneous state of the system, starting form the initial point labeled $t = 0$. Time (not shown) is a parameter that locates the system along the trajectory.

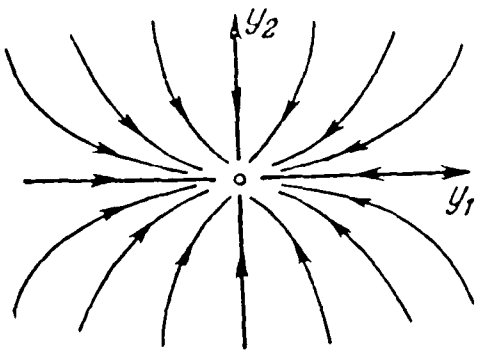

Figure (2.1.2) The collection of trajectories initiated from a set of initial conditions is called a flow field. Here the flow field in the neighborhood of a fixed point is shown. All the trajectories asymptotically converge on the single point in phase space, i.e., they reside in the basin of attraction of the focus.

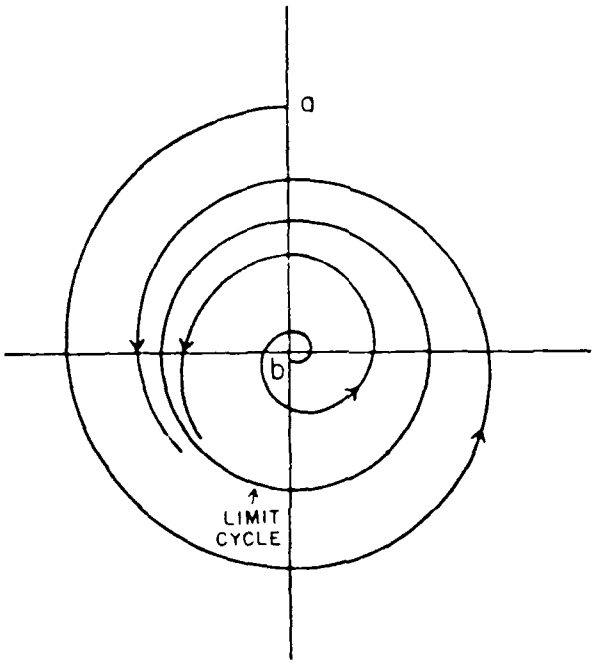

Figure (2.1.3) The two points *a* and *b* in the figure are possible initial conditions for the system. When the system can manifest limit cycle behavior the orbits approach this cycle asymptotically and lose all memory of their initial state.

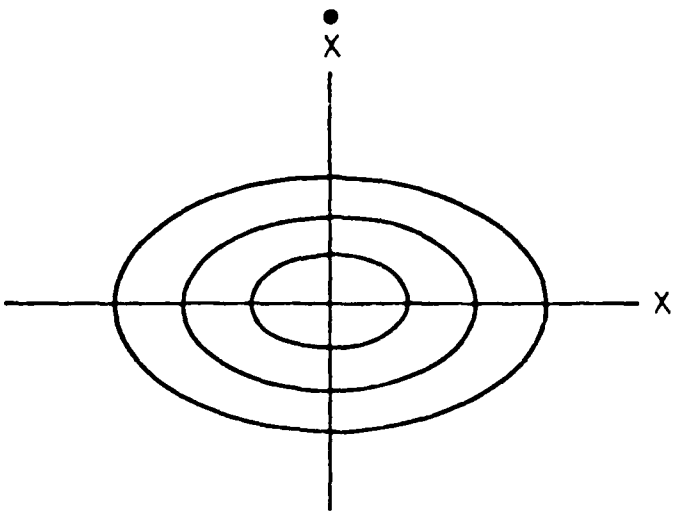

Figure (2.1.4) The $(\dot{x}, x)$ phase space is shown for a harmonic oscillator with a few typical orbits. Each ellipse has a constant energy. As the energy of the oscillator is increased the system jumps from an ellipse of smaller diameter to one of larger diameter.

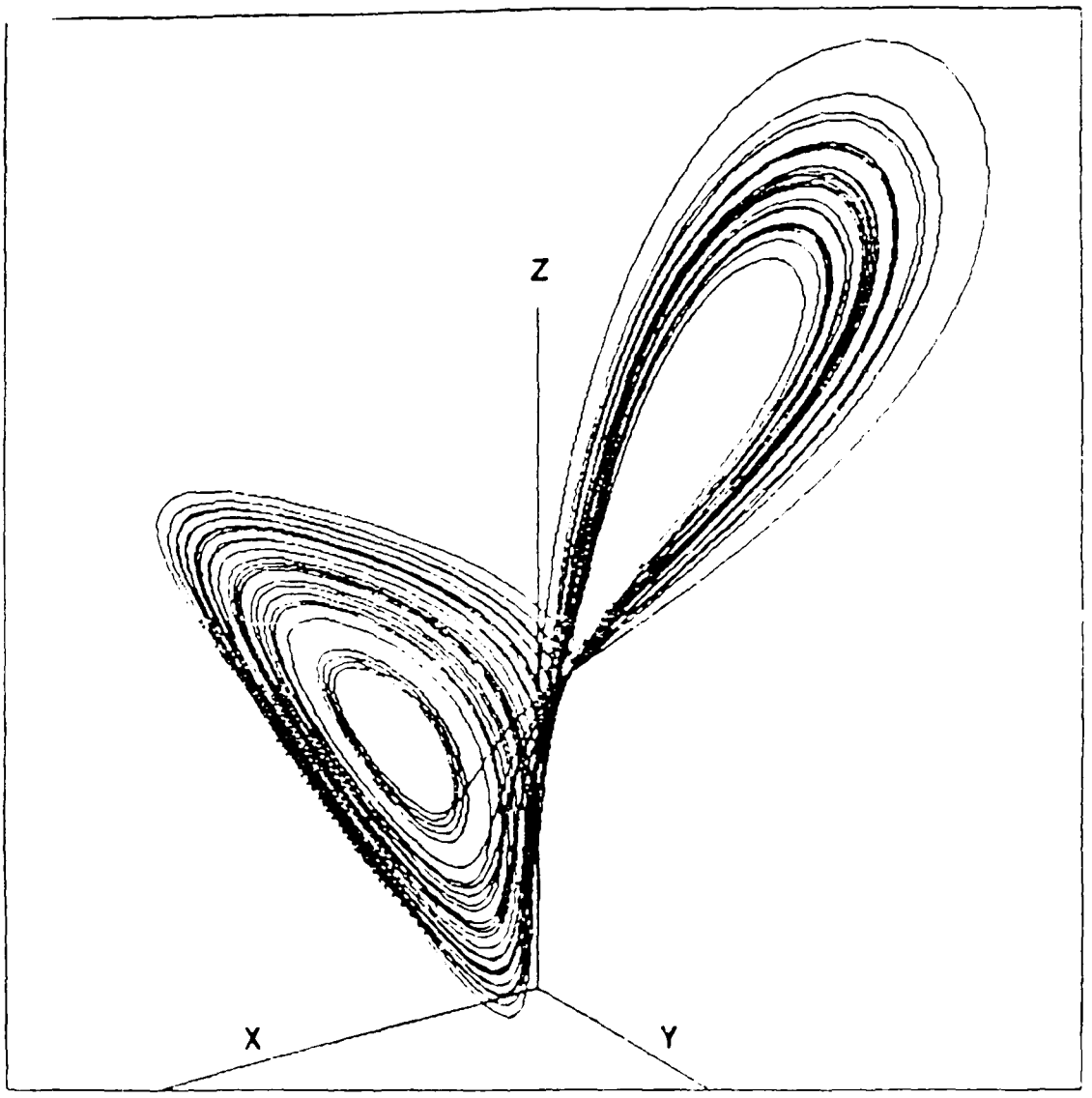

Figure (2.1.5) The attractor solution to the Lorenz system, equations (2.1.2)-(2.1.4), is depicted in a three dimensional phase space (X,Y,Z). The attractor is *strange* in that it has a fractal (noninteger) dimension. (From Schaffer, 1985).

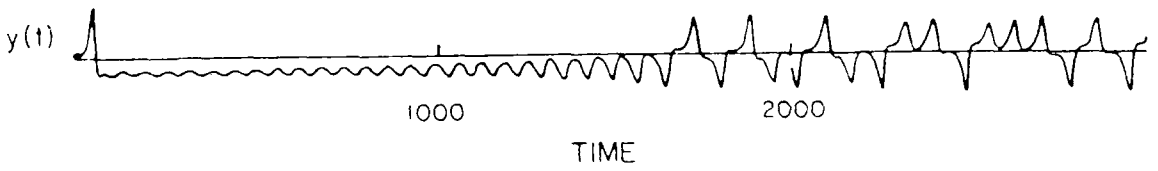

Figure (2.1.6) The time history of the $Y(t)$ component of the solution to the Lorenz system of equations (2.1.2)-(2.1.4) is shown for 3×10^3 time units (from Lorenz, 1963).

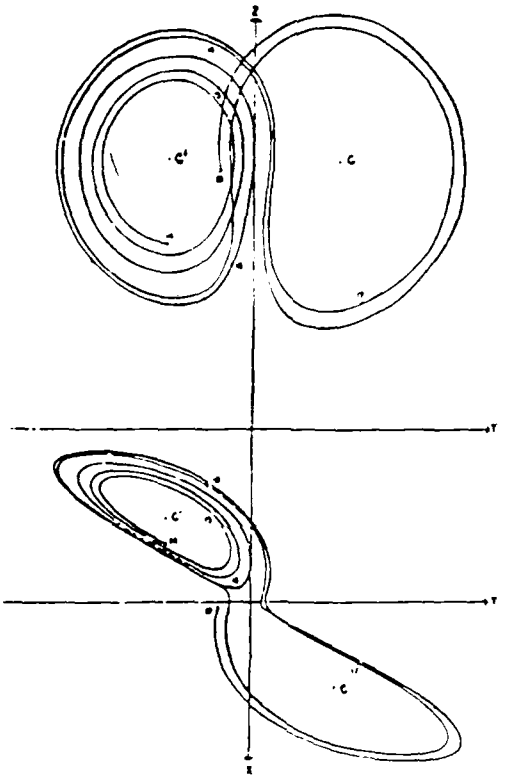

Figure (2.1.7) The three dimensional attractor solution for the Lorenz system is projected onto the (y, z)-plane in (a) and onto the (x, y)-plane in (b) (from Lorenz, 1963).

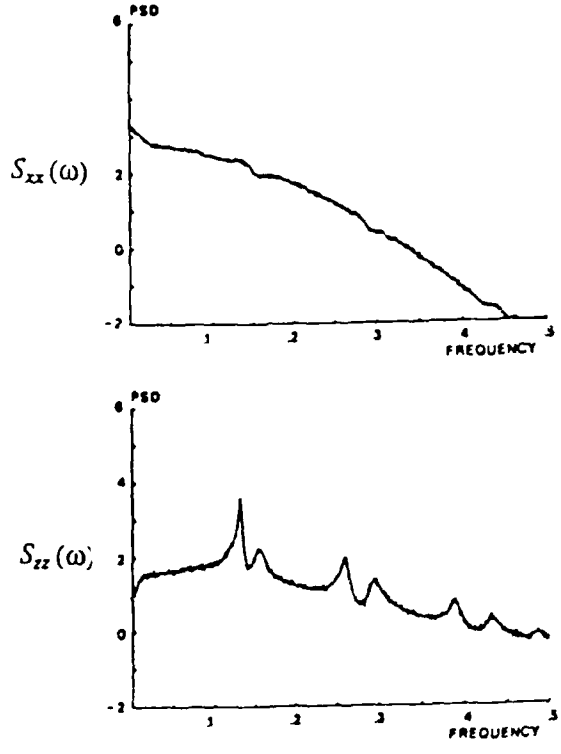

Figure (2.1.8) The power spectral density $S_{xx}(\omega)$ and $S_{zz}(\omega)$ is calculated using the solution for the x-component and z-component, separately, using Equation (2.1.16) (from Farmer et al., 1980).

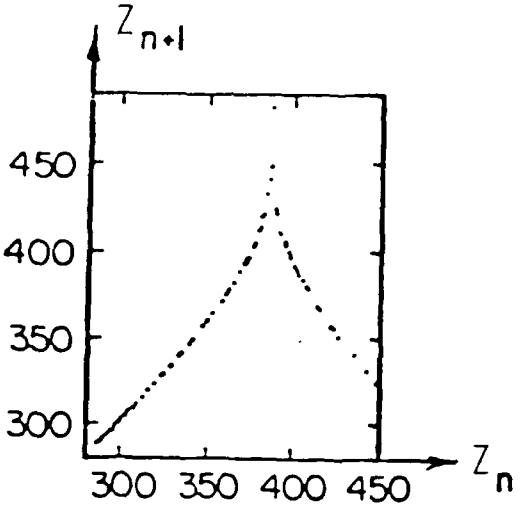

Figure (2.1.9) Corresponding values of relative maximum of Z (abscissa) and subsequent relative maximum of Z (ordinate) occurring during the first 6000 iterations (from Lorenz, 1963).

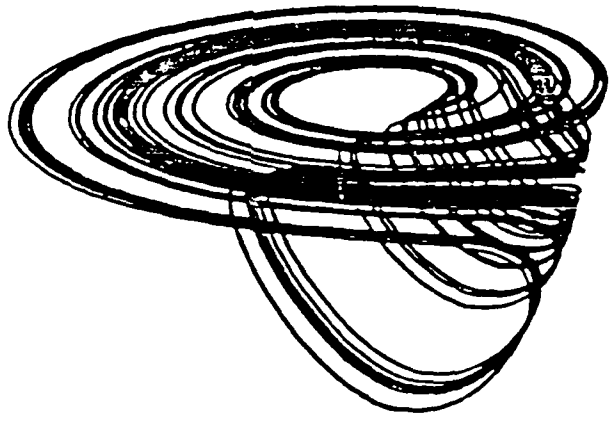

Figure (2.1.10) The "funnel" attractor solution to the Rössler Equations (2.1.12)-(2.1.14) with parameter values $a = 0.343, b = 1.82$ and $c = 9.75$. (From Rossler, 1979).

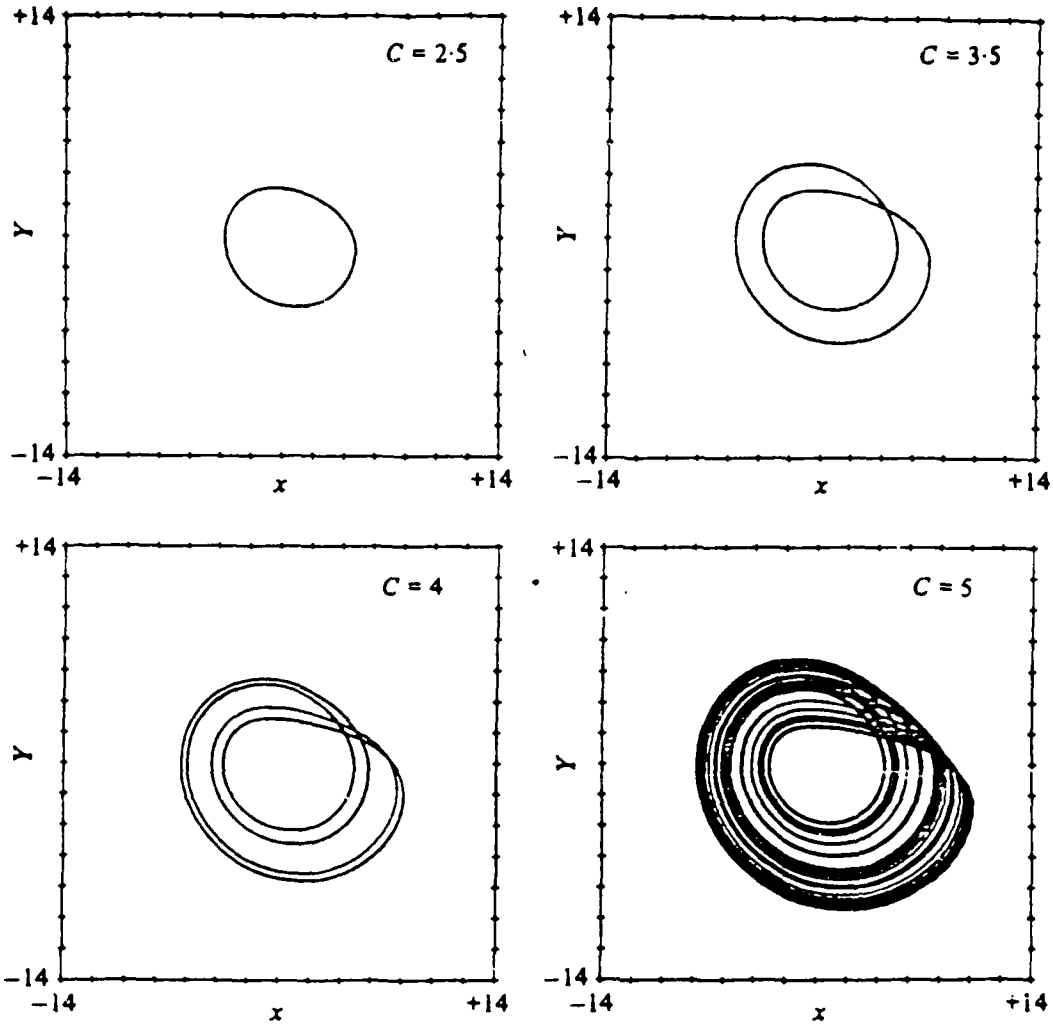

Figure (2.1.11) An $x-y$ phase plane plot of the solution to the Rössler Equaitons (2.1.12)-(2.1.14) with parameter values $a = 0.20$ and $b = 0.20$ at four different values of c indicated in the graphs.

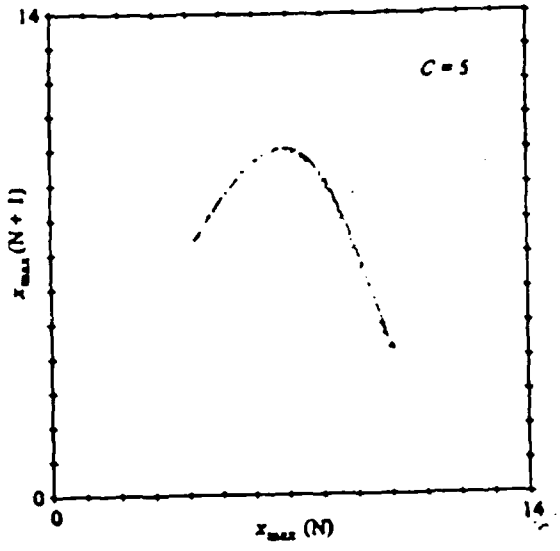

Figure (2.1.12) Next amplitude plot of the Rössler Equation (2.1.12)-(2.1.14) for $c = 5, a = 0.2$ and $b = 0.2$. Each amplitude of the oscillation of x was plotted against the preceding amplitude.

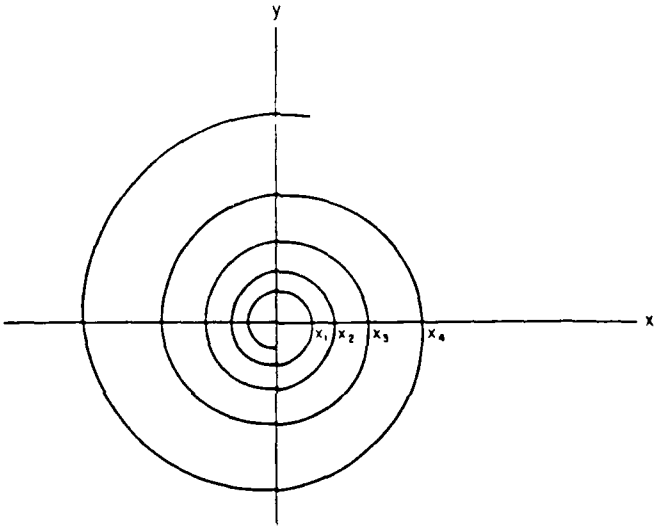

Figure (2.2.1) The spiral is an arbitrary orbit depicting a function $y = f(x)$. The intersection of the spiral with the x-axis defines a set of points $x_1, x_2, \ldots$, that can be obtained from a mapping determined by $f(x)$.

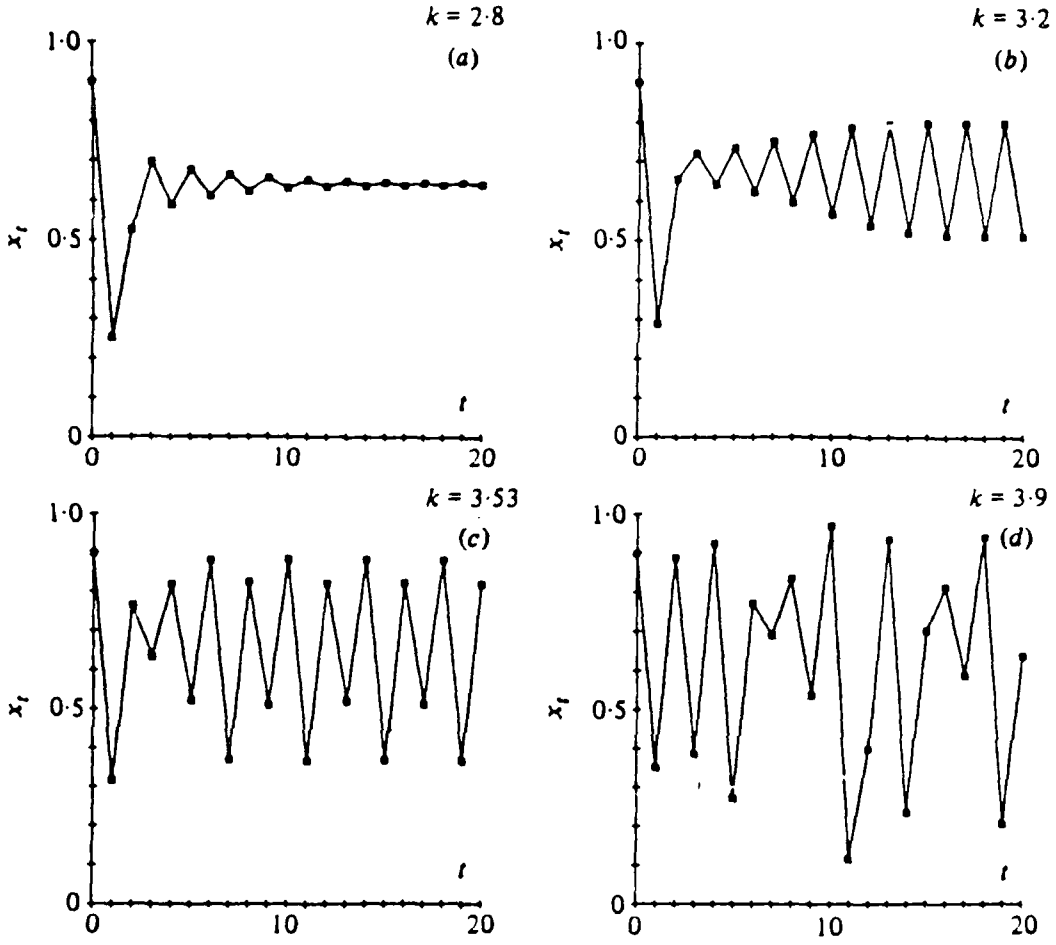

Figure (2.2.2) The solution to the map (2.2.11) is depicted for various choices of the parameter μ. (a) The solution Y_n approaches a constant value as $n \to \infty$ for $\mu = 2.8$. (b) The solution Y_n is a periodic orbit after the initial transient dies out for $\mu = 3.2$. (c) The orbit in (b) bifurcates to a 4-cycle for $\mu \approx 3.53$. (d) The orbit is chaotic for $\mu = 3.9$. (From Olsen and Deng, 1985).

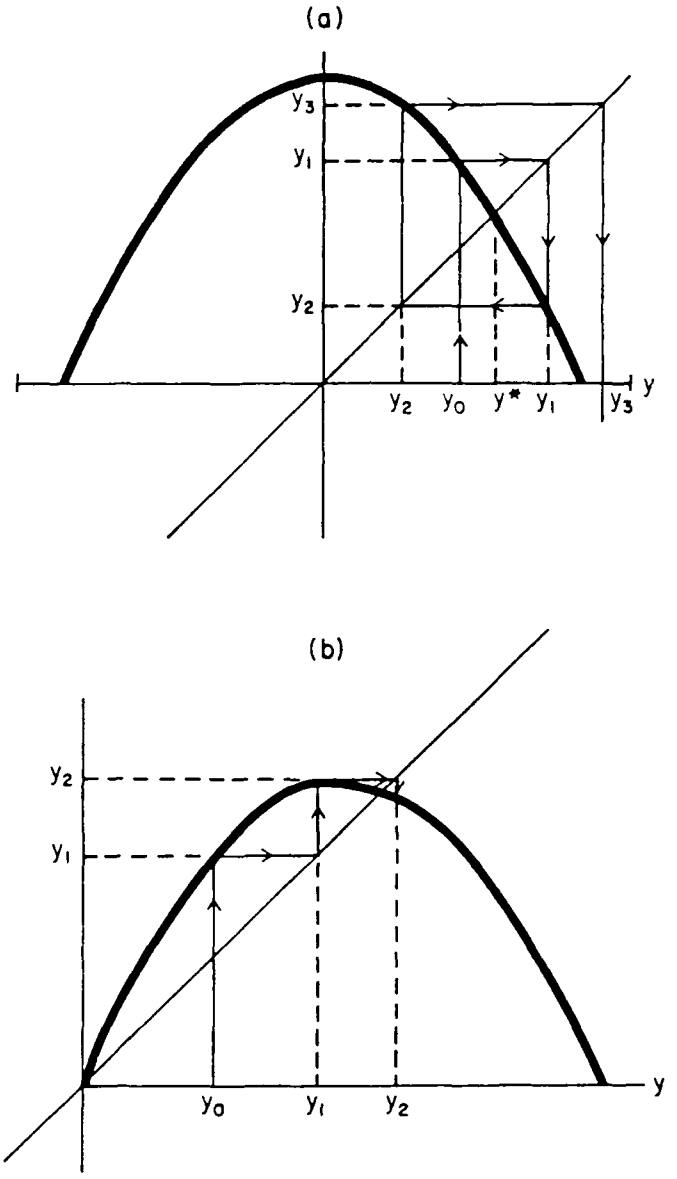

Figure (2.2.3) A mapping function with a single maximum is shown. In (a), the iteration away from the initial point y_0 is depicted. In (b), the convergence to the station point y^* is shown. (From West, 1985).

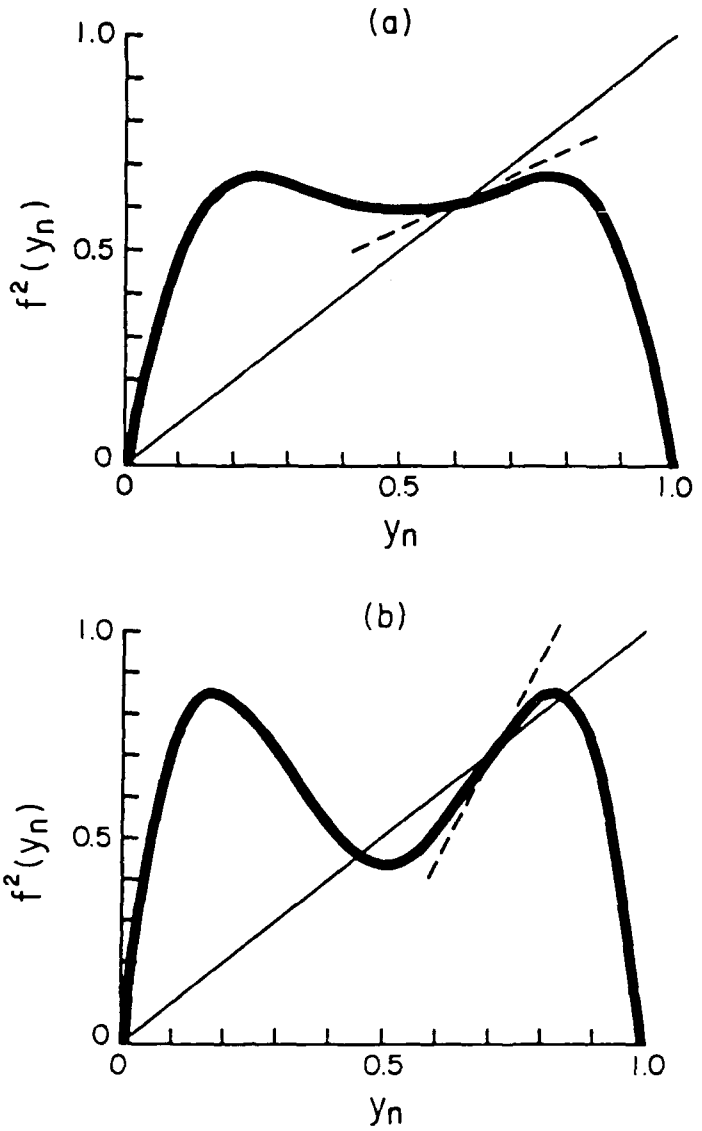

Figure (2.2.4) The map f with a single maximum in Figure (2.2.3) yields an f^2 map with a double maximum. The slope at the point y^* is indicated by the dashed line and is seen to increase as the parameter μ is raised in the map from (a) to (b). (From West, 1985).

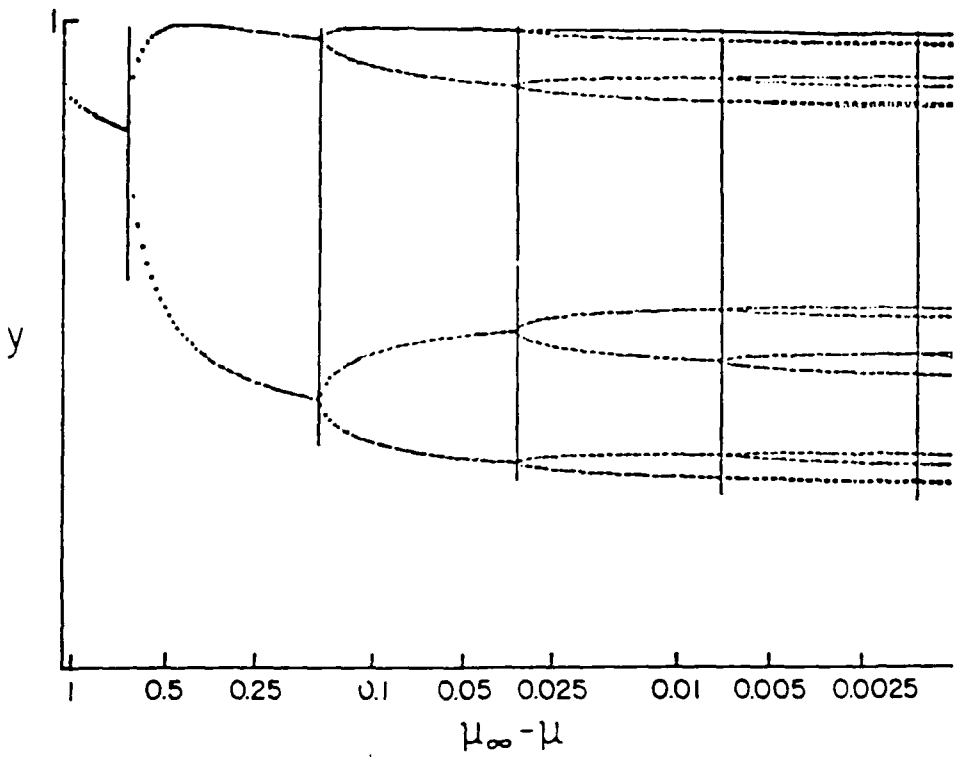

Figure (2.2.5) The bifurcation of the solution to the mapping $x \to 1 - \mu x^2$ as a function of $\mu_\infty - \mu$ is indicated. The logarithmic scale was chosen to clearly depict the bifurcation regions. (From Collett and Eckmann, 1980).

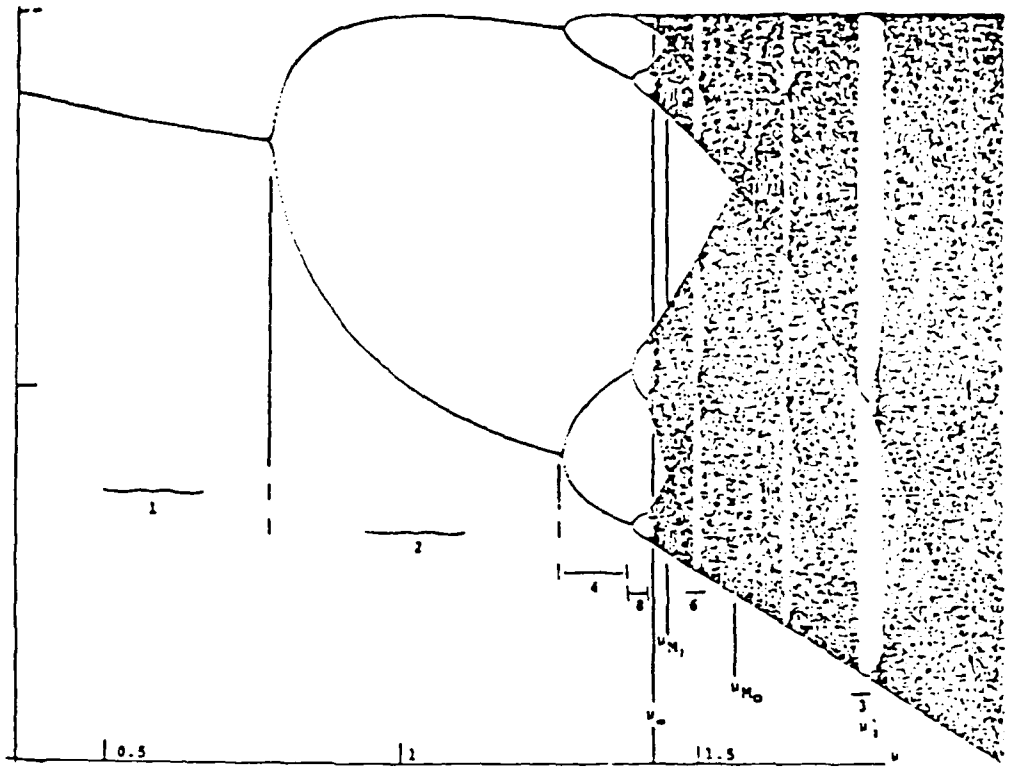

Figure (2.2.6) The same as Figure (2.2.5), but with a linear scale in $\mu_\infty - \mu$ so that the hazy region denoting chaos is clearly observed. (From Collett and Eckmann, 1980).

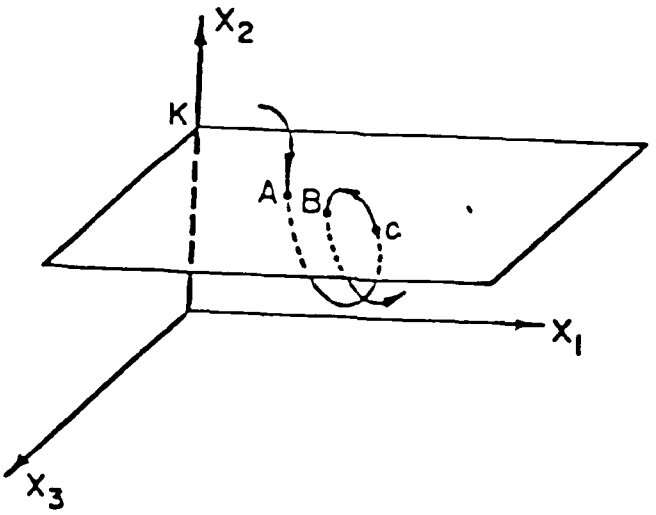

Figure (2.2.7) An arbitrary trajectory is shown and its intersection with a plane parallel to the $x_1, x_3 -$ plane at $x_2 = constant$ are recorded. The points A, B, C,... define a map as in Figure (2.2.1). This is the Poincaré surface of section. (From Ott, 1985).

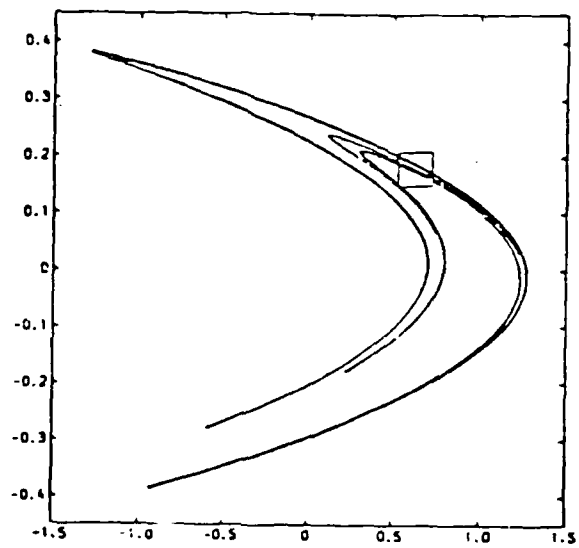

Figure (2.2.8) Iterated point of the map (2.2.2a), for 10^4 iterations with the parameter values $c = 1.4$ and $\beta = 0.2$. (From Ott, 1985).

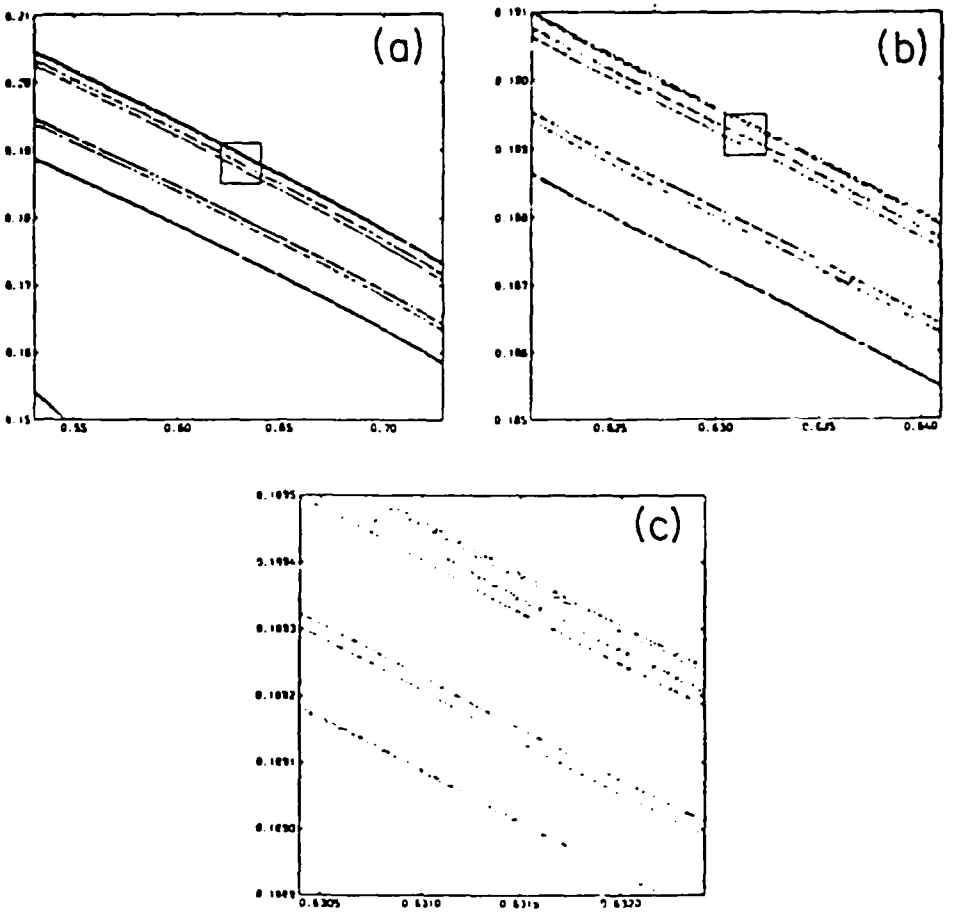

Figure (2.2.9) (a) Enlargement of the boxed region in Figure (2.2.8), 10^4 iterations; (b) enlargement of the square in (a), 10^6 iterations; (c) enlargement of the square in (b), 5×10^6 iterations. (From Ott, 1985).

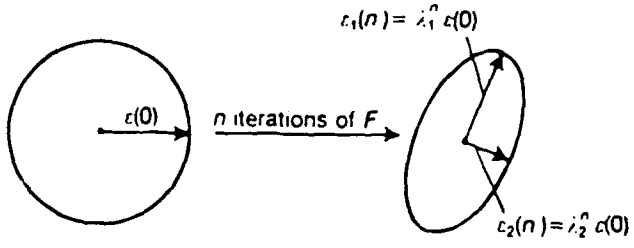

Figure (2.2.10) Lyapunov exponents define the average stretching or contraction of trajectories in characteristic directions. Here we show the effects of applying a two-dimensional mapping to circles of initial conditions. A sufficiently small circle of radius ε is transformed after n iterations into an ellipse with major radius $\lambda^n{}_1\varepsilon$ and minor radius $\lambda^n{}_2\varepsilon$, where λ_1 and λ_2 are the Lyapunov exponents for $n \to \infty$.

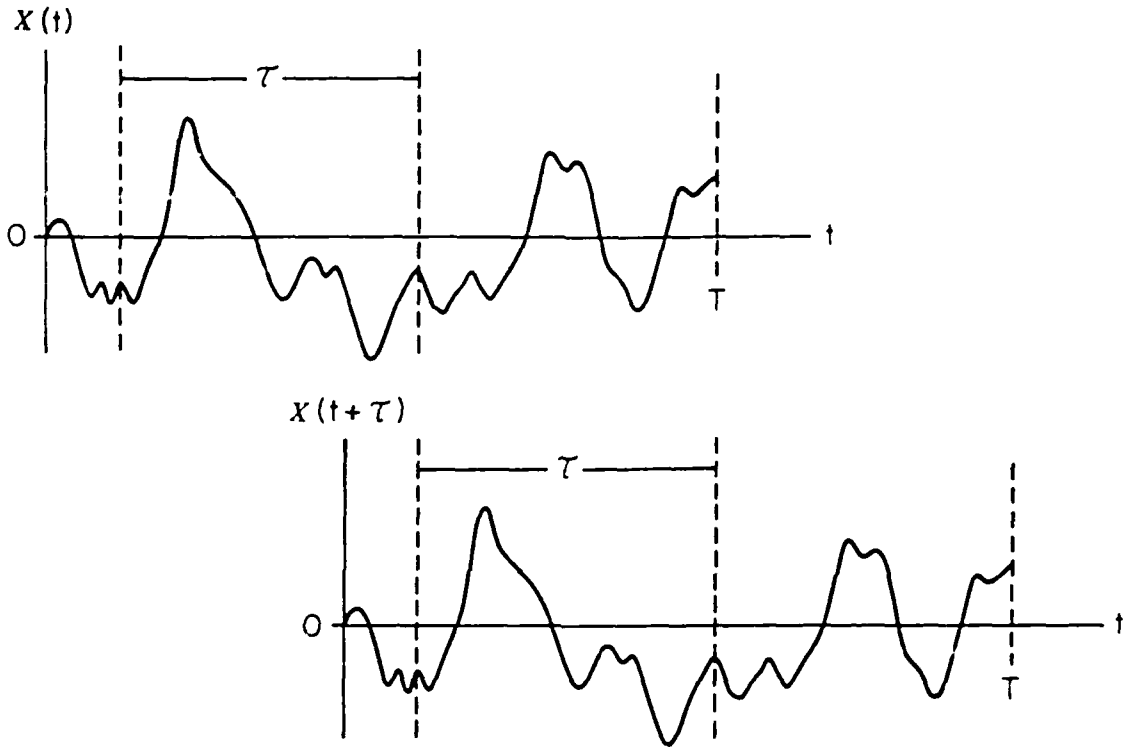

Figure (2.3.1) The time trace of a random function $X(t)$ versus time t is shown in the upper curve. The lower curve is the same time trace displaced by a time interval τ. The product of these two functions when averaged yield an estimate of the autocorrelation function $C_{xx}(\tau,T)$.

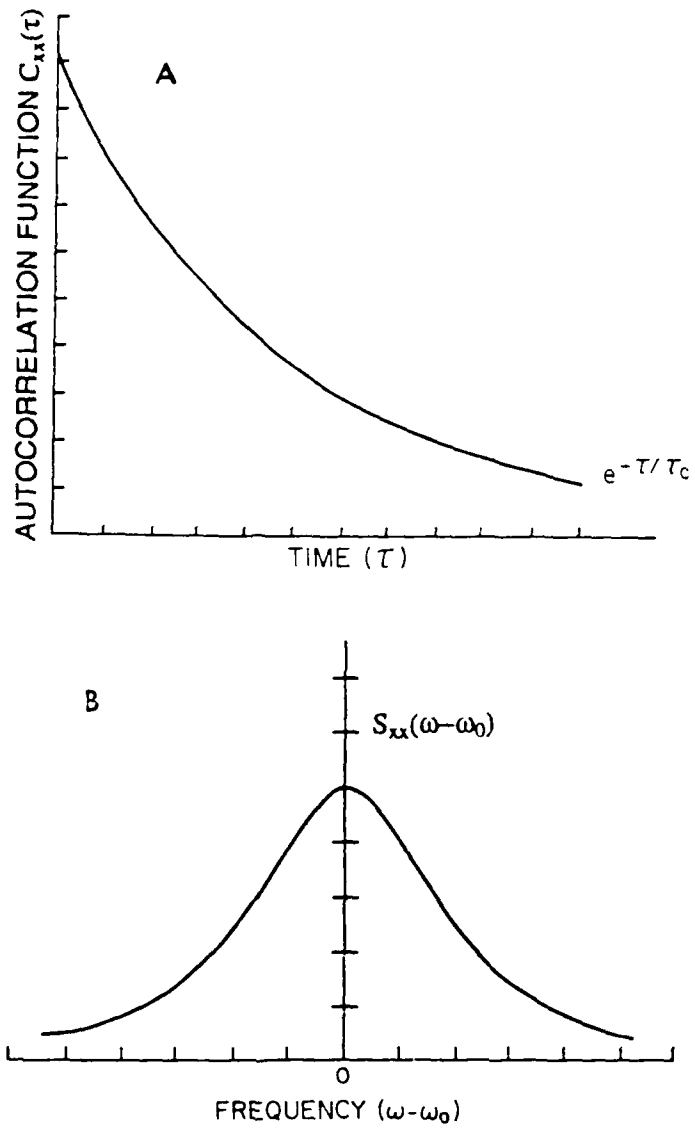

Figure (2.3.2) (a) The autocorrelation function $C_{xx}(\tau)$ for the typical time traces depicted in Figure (2.3.1) assuming the fluctuations are exponentially correlated in time $[\exp(-\tau/\tau_c)]$. The constant τ_c is the time required for $C_{xx}(\tau)$ to decrease by a factor 1/e, this is the decorrelation time. (b) The power spectral density $S_{xx}(\omega)$ is graphed as a function of frequency for the exponential correlation function with a central frequency ω_0.

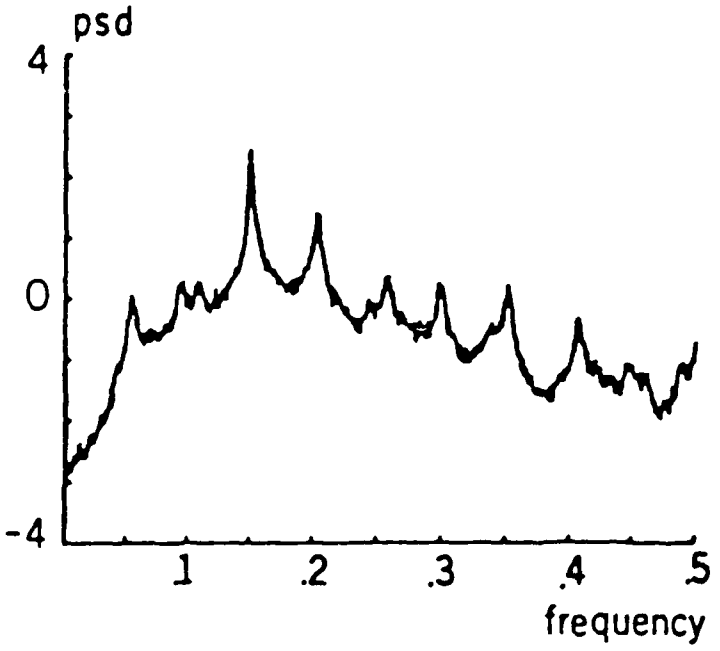

Figure (2.3.3) The power spectral density for the $X(t)$ time series for the "funnel" depicted in Figure (2.1.10).

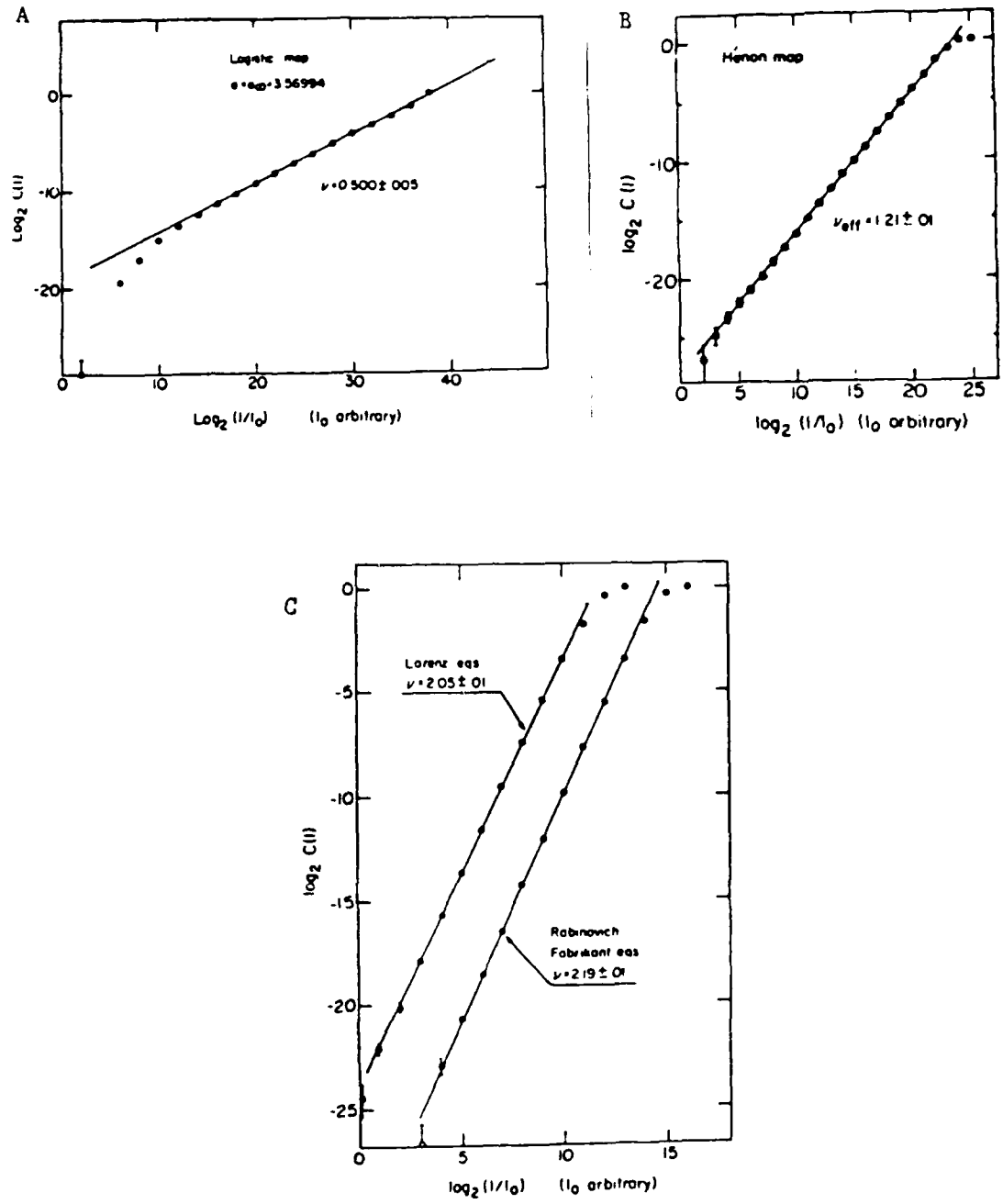

Figure (2.3.4) (a) The correlation integral for the logistic map (2.2.11) at the infinite bifurcation point $\mu = \mu_\infty = 3.699\cdots$ The starting point was $Y_0 = 1/2$, the number of points was $N = 3\times10^4$. (b) Correlation integral for the Henon map (2.2.29) and (2.2.30) with $c = 1.4, \beta = 0.01$ and $N = 1.5\times10^4$. (c) Correlation integrals for the Lorenz equations (2.1.9)-(2.1.11) (dots); for the Rabinovich-Fabricant equation (open circles). In both cases $N = 1.5\times10^4$ and $\tau = 0.25$. (From Grassberger and Procaccia, 1985). (From Grassburger and Procaccia, 1983a).

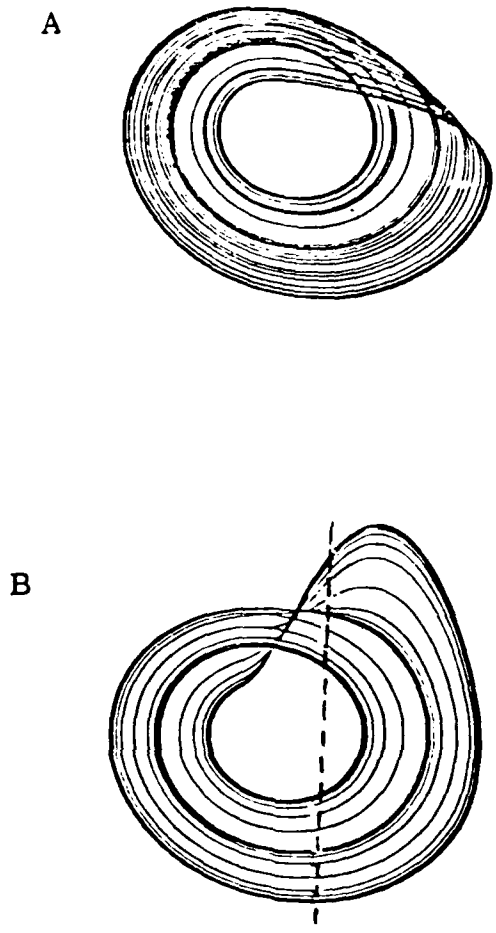

Figure (2.3.5) A two-dimensional projection of the Rossler chaotic attractor (a) is compared with the reconstruction in the $(\dot{x}, x)$ plane of the attractor (b) from the time series $x(t)$. The dashed line indicates the Poincaré surface of section for this attractor (from Packard et al., 1980).

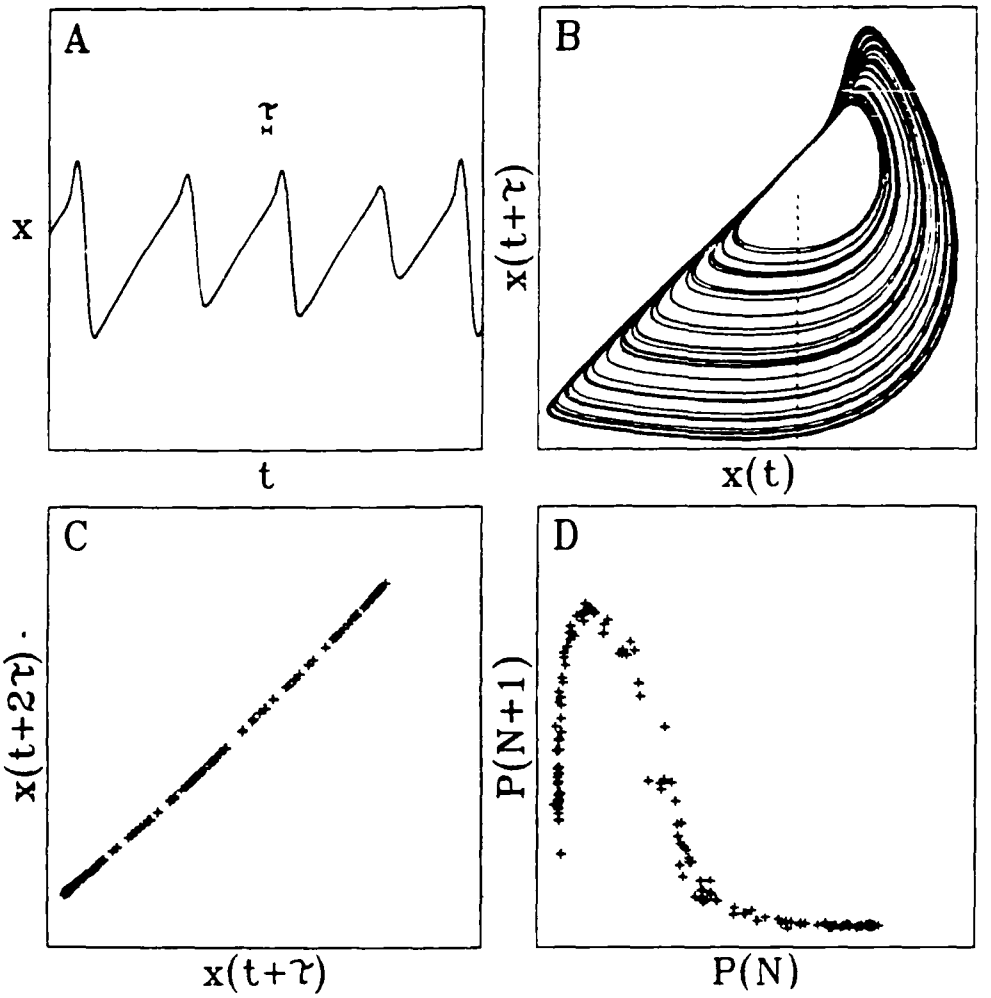

Figure (2.3.6) Attractor from a chemical oscillator. (a) The time series $X(t)$ is the bromide ion concentration in a Belousov-Zhabatinskii reaction. A time interval τ is indicated. (b) Plot of $X(t)$ versus $X(t+\tau)$. Dotted line indicates a cut through the attractor. (c) Cross section of attractor along cut. (d) Poincaré return map of cut, $P(N+1)$ is the position the trajectory crosses the dotted line as a function of the crossing position on the previous turn around the attractor (from Roux and Swinney, 1981).

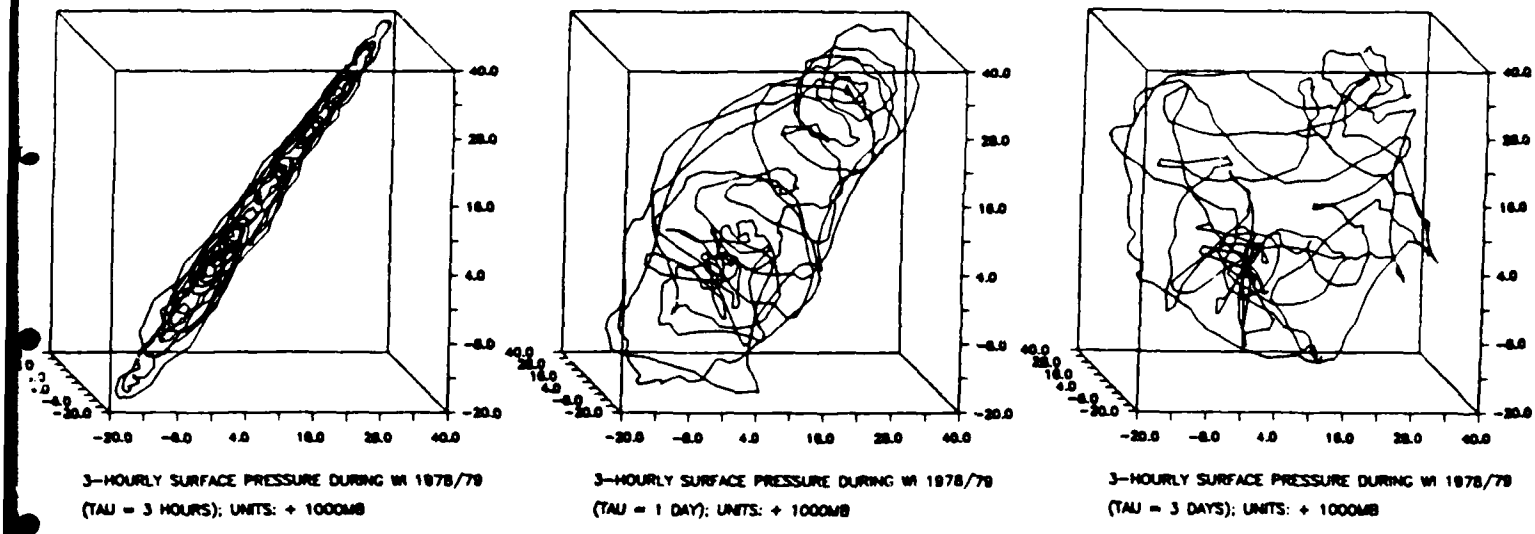

Figure (3.1.1) Time trajectory of three-hourly surface pressure evolving in a three-dimensional phase space of time-lagged pressure coordinates (units: 1000 mb). Horizontal axis: $p(t)$; vertical axis: $p(t+r)$; axis into plotting plane: $p(t+2r)$. From left to right: (a) r = 3 hours, (b) r = 1 day, (c) r = 3 days (from Fraedrich, 1986).

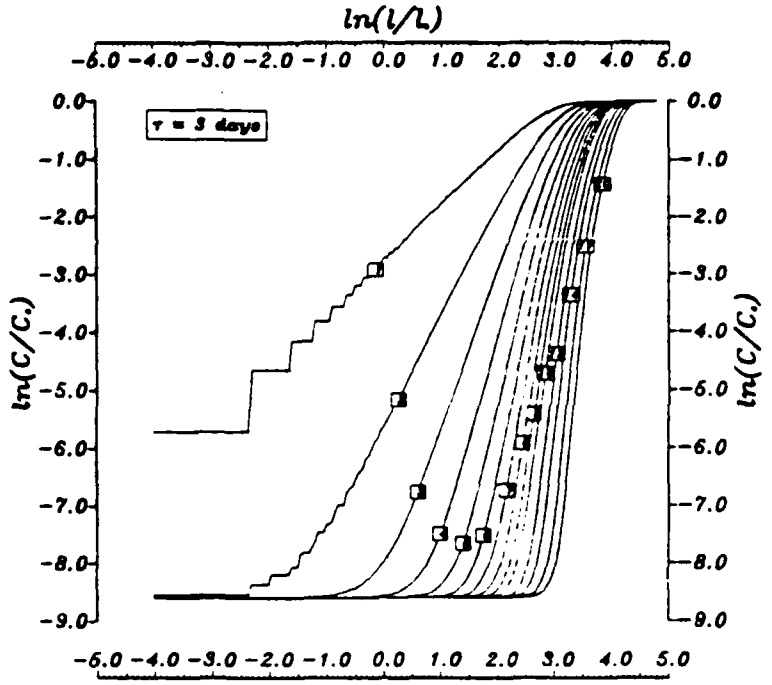

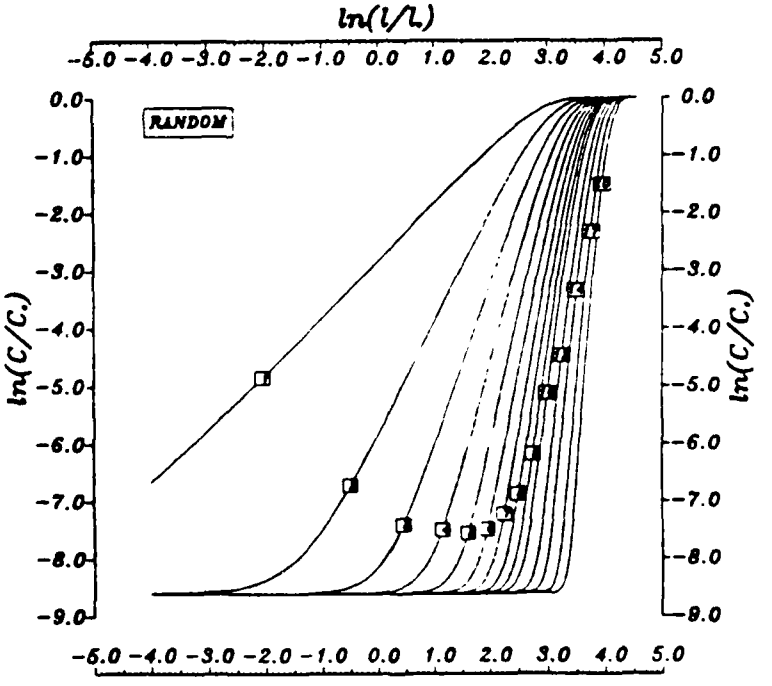

Figure (3.1.2) Cumulative distribution function of distances of the 15-year daily pressure trajectory evolving in m-dimensional phase spaces (m = 1 to 20) of time lagged (r = 3 days) coordinates of the same varible. Top: observed time series; bottom: related random series of same length, mean and variance (from Fraedrich, 1986).

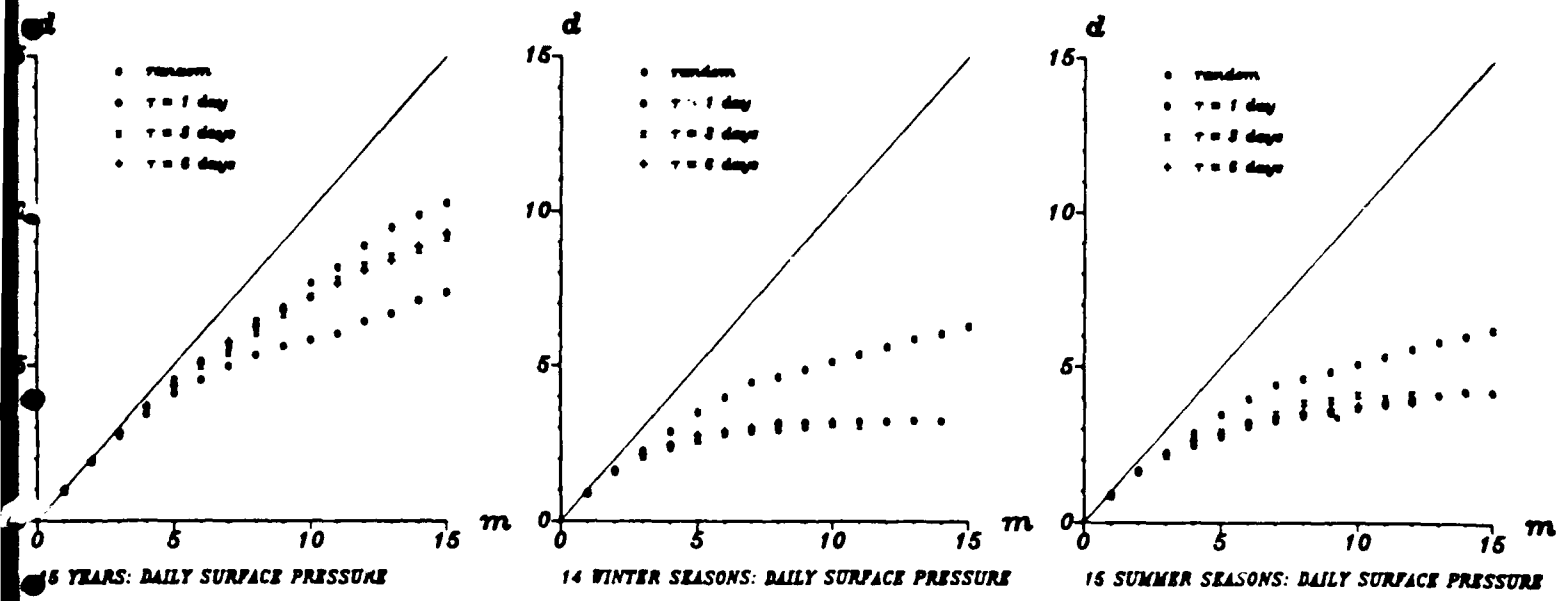

Figure (3.1.3) Dimensionality (d) of the weather attractor as a function of the number m of phase space coordinates, which are determined by multiples (m) the time shifted pressure record (using lags τ = 1, 3 and 6 days). Randomized time series (index c) are compared with observations. From left to right: (a) 15 year record, (b) winter seasons, (c) summer seasons (from Fraedrich, 1986).

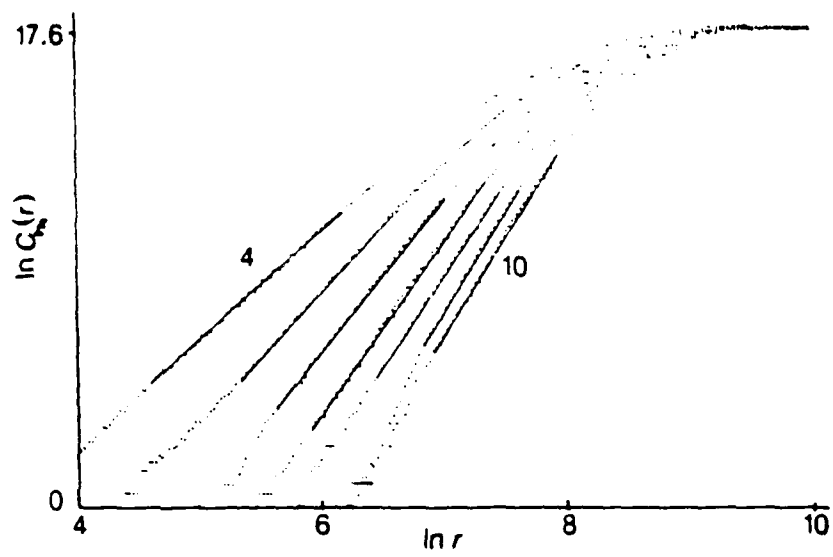

Figure (3.1.4) Plot of $\ln C_m(r)$ against $\ln r$ for embedding dimension, m, from 4 to 10 as obtained by method 1. Note the convergence of slopes as m increases (from Essex, Lookman and Nerenberg, 1987).

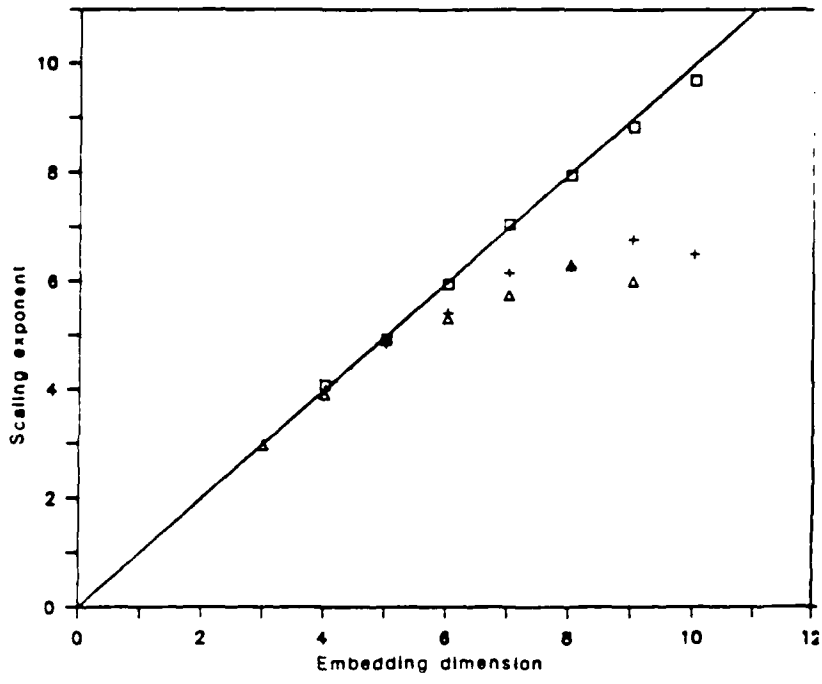

Figure (3.1.5) Summary of results of scaling exponent, $d(m)$ as a function of embedding dimension m, obtained by two methods (method 1, +; method 2, Δ). A random number set of the same size as the data set was used as a control (□). Note the saturation of the exponent arising from the data, for both methods, while there is no saturation for the random number set. This limiting value is identified as ν (from Essex, Lookman and Nerenberg, 1987).

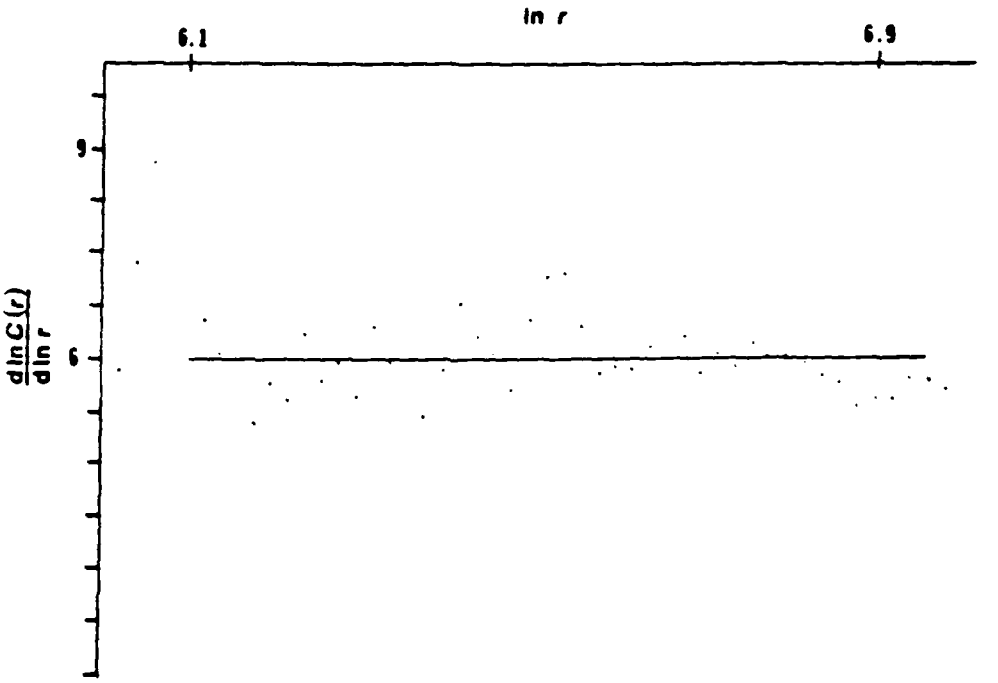

Figure (3.1.6) A sample plot of $d \ln C(r)/d \ln r$ against $\ln r$ showing the scaling region for embedding dimension 9 as determined by method 2 (from Essex, Lookman and Nerenberg, 1987).

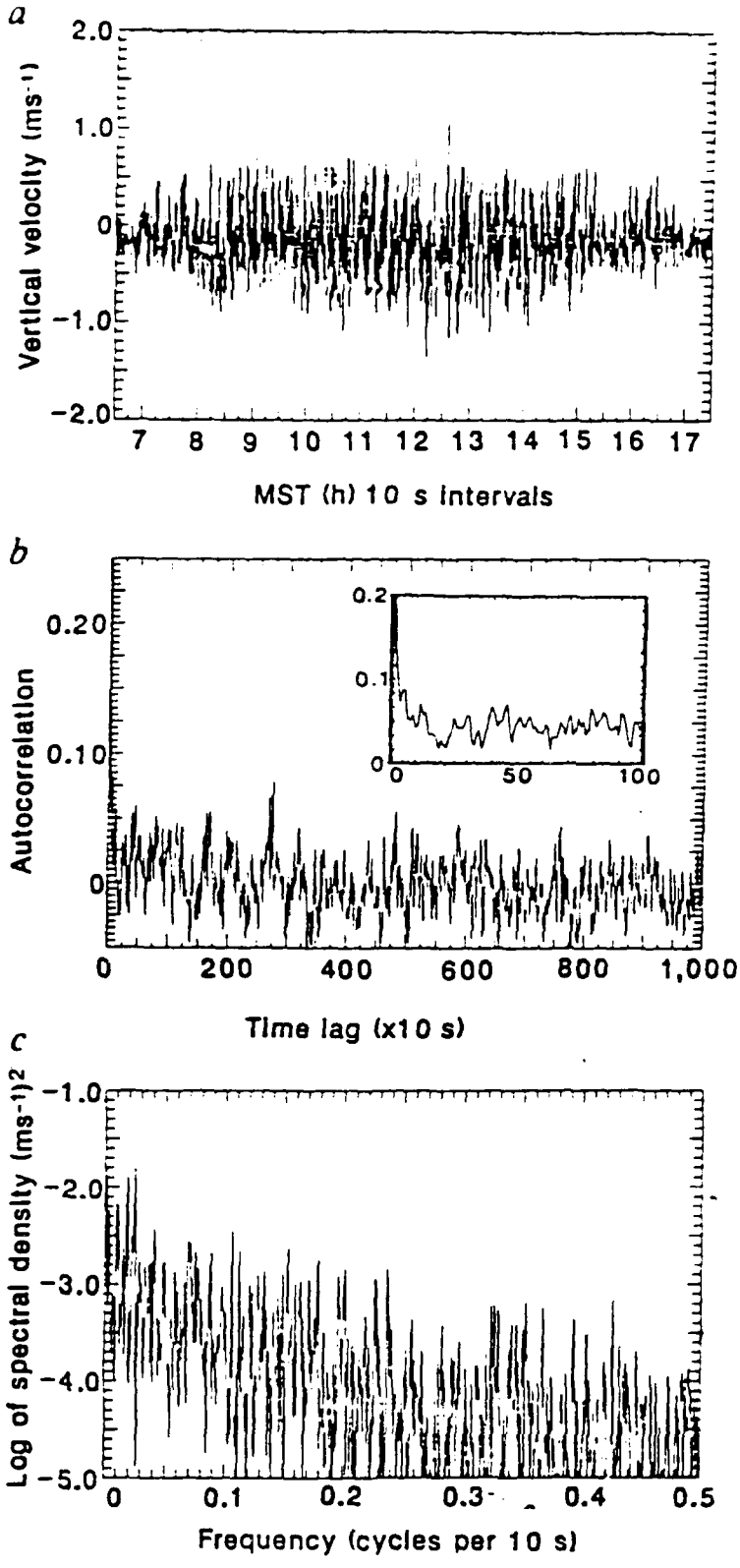

Figure (3.1.7) (a) The data used in this study represent 10-second averages of the vertical wind velocity over 11 hours. The air close to the ground is heated and rises, creating strong convection. Positive values indicate updrafts and negative values indicate downdrafts. (b) The autocorrelation function for the above data. The inset graph is a magnification of the region close to the origin. (c) The logarithm of the spectral density as a function of the frequency for the above data. The spectra show various peaks on a background of a continuous frequency spectrum. This suggests that a strange attractor may be present (from Tsonis and Elsner, 1988).

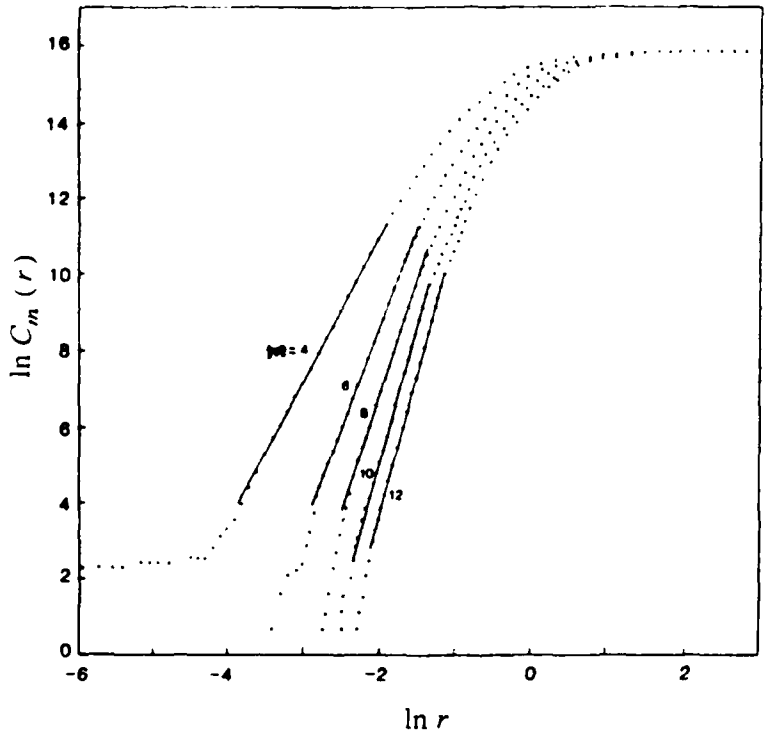

Figure (3.1.8) Plot of $\ln C_m(r)$ against $\ln r$ for embedding dimensions, $m = 4, 6, 8, 10, 12$. Note the convergence of slopes as m increases (from Tsonis and Elsner, 1988).

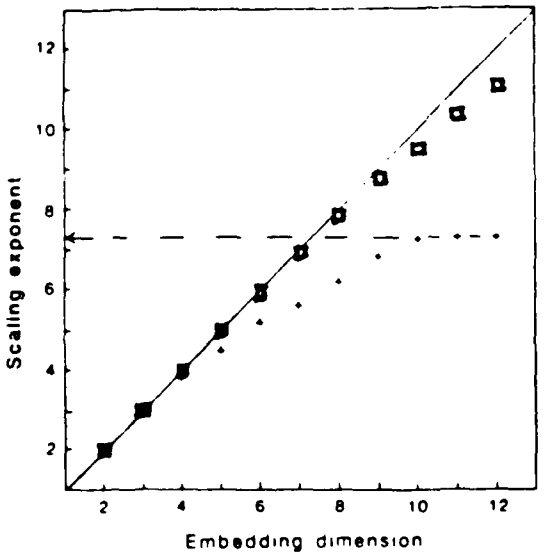

Figure (3.1.9) Scaling exponent, $d(m)$, as a function of the embedding dimension, m. Crosses correspond to the wind velocity data and squares to a random sample of the same size as the wind data. Note the saturation of the scaling exponent observed for the wind data, although there is no saturation for the random set. From this figure we estimated $\nu = d_\infty$ (from Tsonis and Elsner, 1988).

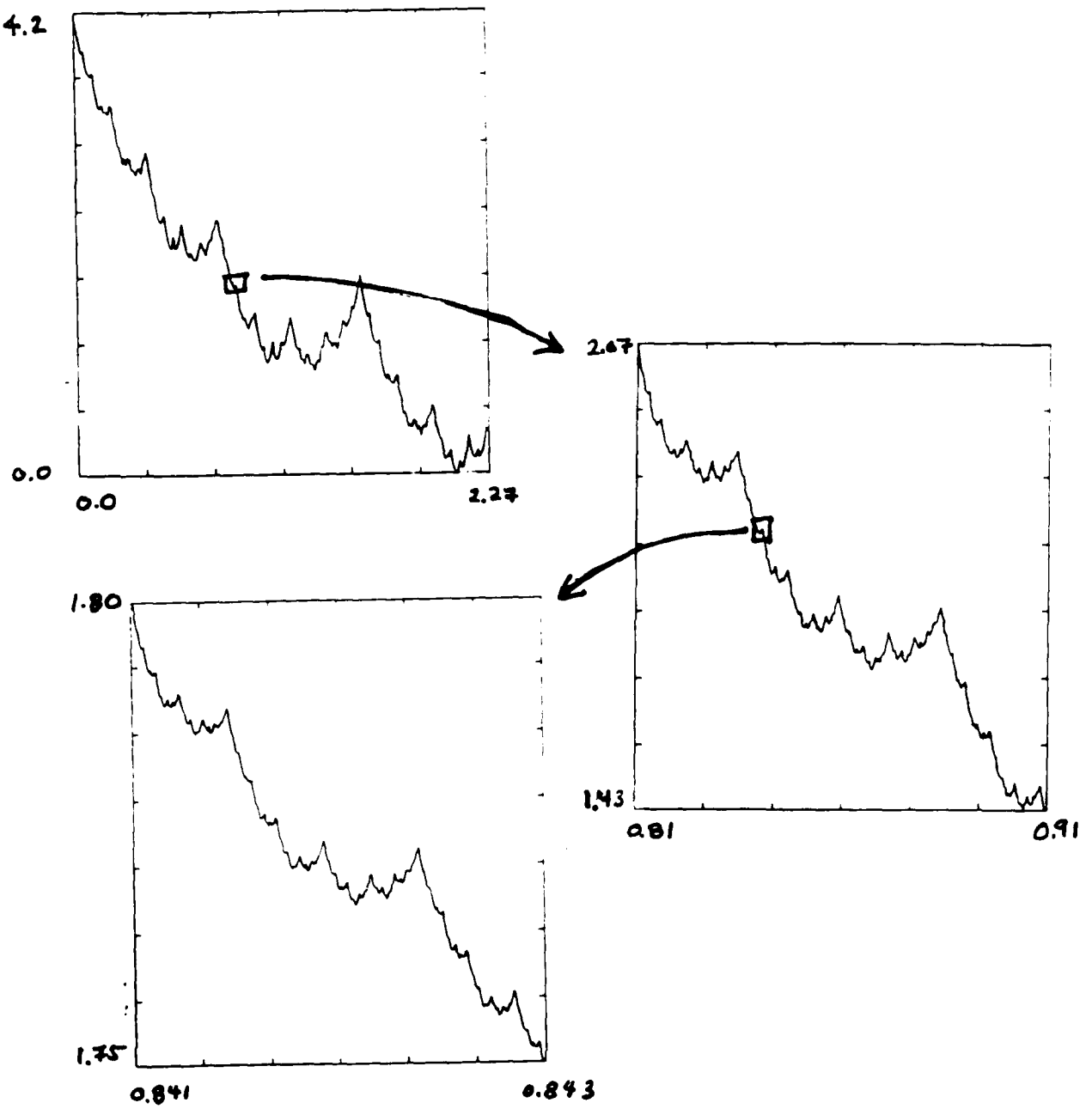

Figure (3.2.1) The Weierstrass function is depicted in (a) for parameter values $a = 2^{2/3}$ and $b = 2$ so that the fractal dimension is 2/3. The curve in (b) is a magnification of the boxed region in (a). The curve in (c) ia s magnification of the boxed region in (b).

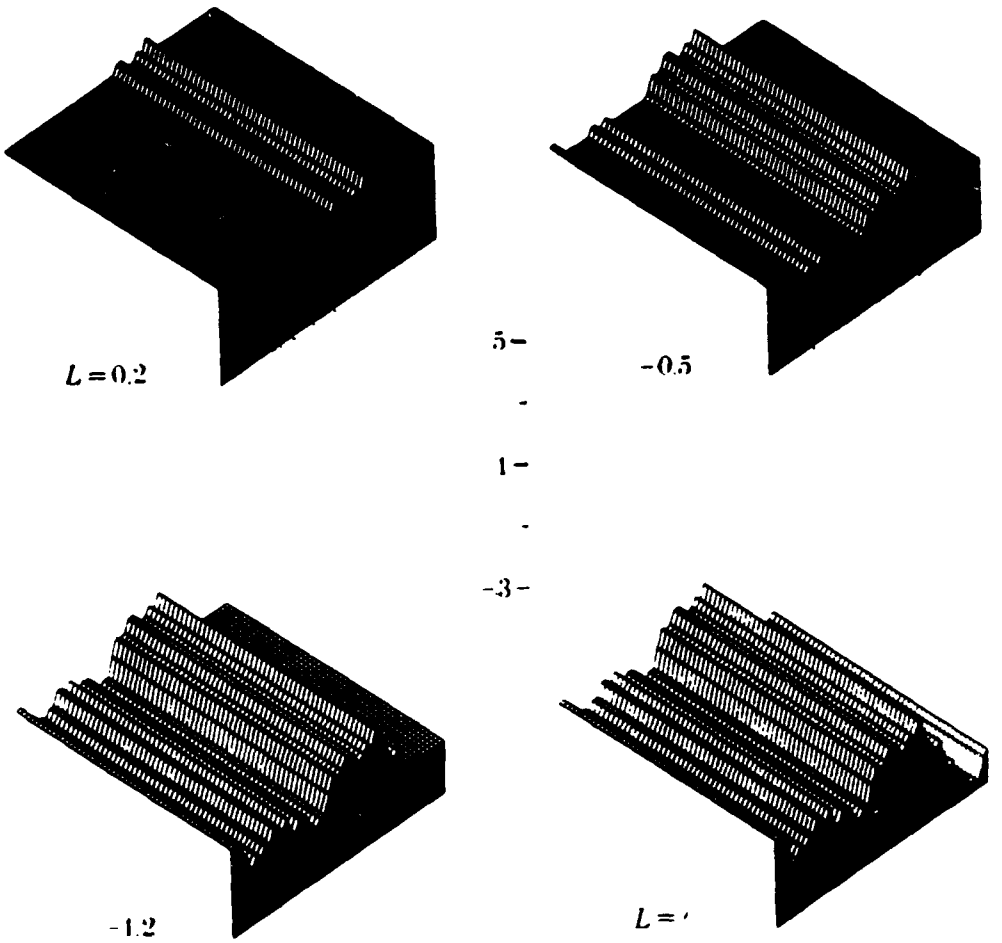

Figure (3.2.2) The Wereistrass-Lévy-Mandelbrot. function with $M = 0$ and random phases. L is the level of an artificial floor which, as it is lowered, reveals more of the surface $(M = 1, D = 2.5, b = 1.5)$ (from Ausloos and Berman, 1985).

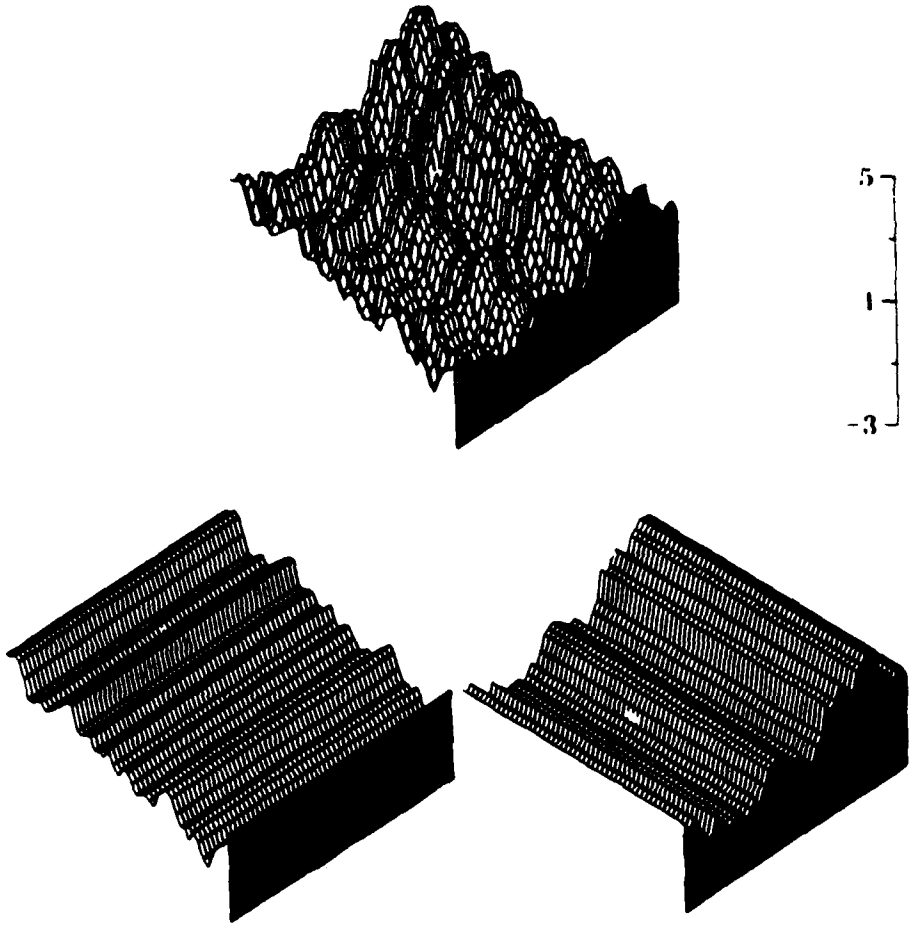

Figure (3.2.3) Surfaces for $M = 2$ with random phases ($D = 2.5, b = 1.2$). The upper surface is the sum of the two lower surfaces (from Ausloos and Berman, 1985).

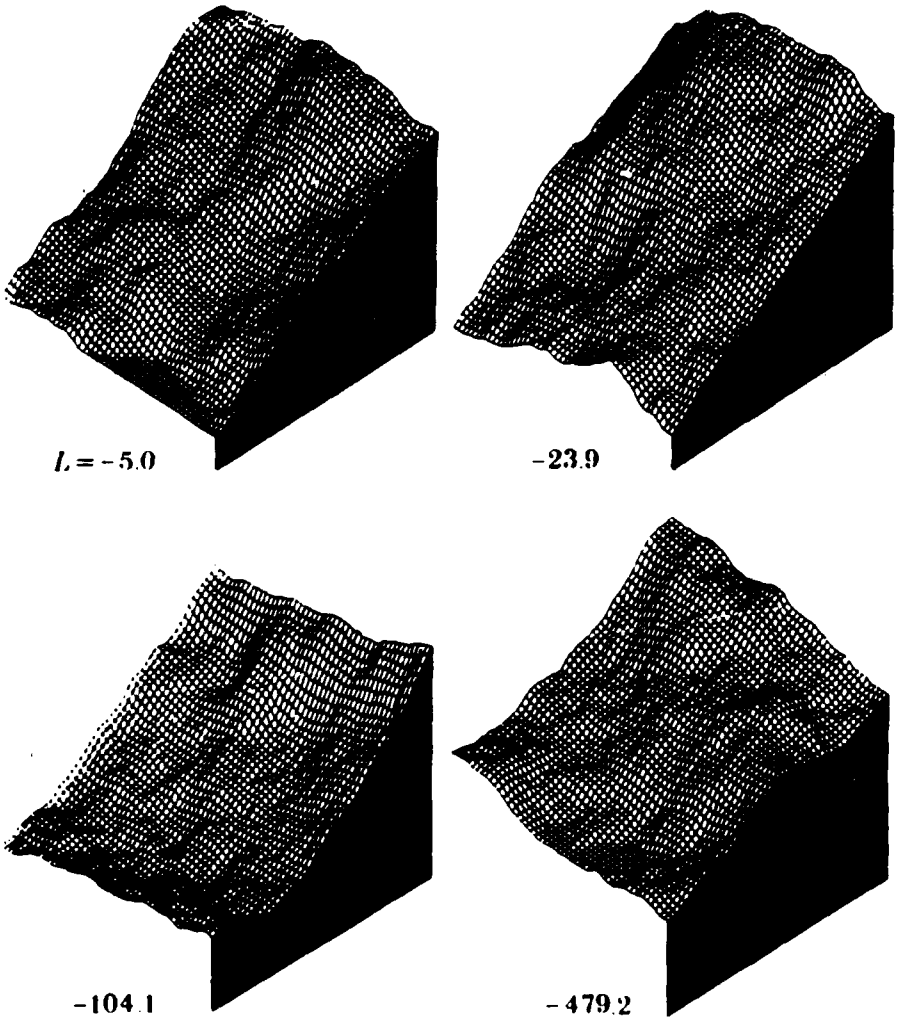

Figure (3.2.4) Four magnifications of the surface for $D = 2.05$, showing self-similarity $(M = 8, b = 1.2)$. The upper right surface is the fivefold magnification of a section of the upper left surface. Similarly, the lower left surface is a fivefold magnification of a piece of the upper right surface and the lower right surface is a fivefold magnification of the lower left surface. The vertical extent is magnified by $5^{(3-D)}$ (from Ausloos and Berman, 1985).

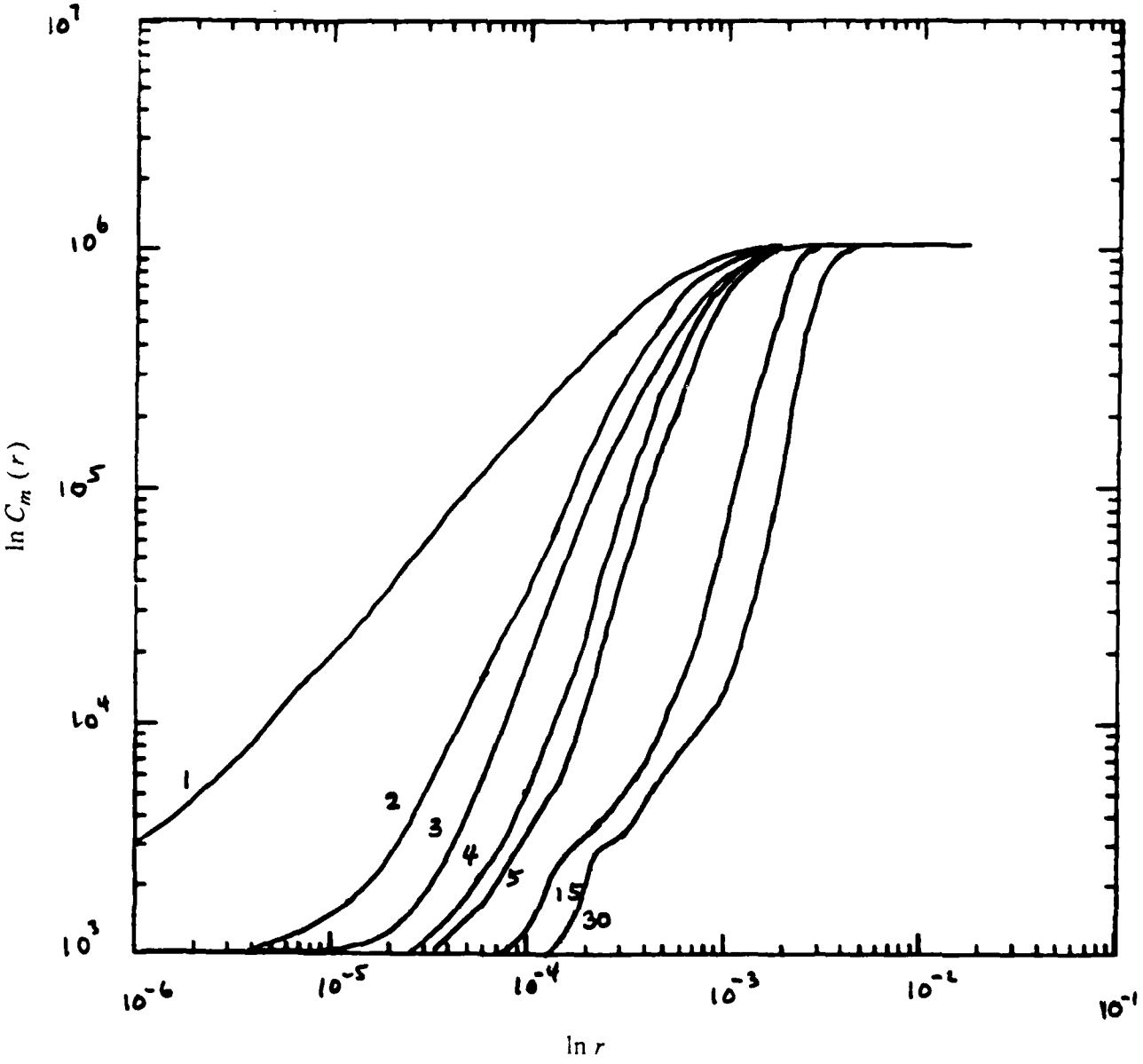

Figure (4.1.1) The logarithm of the correlation function $C_m(r)$ is plotted versus $\ln r$ for a number of different embedding dimensions m. The "time" series is a one-dimensional sea surface over a spatial interval segmented into 1024 data points.

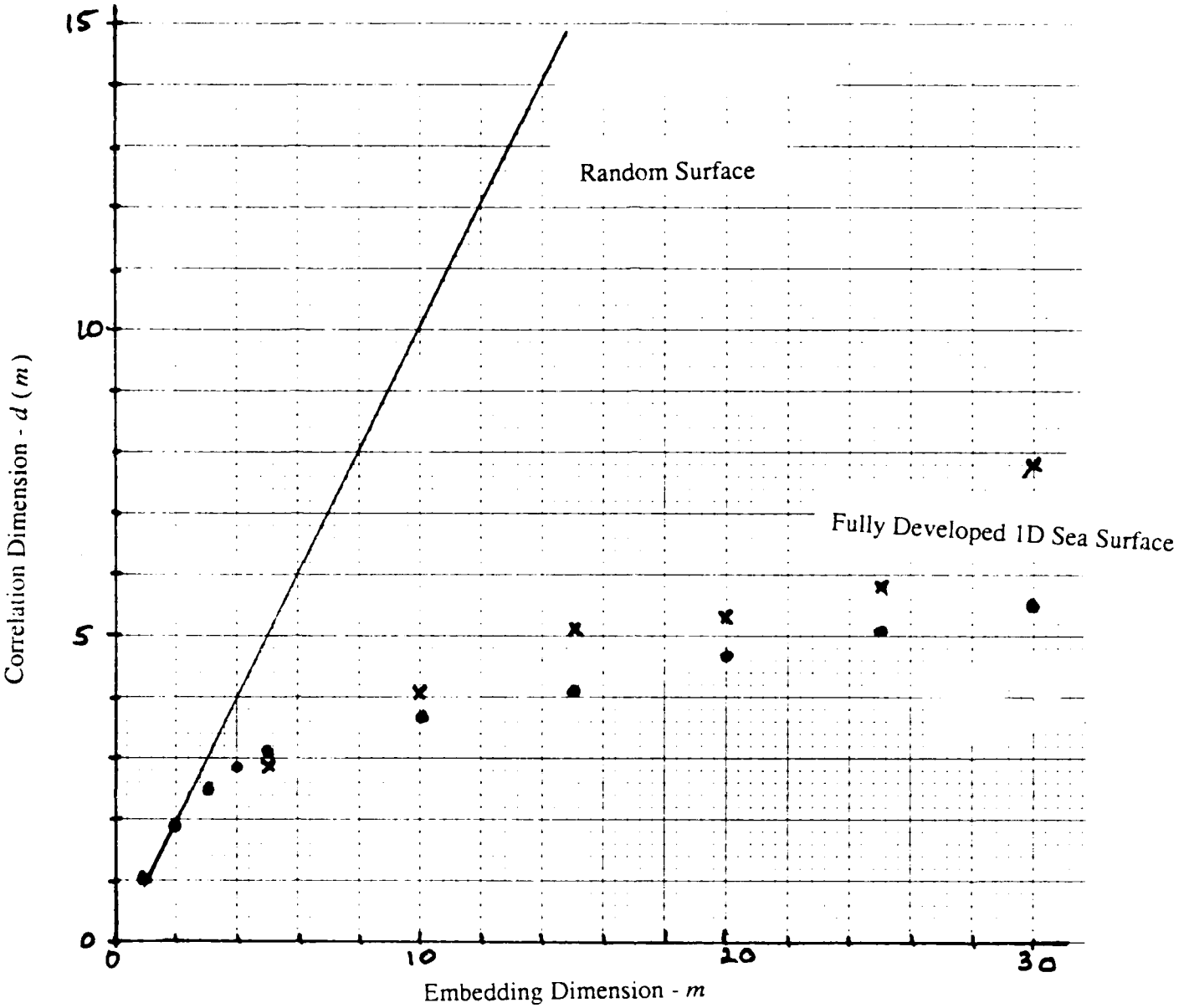

Figure (4.1.2) The correlation dimension $d(m)$ is plotted versus the embedding dimension m for the data in Figure (4.1.1). The solid line depicts the correlation $d(m) = m$ for a calculated random surface. The correlation dimension are as shown for a fully developed one-dimensional sea surface using the "time" shifts $\tau = 8(\cdot)$ and $\tau = 15(x)$.

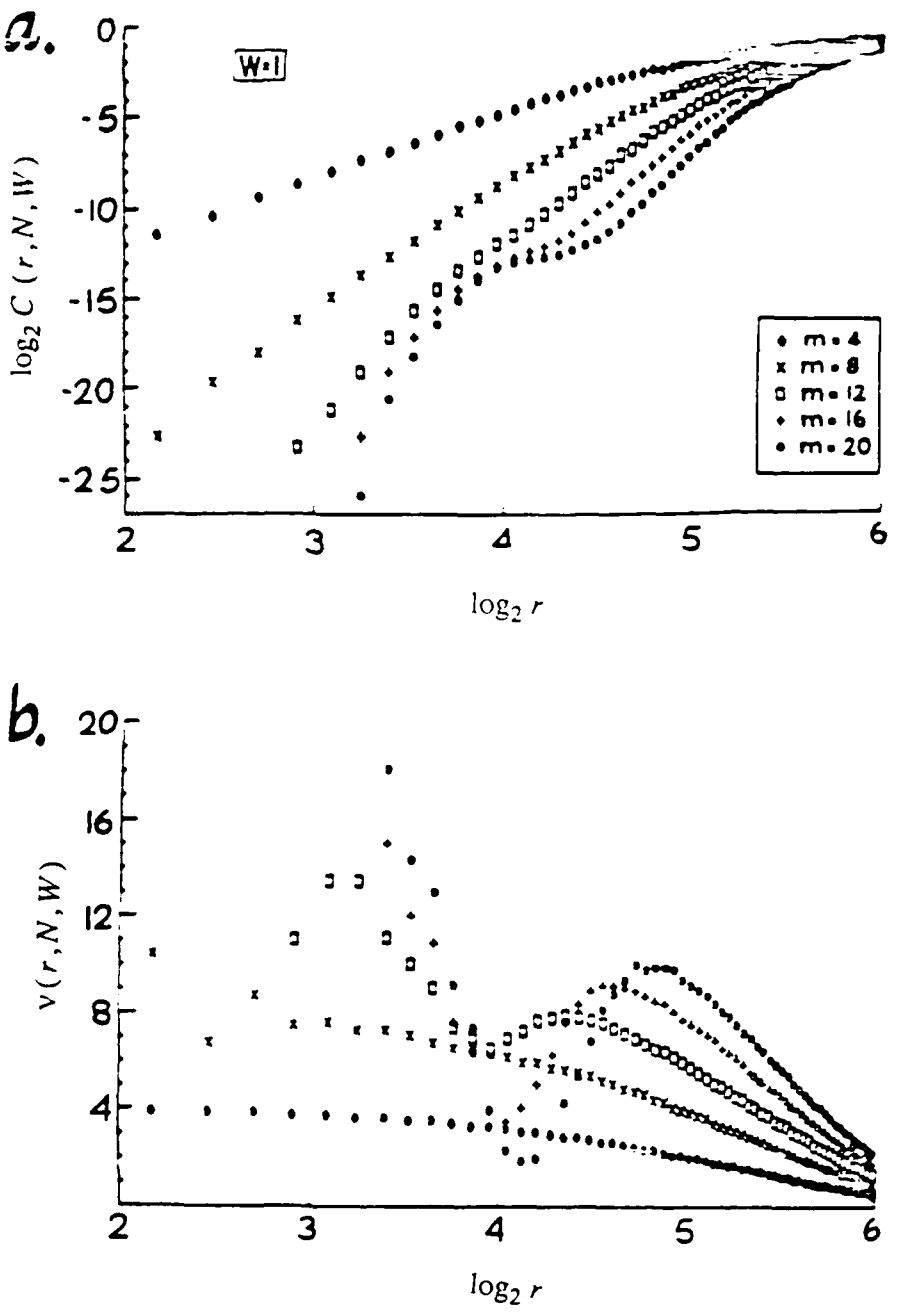

Figure (4.1.3) Standard correlation integrals for autocorrelated random data. (a) Log-log plot of the standard ($W = 1$) correlation integral over a range of embedding dimension m for stochastic data with $N = 10000$ points, standard deviation $\sigma = 20$, and autocorrelation $\alpha = 0.9$.

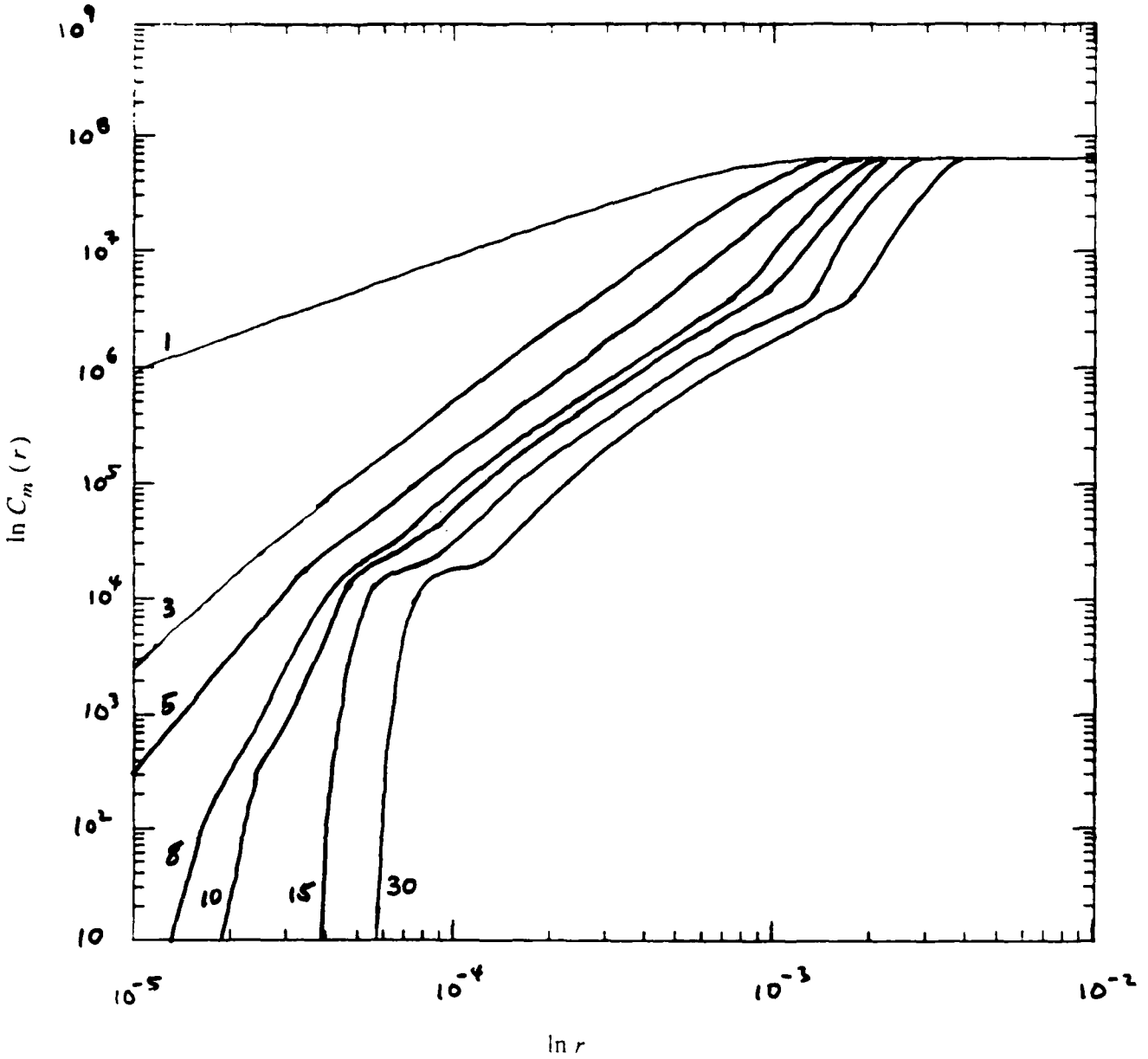

Figure (4.1.4) The logarithm of the correlation function $C_m(r)$ is plotted versus $\ln r$ for a number of different embedding dimensions m. The time series consists of 8031 data points obtained by concatenating the time series from 8 adjacent spatial points. The time shift is 80 units.

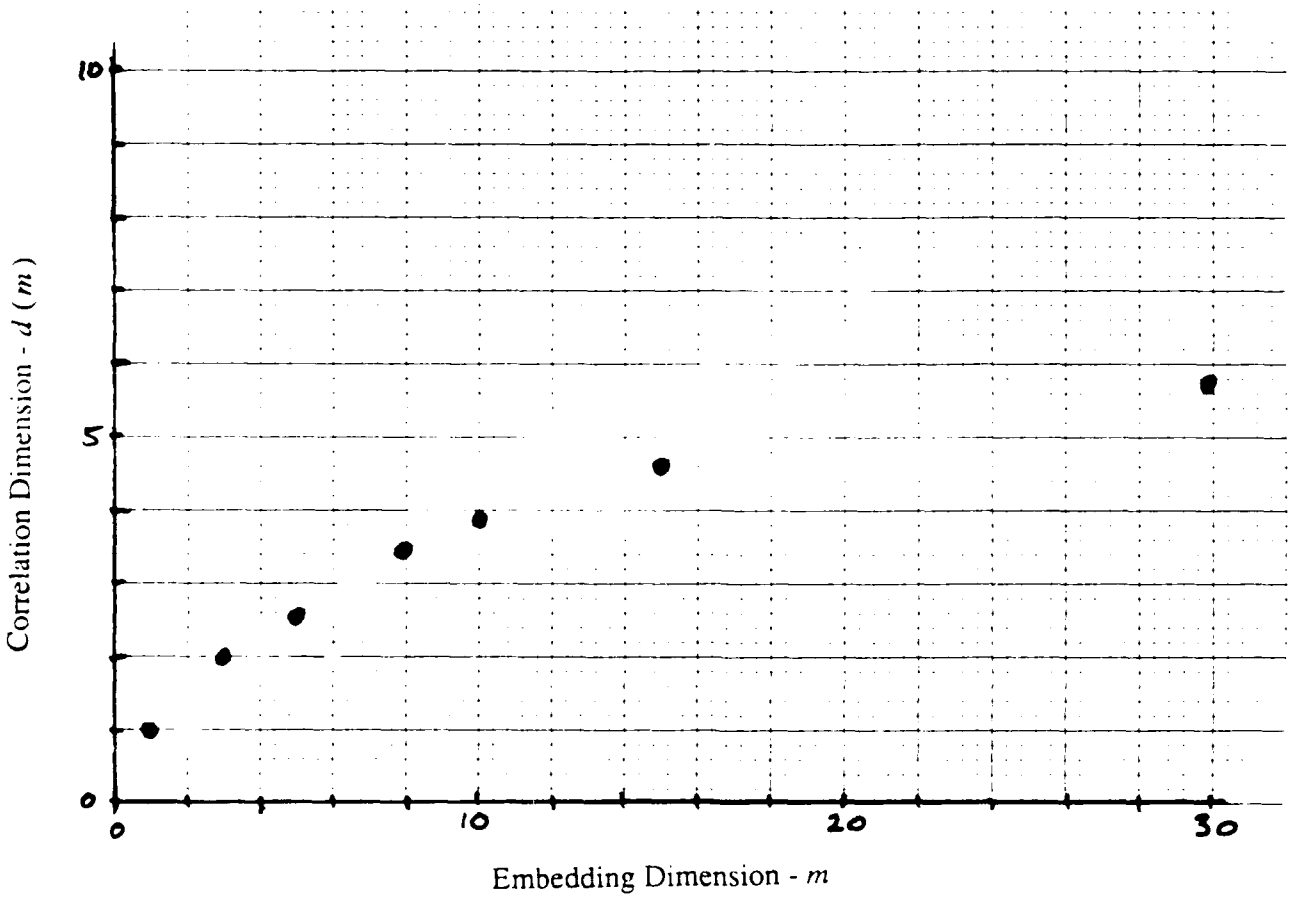

Figure (4.1.5) The correlation dimension $d(m)$ is plotted versus the embedding dimension m for the data in Figure (4.1.4). The time series clearly indicates a saturation in the neighborhood of $\nu = d_{\infty} \approx 6$.